Fusion of Information from Optical, Thermal, Multispectral Imagery and Geologic/Topographic Products to Detect Underground Detonations

Andy Biache, Jr., Carroll L. Lucas, Matthew Heric, and James M. Newlin

Autometric, Incorporated
5301 Shawnee Road
Alexandria, Virginia 22312-2312

Robert Huguenin (Subcontractor)
Applied Analysis, Incorporation
46 Manning Road, Suite 201
Billerica, Massachusetts 01821-3976

12 February 1992

Phase II SBIR Final Report

(Classified Annex Published Separately)

REPORT DOCUMENTATION PAGE

Form Approved
OMB No 0704-0188
Exp Date Jun 30 1986

1a REPORT SECURITY CLASSIFICATION	1b RESTRICTIVE MARKINGS
Unclassified	None

2a SECURITY CLASSIFICATION AUTHORITY	3 DISTRIBUTION/AVAILABILITY OF REPORT
DoD 5220.22M	
2b DECLASSIFICATION/DOWNGRADING SCHEDULE	
None	Unclassified/Unlimited

4 PERFORMING ORGANIZATION REPORT NUMBER(S)	5 MONITORING ORGANIZATION REPORT NUMBER(S)
DF/P2-92/1733	None

6a NAME OF PERFORMING ORGANIZATION	6b OFFICE SYMBOL (If applicable)	7a NAME OF MONITORING ORGANIZATION
Autometric, Inc.	None	Defense Advanced Research Projects Agency

6c ADDRESS (City, State, and ZIP Code)	7b ADDRESS (City, State, and ZIP Code)
5301 Shawnee Road Alexandria, VA 22312-2312	ATTN: NMRO (Dr. Blandford) 3701 North Fairfax Dr. Arlington, VA 22203-1714

8a NAME OF FUNDING/SPONSORING ORGANIZATION	8b OFFICE SYMBOL (If applicable)	9 PROCUREMENT INSTRUMENT IDENTIFICATION NUMBER
U.S. Army Missile Command	AMSMI-PC-BFA	DAAH01-91-C-R033

8c ADDRESS (City, State, and ZIP Code)

AMSMI-PC-BFA/DARPA Project Office
Redstone Arsenal, AL 35898

10 SOURCE OF FUNDING NUMBERS See reverse

PROGRAM ELEMENT NO.	PROJECT NO	TASK NO	WORK UNIT ACCESSION NO
None		None	None

11. TITLE (Include Security Classification)
Fusion of Information from Optical, Thermal, Multispectral Imagery and Geologic/Topographic Products to Detect Underground Detonations (U)

12. PERSONAL AUTHOR(S)
Biache, Andrew Jr., Lucas, Carroll L., Heric, Matthew, and Newlin, James M.

13a. TYPE OF REPORT	13b TIME COVERED	14 DATE OF REPORT (Year, Month, Day)	15 PAGE COUNT
Final	FROM 911108 TO 920225	920225	120

16 SUPPLEMENTARY NOTATION
Ground Truth Annex Published Separately
Classified Annex Published Separately

17 COSATI CODES			18 SUBJECT TERMS (Continue on reverse if necessary and identify by block number)
FIELD	GROUP	SUB-GROUP	Multispectral, Multiple Sensor, Stereoscopic, Nuclear Tests, Digital Image Processing, Sub-Pixel, Hyperspectral, "BEXAR"
None	None	None	

19 ABSTRACT (Continue on reverse if necessary and identify by block number)

This report documents the results of a Small Business Innovative Research (SBIR-Phase II) project conducted for DARPA focusing on the use of all-source overhead remote sensor imagery for monitoring underground nuclear tests and related activities. This documentation includes: 1) the main unclassified body of the report; 2) a separate ground truth Annex; and 3) a separate classified Annex. Autometric's approach was to investigate the exploitation potential of the various sensors, especially the fusion of products from them in combination with each other and other available collateral data. This approach featured empirical analyses of multisensor/multispectral imagery and collateral data collected before, during, and after an actual underground nuclear test (named "BEXAR"). Advanced softcopy digital image processing and hardcopy image interpretation techniques were investigated for the research. These included multispectral (Landsat, SPOT), hyperspectral, and subpixel analyses;

20 DISTRIBUTION/AVAILABILITY OF ABSTRACT	21 ABSTRACT SECURITY CLASSIFICATION
☑ UNCLASSIFIED/UNLIMITED ☐ SAME AS RPT ☐ DTIC USERS	Unclassified
22a NAME OF RESPONSIBLE INDIVIDUAL Carroll L. Lucas	22b TELEPHONE (Include Area Code) (703) 658-4050	22c OFFICE SYMBOL EXRAD

19. stereoscopic and monoscopic information extraction; multisensor fusion processes; end-to-end exploitation workstation concept development; and innovative change detection methodologies. Conclusions and recommendations for further R&D and operational uses were provided: 1) the general areas of sensor capabilities, database management, collection management, and data processing, exploitation, and fusion; and 2) specific multispectral, hyperspectral, subpixel, three-dimensional modeling, and unique unconventional imaging sensor technology areas.

TABLE OF CONTENTS

TABLE OF CONTENTS (Cont'd)

LIST OF FIGURES

LIST OF TABLES

ABSTRACT

This report documents the results of a Small Business Innovative Research (SBIR-Phase II) project conducted for DARPA focusing on the use of all-source overhead remote sensor imagery for monitoring underground nuclear tests and related activities. This documentation includes: 1) the main unclassified body of the report; 2) a separate ground truth Annex; and 3) a separate classified Annex. Autometric's approach was to investigate the exploitation potential of the various sensors, especially the fusion of products from them in combination with each other and other available collateral data. This approach featured empirical analyses of multisensor/multispectral imagery and collateral data collected before, during, and after an actual underground nuclear test (named "BEXAR"). Advanced softcopy digital image processing and hardcopy image interpretation techniques were investigated for the research. These included multispectral (Landsat, SPOT), hyperspectral, and subpixel analyses; stereoscopic and monoscopic information extraction; multisensor fusion processes; end-to-end exploitation workstation concept development; and innovative change detection methodologies. Conclusions and recommendations for further R&D and operational uses were provided in: 1) the general areas of sensor capabilities, database management, collection management, and data processing, exploitation, and fusion; and 2) specific multispectral, hyperspectral, subpixel, three-dimensional modeling, and unique unconventional imaging sensor technology areas.

SECTION 1
INTRODUCTION/BACKGROUND

Historically, the United States has relied on sophisticated seismic monitoring techniques to detect deep underground nuclear testing conducted by other countries. Among the difficulties encountered were those of differentiating nuclear testing from such natural occurrences as earthquakes or detonations produced through such human activities as mining or construction. As treaties were signed limiting nuclear testing to underground detonations of 150 kilotons or less, deceptive means were devised by adversaries to mask, or reduce the range of, unique seismic signals generated by nuclear tests. Currently, seismic monitoring equipment and techniques are severely challenged to identify, unambiguously, covert low-level nuclear testing. Along with the political destabilization of many of the formerly cohesive countries and alliances, has come the emergence of several Third World countries which have the capability to conduct nuclear weapons development.

With political tumult proliferating worldwide, timeliness assumes even greater importance in terms of monitoring the nuclear research capabilities of these emerging nations. The collection of seismic nuclear data from an unsuspected nuclear test site would indicate that research is well along the way for the development of a weapons capability. Such a late warning points to the need for other means to provide for earlier indications of nuclear activities. The difficulty is that much of the initial research is conducted in laboratories where few opportunities exist to identify the extent, duration, or progress of offensive nuclear research.

It is important to establish, early on, that nuclear testing has advanced beyond the laboratory stage with many of these nations, and even more important to be able to identify and monitor further progress.

During the summer of 1989, Autometric, Inc. responded to a DARPA Small Business Innovative Research (SBIR) initiative by proposing a study entitled "Fusion of Information from Optical, Thermal, Multispectral Imagery and Geologic/Topographic Products to Detect Underground Detonations." Since then, the Company has been conducting research to provide insight to the use of current and pending imaging sensors and available collateral data to detect a proliferation of nuclear research and testing in emerging countries. This Final Report, along with its Annexes, documents the results of the research and focuses on means to supplement seismic collections with accessible imaging capabilities.

SECTION 2
PURPOSE OF THE RESEARCH

The purpose of this SBIR was to conduct in-depth analyses of current and pending imagery collection and exploitation capabilities to determine their utility for detecting underground detonations. This was accomplished by monitoring a real-world nuclear event, using a variety of imaging sensors and state-of-the-art data fusion techniques. From these analyses, a set of exploitation tools was developed and documented, along with a workstation concept that takes into consideration the capability to integrate selected analytical and documentation processes. Finally, recommendations were made that specify the electromagnetic windows and spectral bands most useful in detecting the subtle changes that occur at the ground surface due to underground detonations.

SECTION 3
DATA COLLECTION PROCEDURES

Under Phase I of this SBIR, Autometric investigated several means for acquiring periodic imagery over selected sites, as well as for searching large geographic areas for significant changes. Both classified and unclassified sensor access, tasking, capabilities, and products were considered and procedures were established to acquire data on demand. A classified Annex (2) to this report addressed results from National assets. This unclassified report documented the tasking of other collection systems used. Unclassified satellite and aircraft optical and multispectral sensor products, including Seasat radar coverage, were investigated.

Building upon the Phase I methodology, similar Phase II collateral data collection processes were initiated once a test site was selected. The types of collateral collated for Phase II included historical test data, topographic and geological maps, Digital Terrain Elevation Data (DTED), historical and current weather data, as well as historical satellite and aircraft image coverage. All non-digital maps, schematics, and imagery were digitized to maintain data in one medium.

Once the coordinates of the selected test area were known, imagery collection plans were initiated which included scheduled satellite sensor tasking as well as aircraft collections using hyperspectral sensors (see Figure 3-1 and the classified Annex (2)). Procedures for integrating with the test directorate and other test personnel were established with the various Government offices. Details of these processes will be surfaced in the analyses of the products (Section 4).

2
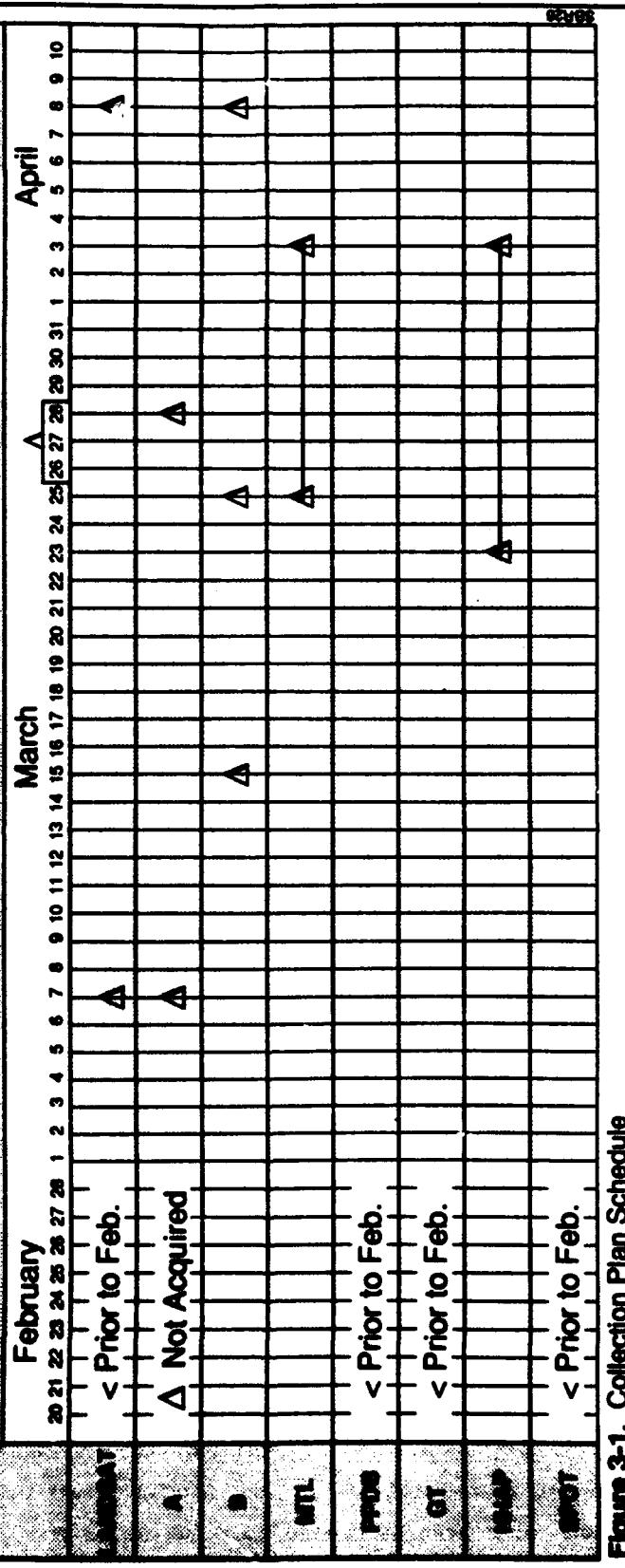
Figure 3-1. Collection Plan Schedule

Figure 3-1 Collection Plan

SECTION 4

UNDERGROUND TEST PARAMETERS

4.1   TEST COORDINATION

Phase I of the SBIR established the feasibility of using multiple sensor products collected through several spectral windows to detect and monitor deep underground nuclear tests. Based on that analysis, a Phase II decision was made to focus on a pending U.S. deep underground nuclear test at the Nevada Test Site (NTS). In November 1990, Autometric initiated the Phase II portion of the SBIR by establishing contact and briefing pertinent organizations who would be involved in the study. Personnel from the DoE, National Photographic Interpretation Center (NPIC), and the NTS were apprised of the study plans, and MTL Systems, Inc. was placed under contract to fly their hyperspectral imaging system over a selected test site before and after the test detonation. With only a few weeks to prepare, Autometric, with excellent support from both the DARPA SBIR COTR and DARPA Headquarters, met with the NTS directorate and arranged to participate in the BEXAR test scheduled for a late March 1991 detonation. The cooperation received from all the participants at the NTS was outstanding. Without their support, much of this research would not have been possible. Special thanks go to Mr. Larry Draper, whose interest and patience were truly appreciated. Mr. Ed Brown of DARPA was also of great assistance in coordinating with other organizations supporting this study.

Working with both the NTS and MTL Systems, an operations plan was produced that would be transparent to the BEXAR operations, yet provide the data needed for the SBIR study. Figure 4.1-1 contains the Operations Plan that was jointly agreed upon and submitted to the NTS in February 1991.

To assure other imaging sensor products would be available for use in the study, an image collection plan was also produced. Historical imagery of the site included Seasat radar imagery, National High Altitude Program (NHAP) aircraft photographic coverage, French SPOT panchromatic imagery, and Landsat multispectral and thermal coverage. The Landsat system was tasked to acquire additional coverage soon after the test so that correlations could be made with previous Landsat data. Arrangements were made with MTL Systems to provide video coverage of the test simultaneous to their hyperspectral collections. The NTS was also asked if they would provide copies of any imagery that they collected during the test. Finally, working with NPIC, the tasking of classified resources was accomplished. A classified Annex (2) to this report provides the details of this tasking and analysis.

Since there was a need to establish ground truth support to compliment the analyses of the imagery, arrangements were made for Autometric personnel to be on-site when the MTL Systems aircraft was collecting its data. Among other ground truth activities, hand-held camera photographs of the test site and surrounding areas were taken. A Ground Truth Report (Annex 1) has been compiled accordingly.

4

Operations Plan
NTS Collection

MTL Systems, Inc. will locate its flight personnel and its twin engine Piper AZTEC aircraft (tail No. N40510) at a site where routine coverage of the selected target can be accomplished. The sensor to be used it the ASIS, along with a conventional VHS video camera. The target site is at coordinate N37°17'46"-W116°18'46". The site elevation is 7037 feet MSL. The collection window is from 1 April to 12 April, bracketing the test and allowing for some weather delays. The first aircraft flight, assuming no delay in test schedule, will occur on 1 or 2 April between 1000 and 1400 hours local time. This will provide coverage prior to the test event. A minimum of two near nadir passes will be made over the test site at altitudes that will provide ASIS coverage at ground resolutions of 8 meters and 13 meters. The second flight will replicate the first flight both in terms of orientation and altitudes so that image superpositioning can be easily achieved. The second flight will be scheduled within 24 hours after the test event, weather permitting, and no later than 7 days after the first flight. Autometric, Inc. will provide an annotated aerial image of the test site to MTL for their planning purposes. MTL will work with the Government, who will specify the parameters of the flight in order to avoid other sensitive sites.

As soon as the test data is firmly fixed, Autometric, Inc., NTS, and MTL personnel will meet at the Desert Rock Nevada Airport on the date of the first flight to review the flight plan and prepare for contingencies. The flight will then originate from the Desert Rock Airport and return. A similar approach will be taken for the second flight.

Autometric personnel will be in the test area during the flight to document ground truth with a handheld video camera, and will meet later with MTL and government personnel to review the video camera results and determine the success of the flight.

Autometric personnel plan to be in the test area every day between flights to become acquainted with test procedures. Arrangements will be made with Mr. Lawrence Draper on how this can be best accomplished.

The MTL aircraft will be flown by Thomas F. Cauley, a certified transport pilot, certification number 1572656. He will be accompanied by instrument operator Robert L. Stevens, SSN 121-54-2573.

The Autometric personnel that will be on site between 15 March and 12 April 91 are:

Mr. Carroll L. Lucas	SSN	003-12-4297
Mr. Mathew Heric	SSN	252-74-3309
Mr. Paul Richard	SSN	218-36-7323

The backup person, should one of the above not be available, is Mr. Maurice Barry, SSN 052-56-0708.

Mr. Lucas will work closely with the NTS personnel to assure that the aircraft and the participation on the ground by Autometric personnel is transparent to the test operations.

Figure 4.1-1
Operations Plan

4.2   TEST LOCATION AND DESCRIPTION

The BEXAR site was in a northwestern section (19) of the NTS. Specifically, BEXAR was atop a mesa whose elevation was approximately 2134 meters above sea level (Figure 4.2-1). The mesa was bounded on the north by a terrain feature called Dead Horse Flat, and on the west and south by Silent Canyon. Geologic collateral data indicated that the mesa was comprised of rhyolitic ash flow tuff underlain by quartz latite ash flow and mafic/rhyolite tuff to a depth of over 600 meters (Figure 4.2-2).

Vegetation in the area was sparse, consisting primarily of stunted cedar and other evergreen trees/bushes. Small patches of snow and ice were observed on the north sides of slopes and clumps of vegetation.

BEXAR ground scars designating site activity and road building were not evident on the earliest historical imagery collected by the French SPOT sensor in September 1988, indicating that the site was new and uncontaminated by previous tests. The later SPOT coverage acquired in December 1989 documented initial scarring and the presence of drilling equipment at the site. A few kilometers away, three other abandoned sites appeared to have similar configurations as the completed BEXAR site; indicating a series of related tests may have been underway. The size difference between the three site scars also indicated BEXAR was the largest and/or most sophisticated of the tests. In 1983, NHAP coverage over the historical sites showed no ground scars.

The BEXAR site was configured as a truncated triangle oriented with its truncated point to the north-northeast of the site. A small square area was also observed attached to the easternmost leg of the triangular scar. The site had been cleared of vegetation, bulldozed, and scraped to produce a level surface and appeared to have been periodically soaked with water and rolled to reduce dust. Two bermed artificial ponds built along the northwesternmost edge of the site scar, contained a small amount of water, rimmed with ice. A continuous circular scar, approximately 300 meters in radius, with the Ground Zero (GZ) as its center, was observed on aerial video imagery (Figure 4.2-3). This was a defoliated trail containing radiological instrumentation used as well as a security measure to keep animals off the site and to alert personnel that they were approaching a sensitive area.

Oriented in line along the southern base of the BEXAR site were ten large metal trailers, a metal two-story temporary building and five other small trailer configurations. Clustered in the rear of each trailer were collections of auxiliary equipment such as air conditioners, humidifiers, generators, etc. as well as personnel vehicles and an occasional piece of heavy equipment, depending on the activity level of the ongoing test. Emanating from the northern ends of the trailers were large white cable bundles which converged just to the south of the GZ, forming one large looping bundle that terminated at the GZ.
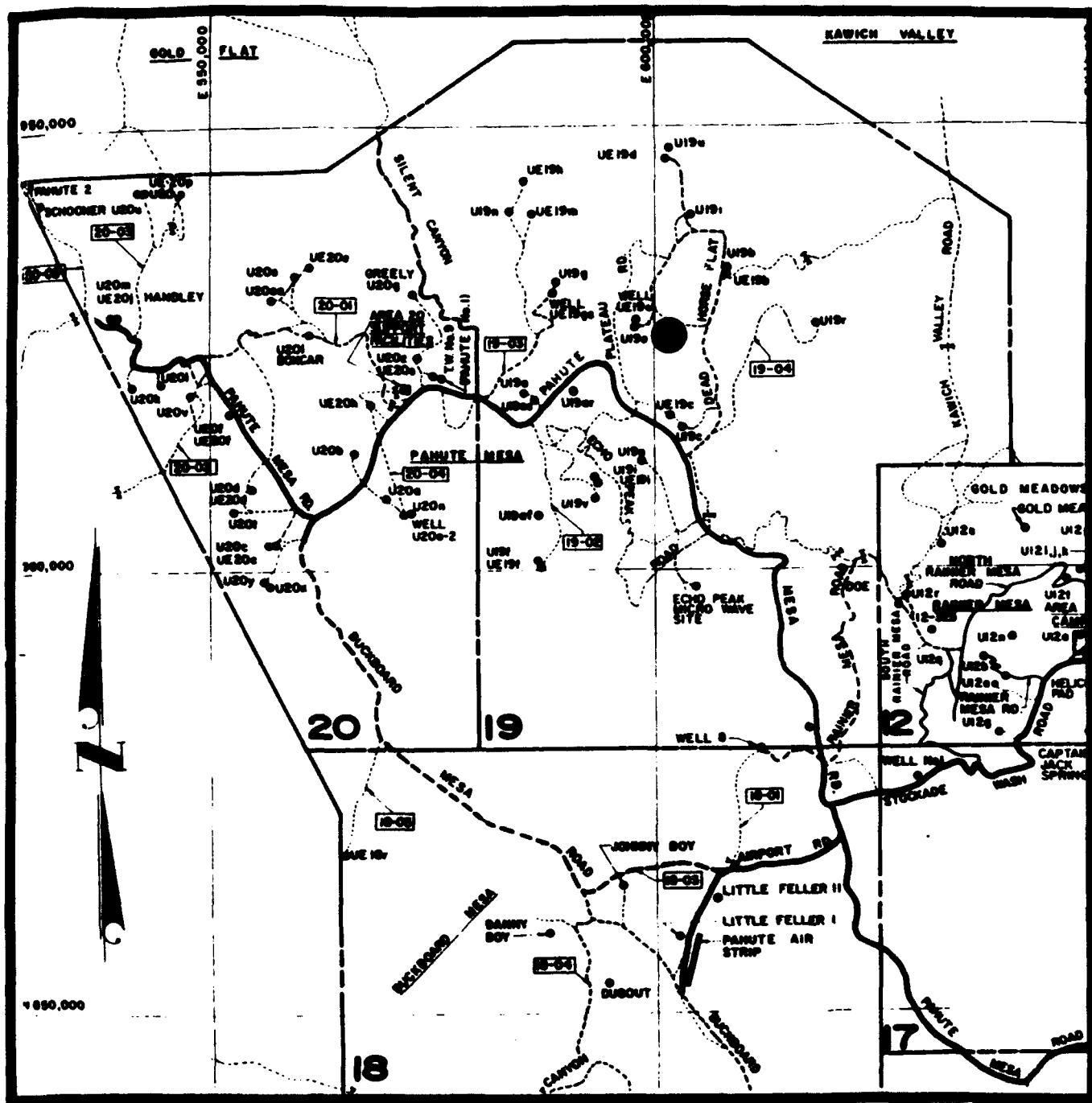
Figure 4.2-1
Site Location Map

Ammonia Tanks Member—Rhyolitic to quartz latitic ash-flow tuff. In areas distal from Timber Mountain, compound, nonwelded to densely welded, in part devitrified; maximum thickness 170 m. On Timber Mountain dome, locally subdivided into intracaldera:

Rainier Mesa Member—Compound cooling unit, nonwelded to densely welded high-silica rhyolite with caprock of quartz latitic ash-flow tuff; generally devitrified center and vitric top and bottom; generally less than 150 m thick, except near west wall of Timber Mountain caldera (Transvaal Hills) where thickness exceeds 350 m

Trail Ridge Member—Multiple-flow simple cooling unit of comenditic rhyolite ash-flow tuff with thin ash-fall pumice lapilli and local pebbly tuffaceous sandstone at base; as much as 80 m thick

Paintute Mesa and Rocket Wash Members—Composite ash-flow tuff sheet of high-silica sodium-rich rhyolite comprising four cooling units that locally coalesce to a single or compound cooling unit; as much as 180 m thick. Includes a thin bedded ash-flow and ash-fall pumice lapilli base

Alluvium and colluvium (Holocene, Pleistocene, Pliocene, and Miocene)—Unconsolidated to moderately cemented, locally deformed, alluvial fan, flood plain, stream bed, talus, slope wash, and eolian deposits; thickness variable, as much as 600 m thick

Figure 4.2-2
Geological Map of BEXAR Test Area

8
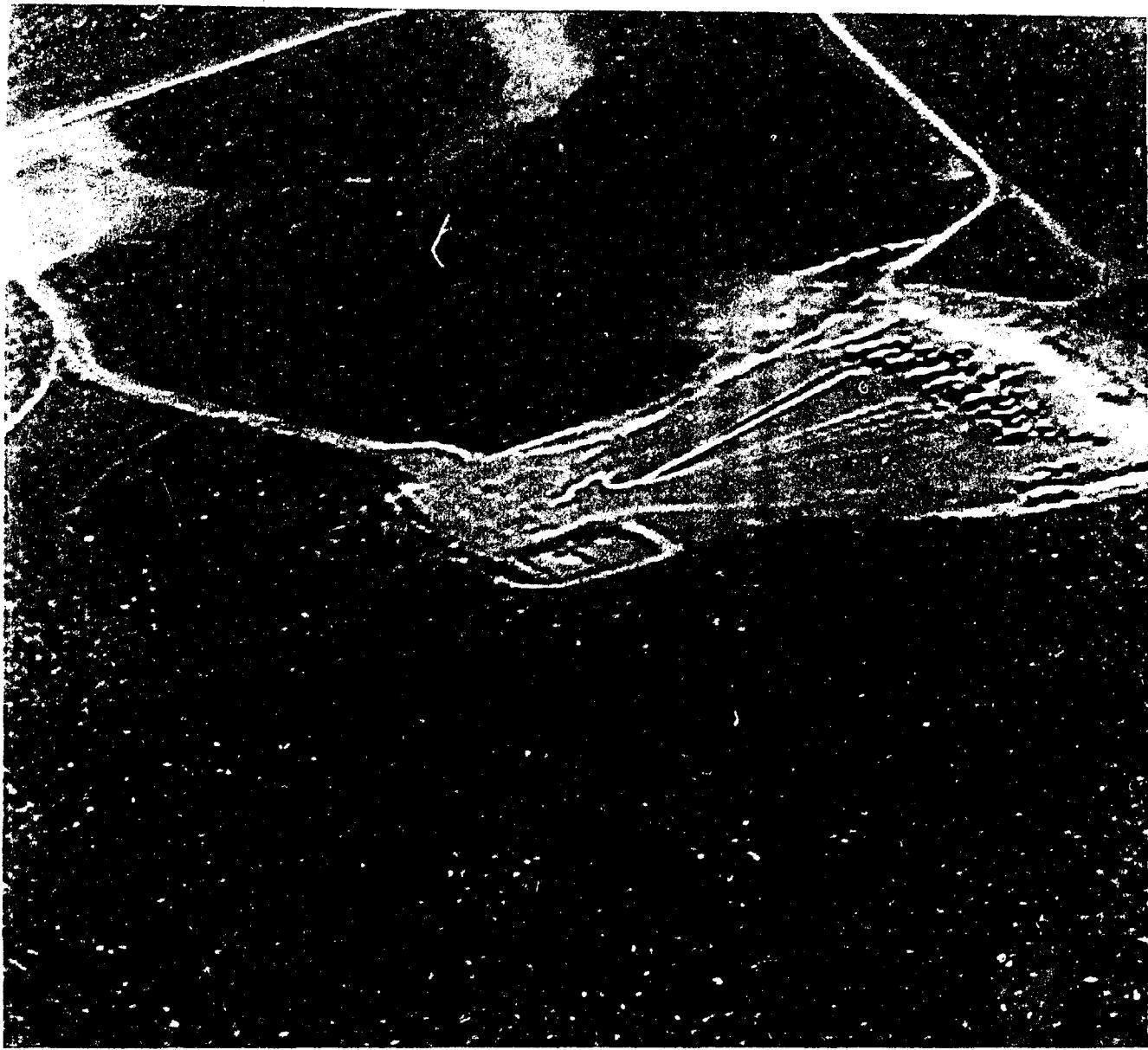
Figure 4.2-3
Aerial Video Imagery of BEXAR

4.3   TEST CHRONOLOGY

BEXAR was initially scheduled for the last week in March 1991; however, test preparations delayed Time Zero (TZ) until 3 April, at 09:00 hours (local time). Autometric personnel were on site on 1 April to be pre-briefed on the test and to acquire ground photographs of the area prior to detonation. On 2 April, at the GO/NO GO weather briefing, the TZ was moved to 09:00 on 4 April due to unsatisfactory projected wind velocities and directions.

All activities at the site ceased early in the morning of the rescheduled test. Wind direction problems, though, delayed the TZ an additional two hours on 4 April; however, a successful detonation occurred at 11:00 hours. The test produced a small debris cloud that moved to the north of the site and within 2.5 minutes it had dissipated and was no longer visible to overhead imaging sensors.

By 14:00 hours, above-ground activity at the site had resumed. Vehicular and personnel activities were observed throughout the afternoon, fixing the critical test timing and indicating a successful test. Finally, approximately 24 hours after the test, on 5 April, Autometric personnel visited the site and acquired post-detonation ground photography. Additional information concerning site activity and conditions shortly before, during, and after the test is documented in the Ground Truth Report (Annex 1).

4.4   HISTORICAL TIMELINE CHRONOLOGY

The United States has been conducting contained underground nuclear tests at the NTS since 1957, a year before the signing of the Limited Test Ban Treaty. Close to 700 well-documented underground tests have been conducted to date, providing considerable historical textual data of the surface effects produced by the detonations. During the 1980s, more emphasis was placed on acquiring imagery of the tests, and such data has shown interesting correlations. The Defense Nuclear Agency (DNA) has also been conducting above-ground simulated nuclear tests since the 1970s. Under the initial Phase I of this study, these data were combined and used to establish a Generic Testing Timeline of events that occur during test preparation and conclusion.

Subsequently, the initial timeline has been refined and modified with data that have been produced through the monitoring of the BEXAR test. Figure 4.4-1 depicts the revised data and justifies the generic nature of the information (at least under similar environments). International aspects of these data are addressed in the classified Annex (2) of this report.

Generic Testing Time Line (U)

OBSERVABLE SURFACE KEYS

T-6-12 MONTHS	T-1 MONTH	T-48 HOURS	T-2 HOURS	DETONATION T+16 HOURS	T+3 DAYS T+MONTHS
DRILLING	CONTINUOUS ACTIVITY	CONTINUOUS ACTIVITY	TEST REHEARSAL	NO ACTIVITY	CRATER COLLAPSE	CLEAN UP	VEGETATION CHANGES

INITIAL GROUND ZERO

INITIAL GROUND ZERO	CONTINUOUS ACTIVITY	CONTINUOUS ACTIVITY	TEST REHEARSAL	NO ACTIVITY	DETONATION	CRATER COLLAPSE	CLEAN UP	VEGETATION CHANGES
DRILLING APPARATUS FIELD APPARATUS FIELD COMPONENTS SECURITY CONTROLS GZ STAKES	DRILLING APPARATUS RIGGING APPARATUS CALIBRATION OF TRENCHES CONSTRUCTION OF UNDERGROUND STRUCTURES TESTING EQUIPMENT GENERATORS & BUNKERS PHOTO SUPPORTS & MARKER PYLONS EXPLOSIVE HANDLING FACILITY CONSTRUCTION OF CHARGE CONTAINER COVERING CABLE TRACKS TEST VANS CREW QUARTERS MOTOR POOL WATER STORAGE	COMPLETION OF CHARGE CONTAINER ARRIVAL OF EXPLOSIVE COMPONENTS SPECIAL TARGETS ARRIVE & ARE EMPLACED INCREASE IN PERSONNEL & MOVE SECURITY PERIMETER ON TEST BED (CHAIN LINK & CONCERTINA WIRE) GUARD SHACKS AROUND SITE PREPARATION OF EXPLOSIVE AT HANDLING FACILITY LOAD EXPLOSIVE INTO CONTAINER INSTALL CAMERAS ON PYLONS MAXIMUM TRAILERS & SUPPORT EQUIPMENT ON TEST BED COVERING UNDERGROUND STRUCTURES WEATHER STATIONS IN PLACE	TEST AREA BEING CLEARED MAX NUMBER OF PERSONNEL WX BALLOONS IN PLACE DUST COLLECTING MISSILES REMOVAL OF TRAILERS & SUPPORT EQUIPMENT SPECIAL AIRCRAFT AT NEARBY AIRFIELDS NIGHT ACTIVITY	TEST SECURITY NO ACTIVITY WX BALLOONS LAUNCHED VIP KEYS (SPECIAL TRANSPORT) ROAD BLOCKS CALM WIND WIND DIRECTION AWAY FROM URBAN AREAS	DETONATION DEBRIS CLOUD VENTING DUST AIRCRAFT MISSILES NO PERSONNEL ON SITE SEISMIC ACTIVITY FAULT ACTIVITY	PERSONNEL ON SITE VEHICLES AT SITE DEBRIS FRACTURES CRATE SPALLING EQUIPMENT DAMAGE FAULTING SOIL TEXTURE CHANGES CAMOUFLAGE (DAD) DUST ON VEGETATION	TEST BED CLEAN UP VEHICLES PERSONNEL SURFACE SUBSIDENCE TRAILERS & SUPPORT STRUCTURES IN PLACE RECOVERY OF EXPERIMENTS EXCAVATION AT UG STRUCTURES WITHDRAWING TRAILERS & SUPPORT EQUIPMENT	VEGETATION CHANGES DRAINAGE CHANGES SUBSIDENCE EXCAVATIONS OF UG EX- PERIMENTS EXCAVATION OF CRATER FILL IN CRATER NO ACTIVITY

Figure 4.4-1 Generic Testing Timeline

SECTION 5
PRELIMINARY VISUAL ANALOG IMAGERY ANALYSES

Both original analog and digitally-processed analog imagery were analyzed in Section 5. Section 7.1 provides descriptions on the specific digital techniques used prior to the preliminary visual anlayses.

5.1   HISTORICAL IMAGERY

5.1.1   Point Positioning Data Base (PPDB) Photographs

PPDB photograph numbers 27 and 28 from control number 77-01200, acquired in calendar year 1977, provided excellent high-altitude stereoscopic imagery of the BEXAR site. (The PPDB is a worldwide database but is rapidly becoming obsolete due to difficulties in updating the imagery. The vast majority of the database was produced prior to 1982.) The ground resolution of the imagery appeared to be approximately one meter. There was no indication of ground scarring or road building at the site. Sparse vegetation and low shrubs or trees covered the area at the top of the mesa and a recent linear man-made ground scar parallels a fault line south of mesa connecting to the major north/south road servicing other tests to the northeast of the site. The dark-colored, non-reflective cover at the site would have provided a sharp contrast to any natural or manmade scarring. The photogrammetric fidelity of the PPDB imagery allowed for the topographic mapping of the area to within a meter in both relative altitude/height and geographic positioning. This provided an excellent database for future comparative analyses.

5.1.2   Seasat Radar Coverage

Seasat coverage of the NTS occurred in 1978. Seasat is an "L"-band synthetic aperture radar sensor that was in orbit for a relatively short period of time. Spatial resolution is in the order of 38 meters and, under Phase I of this research, Autometric determined Seasat recorded the existence of collapsed craters and of significant road construction. Since the BEXAR site was undeveloped in 1978, however, only the general terrain surface data was detected. If significant ground scarring or road construction had been underway, Seasat would have likely detected it and would have confirmed changes over previous NTS imagery acquired by a variety of sensors. The strength of a Seasat-like radar sensor is in its ability to respond in critical situations; namely, regardless of time of day or weather

conditions. This may offer little in terms of long-term tests, but may well be able to detect final test preparations as well as cratering and large equipment concentrations occurring directly after a test.

5.1.3   National High Altitude Photography (NHAP)

NHAP exists only over the United States and some of its possessions. It is indicative, however, of high spatial resolution photography in many country inventories which could be made available on demand. The latest available NHAP coverage over the BEXAR area was flown on September 10, 1983. Two stereoscopic flight lines were accomplished, one with black and white film, the other with color infrared film. Frames 123 and 124 of black and white Mission 371614-HAP-83 provided good stereo coverage of the site area at a nominal ground resolution of one meter. The BEXAR site showed no scarring; although the mesa promontory to the northeast of the site showed scars of previous activity containing a square cleared area and a road connecting the area to the main north/south road. Usually the black and white photography provides better ground resolutions than color infrared film products; however, in this case the color infrared flight was flown at a significantly lower altitude and provided stereoscopic coverage and ground resolutions of less than one meter. As an example of the quality of the film, in viewing frames 170 and 171 of Mission 371614-HAP-83F color infrared film, vehicles can be detected on the roads, and the cabs of large vans can be differentiated from the bodies. Since the NTS is arid and the date of the flights was in September, the color infrared film showed minimal red tonal information (depicting healthy vegetation). The near monochromatic blue of the image provided limited additional spectral information beyond that of the black and white film. Original NHAP film products provide excellent stereo coverage of a given flight line and, once registered, provide photogrammetric fidelity similar to PPBD data. Figure 5.1.3-1 is a rectified high spatial resolution color infrared image of the BEXAR area prior to construction. This was used to compare with later coverage dates to monitor changes as they occurred.

5.1.4   Landsat Thematic Mapper (TM) Imagery

One source of Landsat data available for this study was a 1:100,000 scale image map of Pahute Mesa, Nevada, produced in 1984 by the U.S. Geological Survey (USGS). The image map was compiled using Bands 2, 3, and 4 of the TM data. The 1984 TM coverage site showed no indication of activity. Vegetation covering the top surface of the mesa remained undisturbed, and there was no indication of new road construction to the site area. The vegetation appeared to be lusher than in previous NHAP

Figure 5.1.3-1
NHAP Color Infrared

coverage, indicating the seasonal changes recorded through periodic coverages. Because there were no signs of BEXAR activity, it was decided to forego acquiring the data tapes and to acquire coverage closer to test TZ. Figure 5.1.4-1 can be used to compare with later date TM coverage to determine the ease of detecting test activities with a 30-meter large-area-coverage sensor. Examples of this are shown in Section 5.2.

5.1.5 SPOT Panchromatic Imagery

The French SPOT system can provide stereoscopic images of a target area through two operational modes. The first, and most used, is the capability of acquiring coverage over the same area from adjacent orbits. The unique sensor pointing ability thus produces stereo images that have a time difference of approximately 90 minutes and assures that little change has occurred between the two images. A second capability provides for stereo images to be acquired along the same orbital line, but with days or months separation in time. This capability is used when unplanned needs for historical stereo coverage are encountered, multiple monoscopic coverages are available, or tasking of monoscopic data is requested over a previously covered target. Such capabilities also allow for collecting combinations of panchromatic and multispectral SPOT imagery over the target of interest. Although a SPOT image acquires approximately only 10% of a Landsat scene at nadir, it is considered an efficient collector of wide areas.

Autometric had SPOT panchromatic stereoscopic imagery of the BEXAR area in its database from a previous unrelated project. The initial coverage occurred on 17 September 1988, and the other was collected on 14 December 1989. An in-house SPOT stereo mathematical model had been developed that is more accurate than the model sold by the SPOT organization. This was used to register and view the hardcopy stereo image on the Autometric Analytical Photogrammetric Processing System (APPS-IV), and was later integrated into a softcopy workstation for additional analyses. In viewing these data monoscopically, the 15-month time difference was used to detect any changes that occurred at the general BEXAR site.

A cursory comparison of hardcopy images from each collection showed that on the 1988 coverage there was no activity in the area of BEXAR; however, on an adjacent mesa promontory to the northeast, a large cleared and bulldozed area was observed. The high reflectivity of the scarred earth indicated its recent origin, and the detection of large trailers/temporary buildings was a positive indication of an ongoing test. The site was serviced by the major north/south road that joined several previous test areas to the road network connecting the northwest corner of NTS to the rest of the range. The 1989 SPOT coverage provided information that indicated another test had been completed and all equipment had been moved elsewhere. The site scar was much less reflective, indicating weather, sparse

Figure 5.1.4-1
Landsat Thematic Mapper (From USGS Image Map)

vegetation, and the lack of activity was allowing the scar to begin healing. The lack of an obvious crater indicated the test was conducted deeply underground. The 1989 coverage also documented a new road connecting the southern portion of the abandoned test area to the top of the adjacent mesa to the west. A large square cleared area was observed at the terminus of this new road, and a drilling apparatus was detected at the center of the cleared area. The indication was the drilling equipment was moved along the new road either from the old site or across the old site from the north/south road. The wide radius turns connecting the new road to the north/south road indicated the latter to be the most plausible case and lent credence to the fact that the older site had been abandoned. Rudimentary superpositioning of the latest SPOT coverage with aerial coverage of the BEXAR site documented that the square cleared area was the position of the BEXAR GZ and provided a reliable indication of the initiation of BEXAR test activity. Figure 5.1.5-1 is a stereoscopic pair of images from the SPOT coverage. Using the stereoscope supplied in the back of this report, an appreciation of the terrain and changes that occurred between collections can be realized. By simply blinking one's eyes intermittently, changes can be instantly identified.

5.2   CURRENT IMAGERY

5.2.1   Current Landsat Thematic Mapper Imagery

5.2.1.1   Prior to the BEXAR TZ

Tasking for Landsat TM imagery was requested for a period shortly before the TZ of the BEXAR test. On 7 March 1991, the TM imagery was acquired, and tapes were provided in early June 1991. Figure 5.2.1.1-1 is an image comprised of enhanced Bands 2, 3, and 4 from the above imagery. This was used for a direct comparison with the historical 1984 TM data, as well as other coverage acquired shortly after the BEXAR TZ. Immediately apparent in the comparison of this image with the historical data was the evidence of several new test scars situated short distances from the major road network, and connected to the network by short unsurfaced roads with wide radii turns. Three of these scars had similar shapes and configurations or were within a few kilometers of each other. The BEXAR scar showed evidence of activity by the highly reflective line of trailers/buildings along the southern edge of the scar, detected as fluctuating brightnesses, and evidence of water stored in ponds in the northwestern corner of the site. A few kilometers to the south-southwest was another highly-reflective scar similar to, but slightly smaller than, the BEXAR site. The high reflectivity of the soil and the short connecting road indicated the site
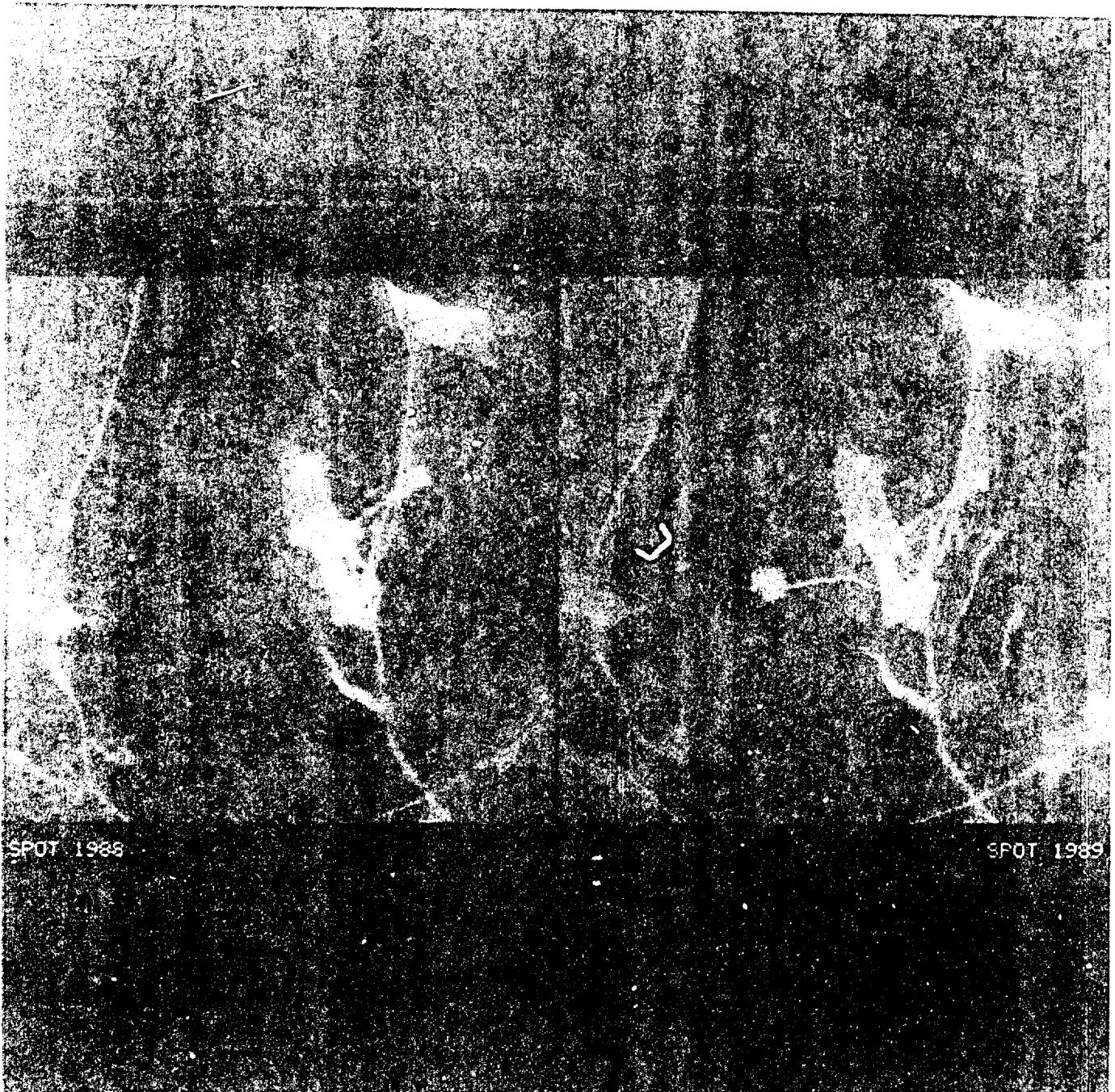
Figure 5.1.5-1
SPOT Stereopair

BEXAR >

Figure 5.2.1.1-1
Landsat Thematic Mapper (TM) Pre-Event

was under construction. Less than a kilometer to the south of this site was another similar site far less reflective. This indicated an earlier test had occurred. The above evidence seemed to indicate that a continuing series of similar tests were being conducted, with another test to be completed within the next several months. Since no collapse craters were apparent, this series depicted deep underground testing.

Another scar adjacent to and on a mesa to the east of BEXAR had a different configuration, yet appeared to be connected to BEXAR by an unsurfaced road. A close examination of this road showed it crossed the scarred area and connected to the major north/south road which services that part of the NTS. This indicated the two adjacent tests were not one integrated test, that the easternmost scar represented a completed test, and the BEXAR test was serviced by two roads connecting it with the range road network.

5.2.1.2   After the BEXAR TZ

On 8 April 1991, the BEXAR area of the NTS was again covered by the Landsat system, and the tapes were provided to Autometric in mid-June, 1991. A visual comparison was made between Bands 2, 3, and 4 of this coverage and the same bands of the March 1991 data. Figure 5.2.1.2-1 depicts the latest TM coverage. Using a mirror stereoscope, some indication of three-dimensionality was achieved and the detection of changes was attempted. The water signature was still evident, but the reflective changes in the area of the trailers were too subtle to differentiate—especially since the changes in solar elevation and atmospheric conditions contaminated the visual signatures. The conventional use of TM Bands 2, 3, and 4 to conduct visual change detection was limited by the 30-meter pixel size of the TM and by the inability to differentiate changes due to human activity from solar and atmospheric changes occurring over time. Using the full spectral capability of the TM and adjusting for non-human changes provided additional opportunities for documenting subtle spectral changes produced by human activities.

No changes could be observed at any of the other test sites described from the March TM coverage. The highly reflective scar to the south of BEXAR appeared identically to the March coverage and still appeared to be under construction. The scar adjacent to and east of BEXAR had not changed. No new scarring occurred in the prepared subscene.
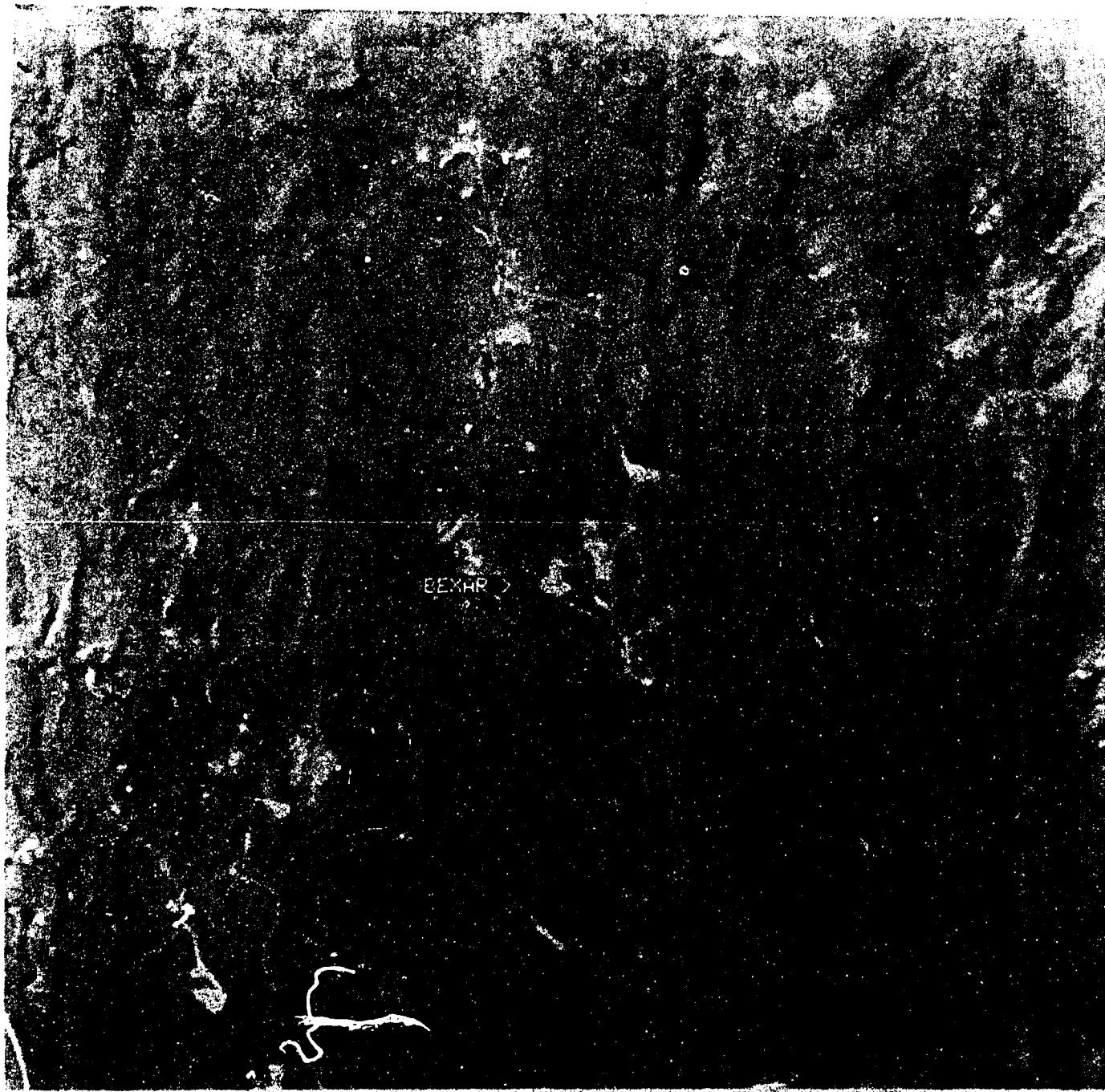
Figure 5.2.1.2-1
Landsat Thematic Mapper (TM) Post-Event

5.2.2 Current MTL Systems Data

5.2.2.1 MTL Coverage Before the BEXAR TZ

On 2 April 1991, MTL Systems flew its Airborne Spectroradiometric Imaging System (ASIS) in a Piper Aztec aircraft over the BEXAR site at two different elevations. ASIS is a spectral radiometer that collects simultaneous data using 63 separate bands throughout the 0.4 to 2.4 micrometer spectral window. The data were calibrated by MTL Systems, and the tapes were then reviewed at Autometric. The means devised to review efficiently these data are discussed in Section 7.4 of this report. The intent of the study was to determine which bands provided the most reliable information concerning changes that might occur due to underground detonations. Although hyperspectral data are not designed for visual exploitation, Figure 5.2.2.1-1 provides an example of one of the 63 bands (Band 10).

5.2.2.2 MTL Coverage After the BEXAR TZ

The final coverage of the BEXAR site by the ASIS occurred within three hours after TZ and because of atmospheric cloud conditions, was flown only on the scheduled low altitude flight plan. The data were reviewed at a digital display station. More detail on ASIS Analysis is provided in Section 7.4.

5.2.2.3 Nevada Test Site (NTS) Video Data

Before, during, and after the detonation, NTS collected low-altitude video data of the BEXAR event. Primarily, these images were used by the researchers as a ground truth component, and more information on the video is provided in Annex 1. The video complimented the other data and provided a means to establish key observable event-related phenomenon (Section 5.3).
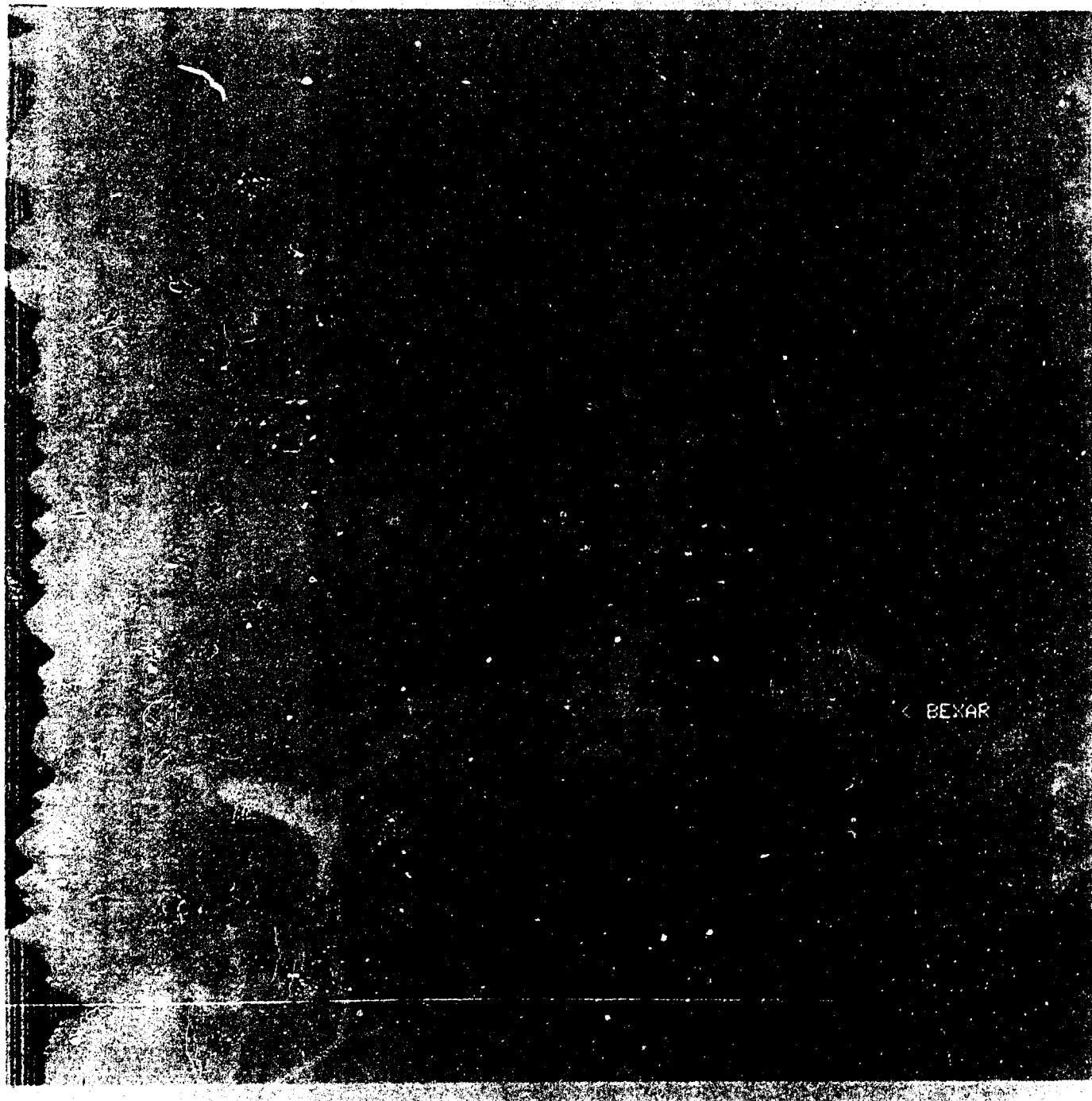
Figure 5.2.2.1-1
Airborne Spectroradiometric Imaging System (ASIS) Band 10 Example

5.3 KEY SPECTRAL OBSERVABLES FOR PENDING DIGITAL ANALYSES

After the abovementioned analog data were reviewed, several spectrally-oriented observations were made by the research team. These served as the foundation for the pending digital analyses conducted by Autometric and AAI, Inc. (subcontractor).

As a result of the detonation, surface disruptions were seen in the vicinity of BEXAR's drill hole. In particular, surface material was thrust into the atmosphere as a dust cloud, and after the event the dust drifted to the northeast away from the blast site. Indeed, the surface effects from the blast were concentrated in the immediate area of the drill hole, and although watered down and trafficked, this loose spoil material was relatively unpacked and unstable and therefore susceptible to resettling.

It was apparent from the data that the local surface geology and topography influenced the surface expression of the underground blast. The area of major surface disruption appeared to stop abruptly at linear boundaries on the east and west side of the drill hole. Apparently, a small geologic surface lineament on the east side and a steep topographic slope on the west side of the test mesa may have restricted and narrowed the area of major surface disruption. No visible surface disruption occurred on the outside of the lineament or the steep slope.

A steep topographic slope occurred off the northwest side of BEXAR. In the NTS video, a linear cloud approximately 300 to 500 meters long developed above this steep slope. It was possible that the soil material on the steep slope may have been loosened and subsided as a result of the blast, and the down-slope subsidence may have entrained the observed dust. The particulates in this cloud were slightly darker in color than the particulates in the clouds thrust from the drill hole area.

There were several potential spectral changes which may have been detected. The detonation caused substantial surface fracturing in the spoil pile. These fractures were centimeters across and less than a meter in length and were shadowed. Collectively they may have changed the spectral signature of the spoil pile. Shadowed areas are illuminated by diffuse hemispherical sky radiance rather than directly transmitted solar irradiance and thus have different spectral characteristics.

Another possible change to the spoil pile and unvegetated areas was a redistribution of particles due to vertical displacement. Before the blast, fine particulates in the soil and spoil pile were likely settled into cracks, crevasses, and other gravitational wells. The larger coarser particulates, which could not as easily be eroded, remained on the surface. During the blast, fine particulates became entrained by the vertical displacement. Some were suspended in the cloud of particulates and transported away, while others may have been deposited on the spoil pile surface. Some may have been simply mixed on the surface. The net result may have been an increase in the fraction of fine material on the surface.

Another change may have been an expansion of the spoil pile. The spoil material was distributed up to a meter or higher in depth over the top of the mesa and in a manner which created a rather distinct spoil pile edge with some of the edge having steep slopes. Some of the edges may have

24

been unstable. Most of the spoil pile was trafficked and watered down to prevent dust raising. It was unlikely the spoil pile edge was packed by vehicle traffic. The seismic displacement during the blast could have caused the sloping edges of the spoil pile to "settle out" or subside. This would have caused the spoil pile to expand.

The fine particles which were entrained into the atmosphere as a result of the blast traveled down-wind, in a northerly direction, away from the spoil pile. In the video, the dust could appeared to dissipate slowly as it moved. It was suspected that the fine particles in this cloud were deposited onto the vegetation and ground.

It was likely that the surface displacement during the blast caused both direct physical changes to the vegetation and, after the blast, indirect physiological changes. Potential direct physical changes included uprooting and toppling trees, breaking branches and limbs, and leaf/needle loss. From a remote sensing perspective, these disturbances to the vegetation may have resulted in the exposure of more forest floor material.

Surface displacements could have also caused harm to the root systems of plants resulting in plant stress. Typically plant responses to stress include decreased relative turgidity, decreased leaf moisture content and nutrient supply. Prolonged stress can produce changes in certain plant pigment concentrations, such as chlorophyll, carotene, and xanthophylls. Most plant disturbances cause an increase in 0.4 - 0.7µm reflectance, and plant dehydration and decreased turgidity cause increased reflectance in the 0.5 to 2.5 region. These vegetal responses to stress created by the blast were therefore potential observables.

Although plant physiological responses to the blast event would have started at the time of the blast, it would have taken time for these effects to become prominent. This time period could be as long as it takes for a given plant to die. It was assumed no radiation from the blast affected the vegetation.

The surface effects of the blast may have been more prominent in areas more susceptible to seismic displacement. Geologic lineaments, for example, are often deposition zones of recently settled soil material and sometimes have sharp topographic slopes. Steep topographic slopes are subject to mass soil movements such as soil creep and landslide. Massive soil movements typically bury vegetation and expose bare soil. Dirt roads and other areas where the natural soil and plant material has been removed are sources of easily erodible material. Bodies of water can change configuration, and their waters serve as depositories for silt and debris.

Each of these phenomena were potential indicators of an underground detonation. These observables, however, were specific to BEXAR. Another test site with different vegetation and soil, and where the test site was prepared differently, may require an entirely different set of observables. Observables less dependent on specific environmental characteristics (such as the presence of well-defined geologic surface lineaments) have greater potential for universal applicability. The observables based on the spoil pile characteristics are not specific to any one type of environment but are

applicable to any test site prepared in a similar fashion to BEXAR. Covert underground testing might require different observables; particularly if the spoil material is transported away from the drill hole.

5.4   SUMMARIZED UTILITY OF VISUALLY-INTERPRETED ANALOG IMAGERY

As provided in the previous report sections, experienced imagery analysts interpreted the analog data and ascertained its overall utility for supporting the detection of underground testing. The most glaring deficiency noted was the lack of an up-to-date unclassified high spatial resolution imagery database. The PPDB, while satisfying the spatial resolution criteria, is not being updated and is becoming less useful, especially in urban areas. The criteria that it did satisfy was that of providing an excellent metric database from which accurate maps of the area of interest could be produced. The next viable sensor product was the Landsat TM imagery. With its large area coverage and the capability to update continuously its coverage every 16 days, it satisfied two of the necessary criteria for monitoring global issues. However, with its current spatial resolution of approximately 30 meters, the products could not be interpreted to produce definitive information on facility or test parameters. The strength of the TM was that it could record such activities as scarring and road building which accompany underground test activities. With continuous global coverage, the TM should be used to monitor areas designated as potential test sites, and to document major changes, such as road building, clearing or scarring. Although hardcopy imagery interpretation can be accomplished if digital exploitation means are not available, the seven-band spectral data that are collected digitally can be exploited more efficiently digitally, and the additional spectral information may compensate for much of the relatively poor spatial resolutions. The Seasat radar coverage pointed out that if there were a need to acquire data during poor weather or at night, these means could be used, if available, to support such requirements. However, the spatial resolutions were such that only gross changes in activity would be delineated. Since the preparations for testing can be observed for months, the need for immediate coverage assumes a low priority (except for alerting inspection or verification teams prior to detonation). The SPOT system products provided better spatial resolutions than either the Landsat TM or the Seasat data; however, each image covered only about 10% of a Landsat TM image, and acquires only three spectral bands vs. the seven Landsat TM bands. Its strengths lie in its capability to provide stereoscopic coverage of an area and to monitor an area from adjacent orbits. The maps that can be produced could provide accuracies in the vicinity of 10 meters as opposed to one meter from the PPDB. However, SPOT provides continuous global data so that recent changes can be recorded as areas of interest evolve. One other difficulty encountered with SPOT imagery is that the priorities for coverage and dissemination are at the discretion of a foreign country that may or may not wish to comply with a request or be a part of the verification apparatus. Visual interpretation of the MTL ASIS 63-band data in hardcopy was not an

efficient means to exploit the material. To view the large amount of data, it was necessary to use special digital tools and a display station. These techniques will be described in a later portion (7.4) of this report.

To utilize fully the products investigated, it was necessary to exploit the strengths of each product. As an example, to conduct global test detection and monitoring, the Landsat TM would best answer this requirement. Once a suspect site is detected, the PPDB data can provide a good historical and map base for further integration of other data. Should the PPDB data need to be metrically updated, then the SPOT system data can be used; provided that the imaging requirement would be honored by the country that sponsors the system. The capability for classified systems to support such requirements will be discussed in the classified Annex (2) of this report.

SECTION 6

6.0 HARDCOPY THREE-DIMENSIONAL ANALYSES

For the past several years, Autometric has been producing and installing their APPS-IV for military/intelligence community customers. The APPS-IV is an analytical plotter designed specifically for the generation of digital databases directly from stereo models of most types of imagery. It has been used primarily to support sensor tasking, targeting, and support to the Cruise Missile program. However, it also has the capability for database generation and mapping. Input to the APPS-IV includes hardcopy transparencies of the area of interest, the mathematical model of the collection sensor, and proprietary software. Output is in the form of three-dimensional viewing, and/or the production of thematic three-dimensional databases, including precise terrain contouring. A pen plotter produces the final product.

The decision was made to determine whether a generic analytical plotting device, represented by the APPS-IV, would provide unique and/or efficient capabilities to support the detection of underground tests. The initial task was to analyze the PPDB imagery covering the BEXAR test area. Using an in-house developed math model, the imagery was set up on the stages of the APPS-IV and viewed in "3-D" through its optics. Since the PPDB was developed for just such requirements, an excellent stereo image was perceived. Terrain mapping of the site could have been accomplished, but since this is a routine procedure and the PPDB collection was accomplished long before BEXAR was initiated, no formal map was produced. However, a comparison of the data was made with the digital three-dimensional data acquired from the SPOT sensor and displayed on a digital workstation. The loss in spatial resolution between the SPOT data and the PPDB was significant, and further research must be conducted on the utility of high-fidelity mapping to support the detection of underground testing. (Since the SPOT data were digital, losses in spatial resolution occurred when hardcopy renditions were generated). Accordingly, a decision was made to retain as much of the inherent SPOT spatial resolution

as possible by conducting subsequent three-dimensional studies on a digital display station (see Section 7.5).

SECTION 7
DIGITAL PROCESSING AND ANALYSIS

7.1   ARCHIVED MULTISENSOR DIGITAL IMAGERY PROCESSING

Historic multisensor analyses of BEXAR involved the review of both analog and digitally-processed analog data of NTS. The archived imagery was accessed to provide a linear history of the BEXAR site; the primary purpose being to determine what had occurred at the specific test site prior to BEXAR. It was believed initial changes could be tracked easily since BEXAR was in a relatively new part of the NTS range which had comparatively minimal previous use. This Section 7.1 discusses the processing of these data. The analysis of the resultant processed images is reported in Section 5.

As mentioned previously, two sources of archived aerial photography were obtained. These were USGS NHAP and DMA PPDB. Resultant vertical photos from these programs are highly accurate in terms of geometric and spatial fidelity, and because of this, they were considered the most appropriate source for creating the historical database. The obtained photographs are listed in Table 7.1-1.

To compliment these, a 1984 1:100,000 three-band Landsat TM analog print was also obtained.

As discussed in Section 5, upon receipt of these images, two analyses were initiated: (1) analog photographic interpretations and (2) digitally-processed analog interpretations. Each of the images, therefore, had to be converted to digital format. To accomplish this, the above-mentioned images were digitized using a 300 dot/inch Howtek Scanmaster linear scanner. The resultant analog-to-digital (A-to-D) conversions generated 8-bit digital data of the black and white images and 24-bit (8 bits in each additive red, green, and blue color record) of the color images. Subsequently, these data files were transferred to a PC-based image processing system (a Compaq 386/ERDAS 7.4 system) for further review. The resultant image examples are shown as a composite in Figure 7.1-1.

It was apparent in Figure 7.1-1 that due to the varying spatial resolutions and orientations of the original analog images, interpretations would be cognitively demanding. To address this, an additional step in the processing consisted of digitizing a 1978 1:100,000 USGS three-color topographic map for purposes of imagery rectification. The map, in turn, served as the geometric truth, and each archived image was rectified to fit the map. This allowed the georeferenced images to be compared more easily using image overlay and ratioing techniques.

Table 7.1-1
List of Photos

- one stereo pair of NHAP black and white paper photographs (98123 and 98124);
- one stereo pair of NHAP black and white transparent photographs (98123 and 98124);
- one stereo pair of NHAP color-infrared transparent photographs (149171 and 149172);
- one PPDB black and white paper photograph (027);
- one PPDB black and white transparent photograph (027);
- one PPDB black and white paper photograph (028);
- one PPDB black and white transparent photograph (028);
- one 1:100,000 USGS three-color map; and
- one 1:100,000 three-band Landsat Thematic Mapper paper print.
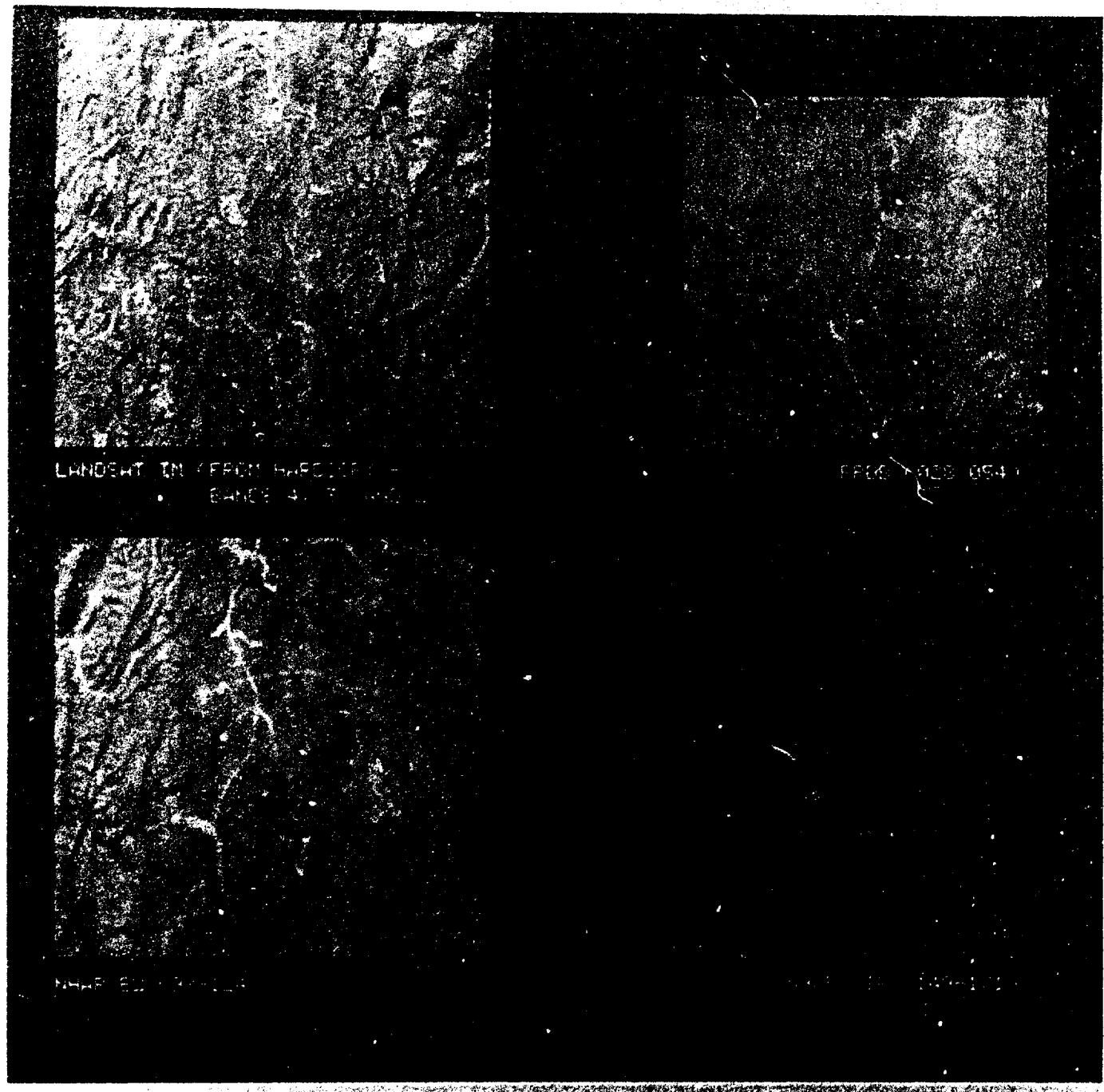
Figure 7.1-1
Composite of Digitized Archived Imagery

As a needed reference in both this section and in Section 7.4 (Hyperspectral Analyses) an overview of the specific rectification process is provided. Specifically, polynomial equations were used to convert source coordinates to rectified coordinates. This was accomplished using first- or second-order transformations computed with 19 ground control points (GCPs). A least squares regression method was used to calculate the transformation matrix from the 19 GCPs. Since the aerial photographs were vertical, or near vertical a linear transformation was chosen. As an example, the transformation matrix for a first-order transformation consisted of six coefficients (ERDAS 7.4 convention), three for each coordinate (X and Y), as follows:

$$
\begin{array}{ccc}
a1 & a2 & a3 \\
b1 & b2 & b3
\end{array}
$$

These were then used in a linear first-order polynomial as follows:

$$X_O = b1 + b2X_i + b3Y_i$$
$$Y_O = a1 + a2X_i + a3Y_i,$$

where:

$$
\begin{array}{lcl}
X_i \text{ and } Y_i & = & \text{source coordinates;} \\
X_O \text{ and } Y_O & = & \text{rectified coordinates; and} \\
a1 \text{ to } 3 \text{ and } b1 \text{ to } 3 & = & \text{coefficients of the transformation matrix.}
\end{array}
$$

When the transformation matrix was calculated, the inverse of the transformation matrix was used to retransform the reference coordinates of the GCPs back to the source coordinate system. A perfect fit for all GCPs, even using higher orders, would have been difficult to obtain; and therefore, some error was acceptable. The accompanying error was determined as a root mean square (RMS) error and was the distance of the input (source) location of a GCP and the transformed location for the same GCP. RMS error was calculated as follows:

$$RMS_{error} = (X_r-X_i)^2 + (Y_r-Y_i)^2,$$

where:

$$
\begin{array}{lcl}
X_i \text{ and } Y_i & = & \text{the input coordinates; and} \\
X_r \text{ and } Y_r & = & \text{the retransformed coordinates.}
\end{array}
$$

RMS$_{error}$ was expressed as a distance in the source coordinates system. An RMS$_{error}$ of two, for example, meant that the reference pixel was two pixels away from the retransformed pixel. Accordingly, for each of the BEXAR digitized images, the RMS$_{error}$ was set $\leq$ 1.0 pixels, and this level of accuracy was achieved for each of the image transformation processes.

The final step in the rectification process was to create the output file. Since the grids of pixels for the source images did not match the grid for the reference image, the pixels were resampled, and new data file values were calculated. These were calculated using a nearest neighbor technique.

To determine an output pixel's nearest neighbor, the rectified coordinates (X_o, Y_o) of the pixel were retransformed to the source coordinate system. This was done using the inverse of the transformation matrix. The pixel closest to the retransformed coordinates (X_r, Y_r) was the nearest neighbor, and the data file values for that pixel became the pixel values in the output image. The nearest neighbor method was used because, unlike bilinear interpolation and cubic convolution processes, it transferred original data values without averaging them, and the extremes and subtleties of the data were not lost.

The images originally shown in Figure 7.1-1 are depicted after rectifications in Figure 7.1-2. These images (and other rectified images not shown in Figure 7.1-2) represented the A-to-D portion of the historical database.

Another element of the archived database was the SPOT imagery. Two SPOT panchromatic scenes, resident at Autometric from another prior research project, were used. One was collected on 17 September 1988 and the other on 14 December 1989.

As background of its sensing capabilities for monitoring underground nuclear tests, a technical overview of SPOT is needed. Originally, SPOT was developed by the French National d'Etudes Spatiales and has a spatial resolution of 10 by 10m in the panchromatic collection mode (20 by 20m in the multispectral mode). The accompanying SPOT system parameters are given in Table 7.1-2

Table 7.1-2 SPOT Sensor Parameters

Characteristics of Sensors	Multispectral Mode	Panchromatic Mode
Spectral bands 1	0.50 - 0.59μm	0.51 - 0.73μm
2	0.61 - 0.68μm	
3	0.79 - 0.89μm	
Instrument IFOV*	4.13 degrees	4.13 degrees
Ground Sampling at nadir	20 x 20m	10 x 10m
Pixels/line	3000	6000
Ground swath width at nadir	60km	60km
Radiometric resolution	8 bits	8 bits
Image data bit rate	25 Mb/s	25 Mb/s

*Instantaneous Field of View (IFOV)
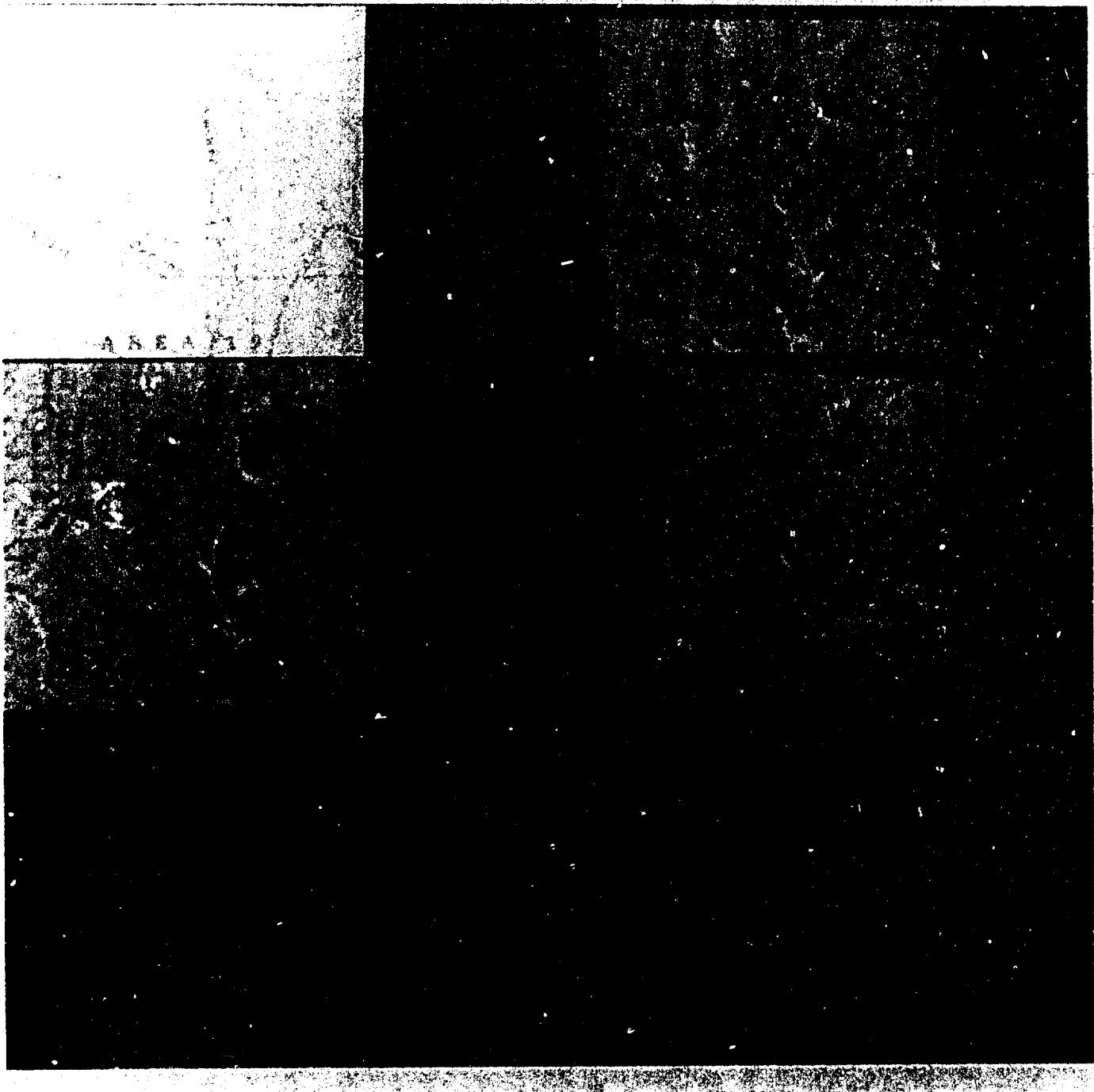
Figure 7.1-2
Composite of Rectified Archived Imagery

The SPOT sensing instruments may be pointed to cover adjacent fields each 60km. In this configuration the total swath width is 117km, and the two fields overlap by 3km. Since the distance between adjacent ground tracks at the equator is approximately 108km, complete earth coverage can be obtained using the fixed field-of-view. It is also possible to point the system off-nadir, and sense any region of interest within a 950km-wide strip centered on the ground track. The width of the swath actually observed varies between 60km for nadir viewing and 80km for extreme off-nadir viewing.

If the sensing devices are set at nadir-viewing only, the revisit frequency for any region of the world would be 26 days. This interval may cause problems for the monitoring of underground nuclear events. Taking into account the steering capability of the instruments, however, during the 26-day period separating two successive SPOT passes over a given point on the earth, a point in question could be observed on seven different passes if it were on the equator and on 11 occasions if at a latitude of 45 degrees.

The SPOT sensors may also acquire stereoscopic pairs of images, and this was the case for the 1988 and 1989 images used in this research. The ratio between the observation base (distance between the two satellite positions) and the height (satellite altitude) is approximately 0.75 at the equator and 0.50 at the latitude of 45 degrees. Stereoscopic imagery obtained using these base-height ratios is useful for a variety of photogrammetric applications such as cartographic work at scales of 1:100,000 and map updating at 1:50,000; and indeed, this capability allowed the generation of the digital elevation data for the BEXAR area (discussed in Section 7.5)

Since the 1988 and 1989 SPOT data of BEXAR were panchromatic and not multispectral, no statistical analyses were performed; rather discriminant visual interpretations were made from the two 10-meter images. This included the production of stereograms. Although because one SPOT scene was taken in September and the other in December, the relative brightness values from date-to-date were considerably different due to variant seasonal energy inputs (and, likely, atmospheric conditions). Accordingly, two sets of stereograms were generated for analysis: (1) the first where both images were unenhanced; and (2) the other where the September image was contrast stretched to 3STD and the brightness values of the December image were linearly remapped based on the spectral space of the September image. These two stereograms are shown in Figures 7.1-3 and 7.1-4, respectively.
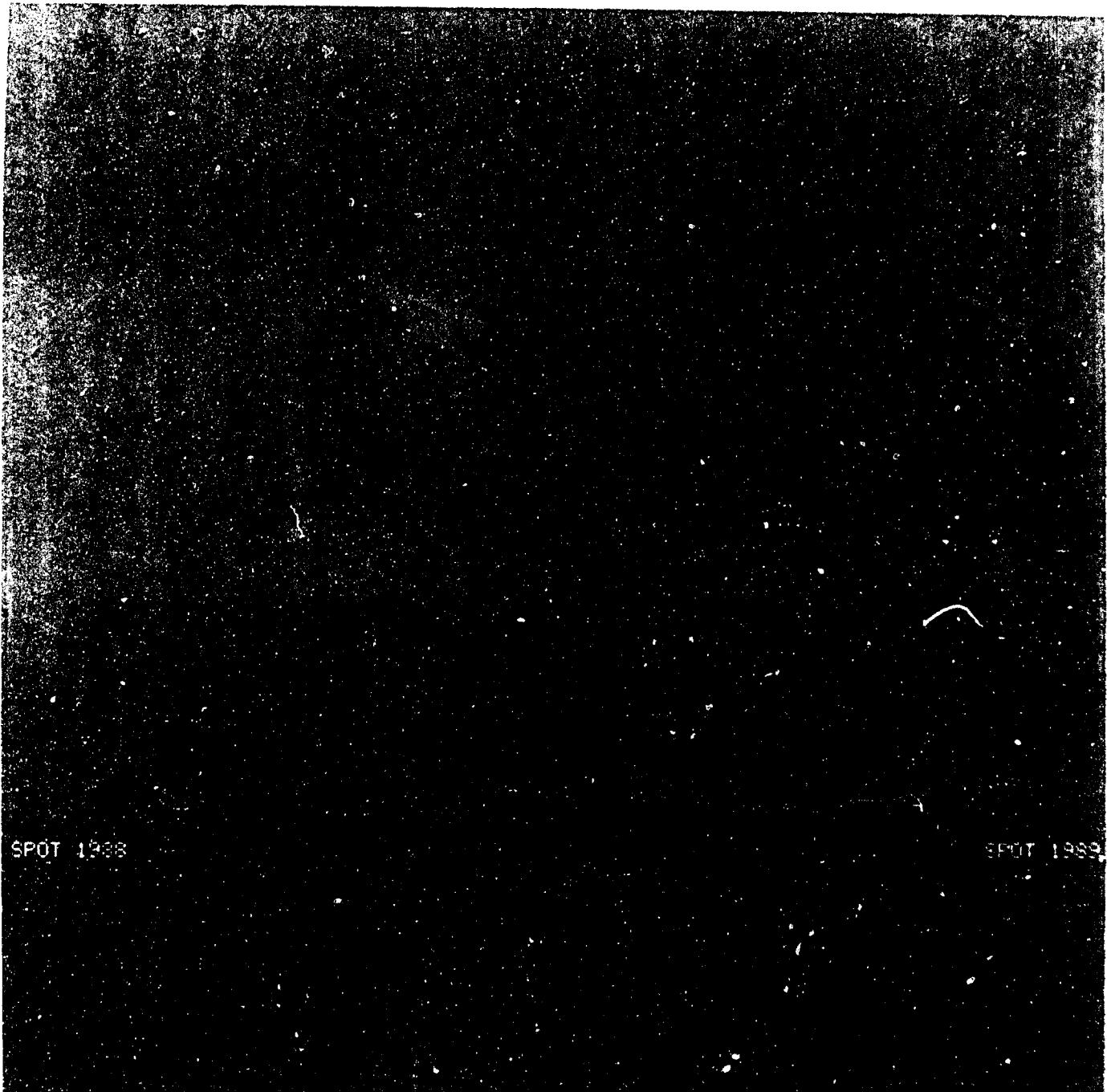
Figure 7.1-3
SPOT Stereogram (Unenhanced)
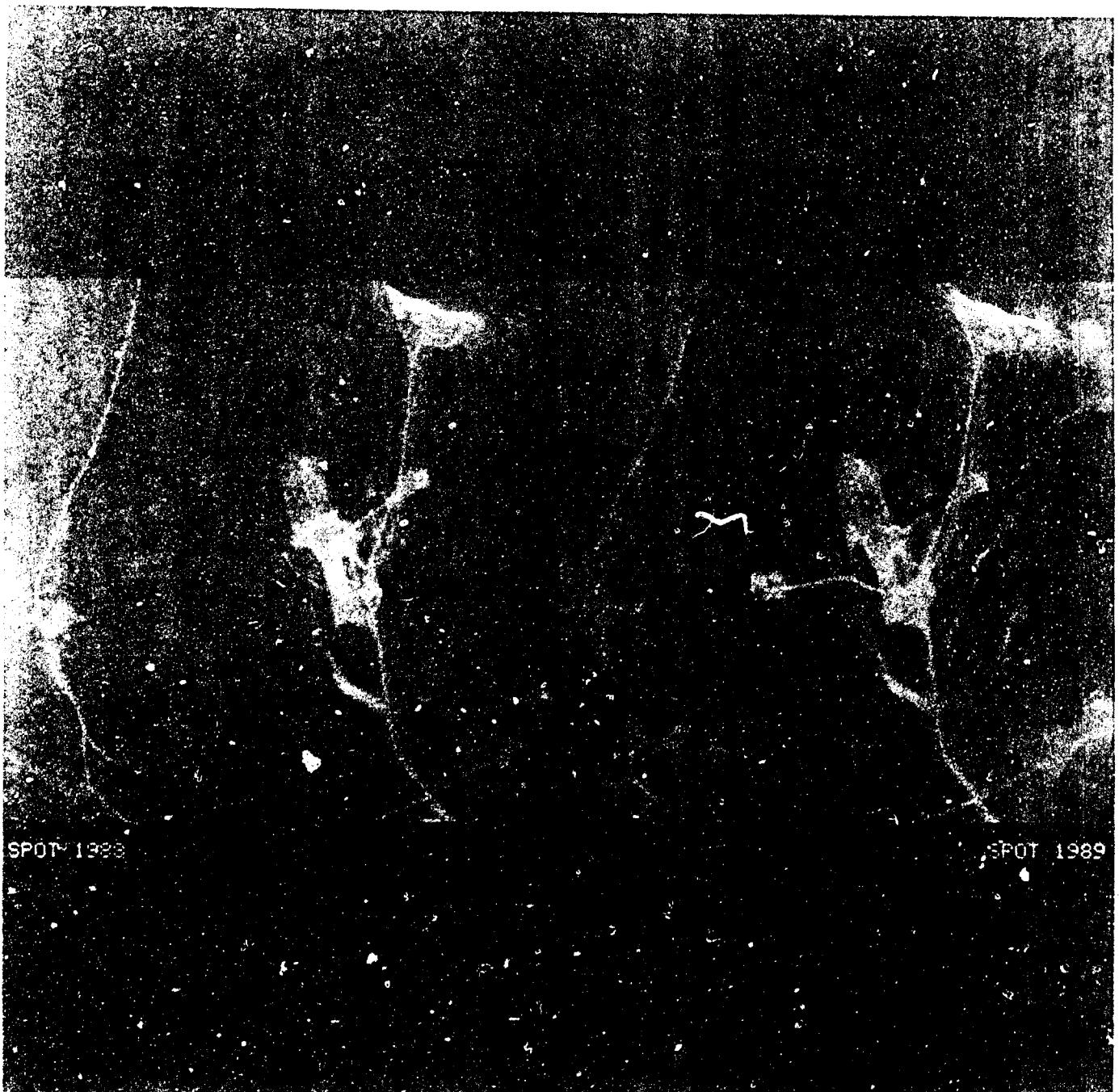
Figure 7.1-4
SPOT Stereogram (Enhanced)

With regard to the Landsat TM data, there were three data sources: (1) the aforementioned three-band analog TM print which was digitized and rectified to the 1:100,000 USGS map; (2) one seven-band digital scene collected before the BEXAR event on 7 March 1991; and (3) one seven-band digital scene collected after the event on 8 April 1991. While the three-band image was discussed earlier, the other two seven-band datasets represented the formal multispectral portion of the research, and as such, they are discussed in Section 7.2

The MTL ASIS was also used to collect data over the BEXAR site. Flown in an aircraft, four scenes were collected using the ASIS: three before the event and one after. With 63 bands, the ASIS data represented the hyperspectral component of the research. Accordingly, these data are discussed in Section 7.4

7.2   MULTISPECTRAL PROCESSING AND ANALYSES

7.2.1   General

For the multispectral aspect of the research, two seven-band Landsat TM datasets were obtained (an archived three-band hardcopy print was used in Sections 5 and 7.1 but was not used here). The BEXAR event took place on 4 April 1991; therefore, the goal was to determine if changes due to the BEXAR event could be detected in the pre- and post-event TM imagery. All analyses in this Section are whole-pixel techniques. Subpixel analyses, being a frequency domain modeling process, are discussed in Section 7.3.

Before discussing the digital analyses of TM imagery, a background of the Landsat V system and its TM imaging capabilities for monitoring underground nuclear events is warranted.

The TM sensor on Landsat V was launched on 1 March 1984. The TM bands were chosen after years of analysis for their value in the discrimination of vegetation type and vigor, plant and soil moisture measurements, differentiation of clouds and snow, and identification of hydrothermal alterations in rock types. TM data have a ground-projected instantaneous-field-of-view (IFOV) of 30 by 30m (the thermal-infrared band has a spatial resolution of 120 by 120m). System parameter information is provided in Table 7.2-1.

Table 7.2-1 Landsat V Thematic Mapper (TM) System Parameters

Spectral bands	1	0.45 - 0.52μm
	2	0.52 - 0.60μm
	3	0.63 - 0.69μm
	4	0.76 - 0.90μm
	5	1.55 - 1.75μm
	6	10.40 - 12.50μm
	7	2.08 - 2.35μm
IFOV		30 x 30m for bands 1-5 and 7; 120 x 120 m for Band 7
Data rate		85 Mb/s
Pixel quantization		8 bits
Altitude		705km

Landsat V (and IV) sun angles, higher than those of Landsat I, II, and III, reduce the amount of shadow in the imagery. This has proven useful for a variety of study applications because shadows drastically modify spectral signatures of phenomena. The equatorial crossing time unfortunately

increases the probability that cloud cover will be present over a given study area. At an orbit of 705km (approximately the same as the Space Shuttle's orbit) repetitive coverage takes 16 days.

In Section 5.3, several key spectral observables were discussed. These included changes to the spoil material at the immediate BEXAR site (i.e., a series of small surface fractures, corresponding shadowing, particulate soil redistributions, and particulate weathering), and vegetative-related conditions from the BEXAR site and surrounding areas. The question at this point of the research was: once the atmospheric and natural changes resident in the TM datasets were removed, could the event-related changes be detected using the date-to-date imagery sets? Thus, before investigating these changes, the changes unrelated to the event had to be analyzed and removed as much as possible.

Most non-event changes in the imagery were generated by differing energy input quantities and associated vegetative cyclical states. Indeed, during the first TM scene collected on 7 March 1991, the solar elevation angle was 37 degrees. and the solar azimuth angle was 136 degrees. Comparatively, during the second collection on 8 April, the solar elevation angle was 48 degrees and the solar azimuth was 129 degrees. There are a variety of methods for removing the impacts of variant energy and cyclical states; and to enable accurate date-to-date change detections, some appropriate method must be considered. Two methods were used to achieve this; one by Autometric, and the other by the contract subcontractor Applied Analysis, Inc. (AAI). Because the validities of the pending analytical sections are dependent on the methods of atmospheric removal employed, these two methods and their accompanying rationales are presented separately in the following sections.

7.2.2   Autometric Atmospheric Corrections

Because the solar elevation angle of the post-event TM image was 11 degrees higher than the pre-event, more input energy was reaching the BEXAR test site on the second collection day. With this increased energy, the BEXAR site and surrounding areas reflected this higher level back to the sensor, and accordingly, BEXAR had a higher relative reflectivity during the second collection. To test for spectral changes related to the event, then, the energy input levels for the post-event collections had to be modeled and scaled to match more accurately the energy input levels of the pre-event collections.

The primary difficulty in determining valid and reliable values of atmospheric parameters such as irradiance and spectral radiance is in accounting for the electromagnetic energy scattered more than once as it passes through the atmosphere. Generally, though, electromagnetic energy reaching the ground is comprised of two components. The first is direct electromagnetic energy (from the sun) which passes through the atmosphere without being absorbed or scattered. The second is atmospheric, or diffuse, electromagnetic energy which has been scattered at least once. The total spectral irradiance on a given surface of the ground is the sum of the irradiances of the direct electromagnetic energy and of

diffuse electromagnetic energy. The spectral irradiance of direct energy can be estimated by the zenith angles of the sun, associated optical path lengths, and monochromatic solar constants. The reflectance of a surface, then, is the ratio of the upward to downward fluxes of radiant energy at the surface. Impacts from these energies combine with spectral compositions of terrestrial phenomena to define the image histogram.

The first step in removing the effects of the two-date imagery involved a review of the respective image statistics. To do this, subscenes centered over the BEXAR test site were extracted for each date, and initial statistics were generated. These are provided in Table 7.2.1-1. As shown, there were considerable differences found in the date-to-date comparisons. From the statistics, it was apparent some changes in the imagery were associated with a combined effect of increased energy inputs and, likely, vegetative cyclical states. For instance, the difference among means for Band 5 (34) suggested there were increased turgidity levels in the area plants. Indeed, this was probably the result of plants absorbing water from recent snow melts (from a mid-March 1991 snow storm). The increases in Bands 2, 3, and 4, however, suggested the plants, although possibly having absorbed the water, have not increased their chlorophyll absorption levels appreciatively. This could have been due to the following: 1) the vegetation of the area was evergreen, and its natural cyclical chlorophyll absorption levels may not have changed considerably within the time-frame of the two imaging dates; 2) the vegetation, having adopted to the harsh desert environment, maintained a relatively constant level of chlorophyll absorption throughout the period; and/or 3) the vegetation had not utilized the absorbed water completely because night-time temperatures in early April remained too cold, and this prevented the vegetation from entering its natural seasonal growth patterns.

In comparison to apparent vegetative changes, however, Band 7 suggested that a substantial amount of the spectral reflectance increase was nonetheless due to the fact that more energy was reaching the BEXAR test site.

To remove the non-event changes from the post-event TM imagery a series of histogram remapping models were employed. Specifically, the histograms from the post-event data were expanded so the lowest occurring value became 0, and then the histogram was linearly scaled so the maximum value became 255. Thus, this histogram expansion process took advantage of the full 8-bit data range. Associated shift and scale factors were then calculated based on the composition of the pre-event and expanded post-event data. For instance, given a calculated shift factor of seven and a calculated scale factor of 0.68, a post-event pixel's brightness value (X1) would be re-mapped using the equation $X1' = X1 * 0.68 + 7$. The process removes considerably the direct impacts of increased energy inputs as well as radiance and shadowing impacts. Original pre-event, original post-event, and corrected post-event statistics are provided in Table 7.2.1-2, and an associated unenhanced image subset for each of the corresponding bands is shown in Figure 7.2.1-1.

Table 7.2.1-1
Image Statistics for Thematic Mapper (TM) Subscenes

Pre-Event Image Statistics

	Band 1	Band 2	Band 3	Band 4	Band 5	Band 7
MIN	59	24	28	30	39	22
MAX	143	78	121	107	177	106
MEAN	77.21	36.57	51.13	53.45	86.41	49.5
STD	12.16	8.11	14.83	10.32	20.76	12.65
MED	74	34	47	51	82	47
MODE	69	31	43	40	75	43

Post-Event Image Statistics

	Band 1	Band 2	Band 3	Band 4	Band 5	Band 7
MIN	78	35	45	49	72	41
MAX	175	94	147	129	218	139
MEAN	99.32	48.63	69.89	70.45	120.8	72.88
STD	13.82	9.27	17.06	11.70	22.81	14.41
MED	95	46	65	68	117	71
MODE	90	43	60	66	116	66

Table 7.2.1-2
Image Statistics for Thematic Mapper (TM) Subscene

Pre-Event Image Statistics

	Band 1	Band 2	Band 3	Band 4	Band 5	Band 7
MIN	59	24	28	30	39	22
MAX	143	78	121	107	177	106
MEAN	77.21	36.57	51.13	53.45	86.41	49.5
STD	12.16	8.11	14.83	10.32	20.76	12.65
MED	74	34	47	51	82	47
MODE	69	31	43	40	75	43

Post-Event Image Statistics

	Band 1	Band 2	Band 3	Band 4	Band 5	Band 7
MIN	78	35	45	49	72	41
MAX	175	94	147	129	218	139
MEAN	99.32	48.63	69.89	70.45	120.80	72.88
STD	13.82	9.27	17.06	11.70	22.81	14.41
MED	95	46	65	68	117	71
MODE	90	43	60	66	116	66

Autometric Corrected Post-Event Image Statistics

|	Band 1	Band 2	Band 3	Band 4	Band 5	Band 7
MIN	68	31	40	47	67	38
MAX	123	66	105	93	156	96
MEAN	79.23	37.78	53.21	54.94	90.14	51.90
STD	11.46	7.62	13.99	9.34	18.54	11.42
MED	76	36	49	52	54	49
MODE	69	31	44.29	49	83	42
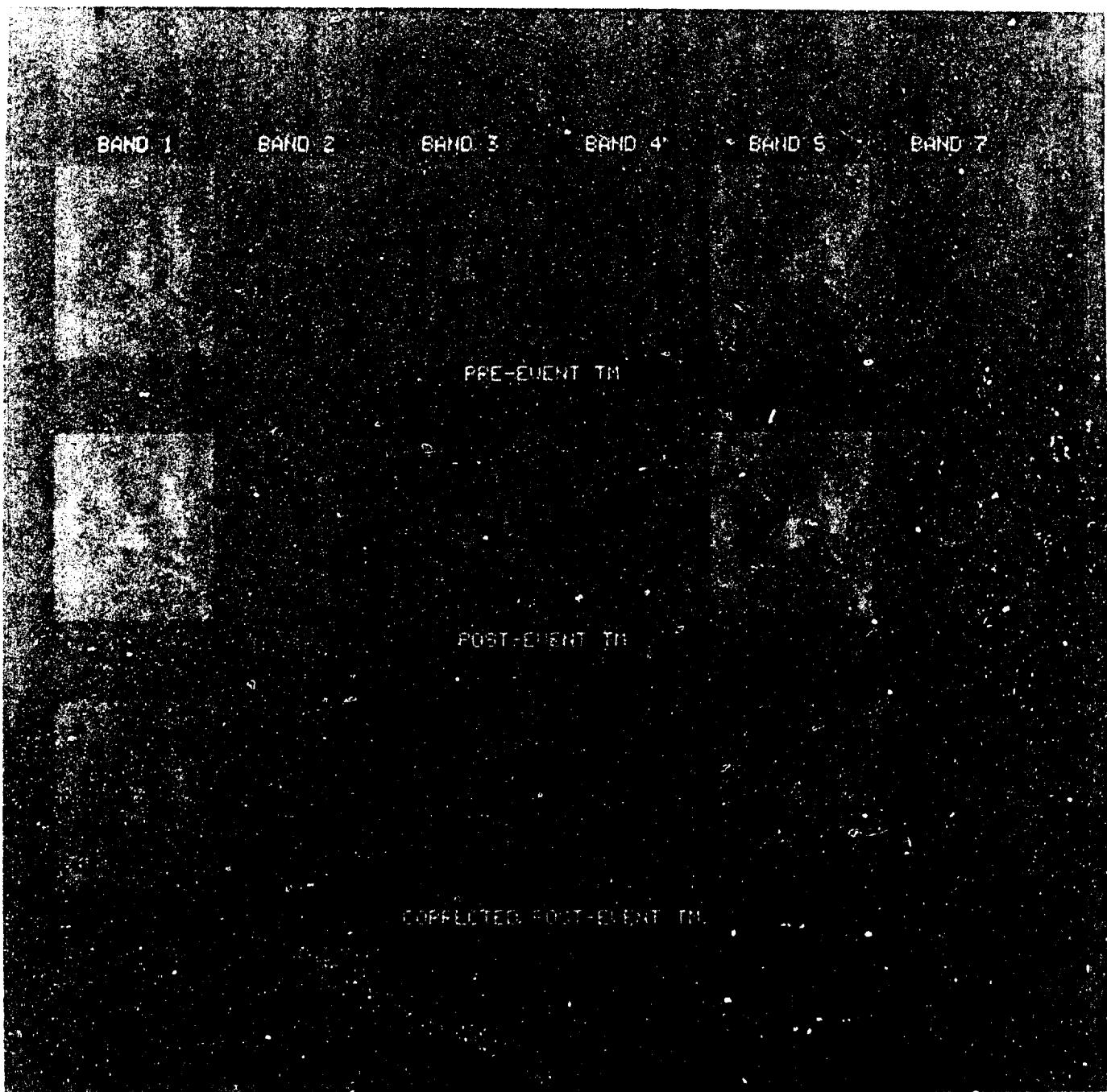
Figure 7.2.1-1
Pre-, Post-, and Post-Event Corrected Landsat Thematic Mapper (TM) Imagery

7.2.3 AAI Atmospheric Corrections

As a subcontractor, AAI was part of the research team. Their primary goal was to implement multispectral subpixel processing techniques for detecting event-related changes. This process is discussed in more detail in Section 7.3. The ultimate subpixel research, however, was built upon multispectral and hyperspectral portions of the research, and components of these were performed both in conjunction with and independently from the Autometric laboratory processings. Accordingly, AAI has developed an atmospheric correction modeling technique within the domain of their AASAP[*]. As the foundation for subsequent complementary AAI subpixel, multispectral, and hyperspectral sections, their method of correcting for the date-to-date collection variations is presented here.

As indicated previously, several multispectral changes were produced by the changes in the solar elevation and azimuth angles between the pre- and post-event scenes. Again, the TM scenes were used for this study were measured on 7 March 1991 and 8 April 1991, and the solar elevation angle increased from 37 degrees (pre-event) to 48 degrees (post-event). Similarly, the solar azimuth angle changed from 136 degrees to 129 degrees.

Among the effects that resulted from change in the solar elevation angle was a change in the relative contribution of radiance from the terrain and atmosphere. Indeed, the incident irradiance was less attenuated by path absorption and scattering in the 8 April scene because solar radiance traversed a shorter path through the atmosphere. Reflected radiances from the terrain and the atmospheric column above the terrain were consequently larger in the post-event scene. The contribution from the terrain increased more than that from the atmosphere, however, due primarily to two effects. First, the fraction of incident solar irradiance scattered from the terrain in the direction of the sensor was controlled in part by the bidirectional reflectance distribution functions of the surface materials, which had different sun angle dependence than that scattered by the atmosphere. For diffusely scattering materials lying horizontally on the surface (and for a nadir viewing sensor), the fraction of radiance scattered from the terrain toward the sensor increased in proportion to the change in the cosine of the solar zenith angle. Second, there was an increase in the fraction of directly illuminated (vs. shadowed) terrain with increase in sun angle. The latter effect had a more complex angular dependence, but in general, was a smaller effect than the former. The estimated combined effect produced about a 35% increase in terrain radiance from 7 March to 8 April, based on radiation transfer model calculations using the AASAP. In contrast, the contribution from the atmospheric radiance increased by a significantly smaller amount due to its strongly forward-scattering character. The increase in scattering was wavelength dependent, but it was in general less than about 14%, based on LOWTRAN 7 model calculations. The spectral characteristics of the terrain and the atmospheric radiance contributions differed significantly, and the

---

[*] AASAP is proprietary to AAI, Inc.

fact that the relative contributions of the two sources changed from 7 March to 8 April implied that some spectral change between the two scenes was attributed to event-unrelated effect.

A second event-unrelated spectral change was attributed to changes in spectral characteristics of the terrain radiance, due to changes in the extent of shadowing from 7 March to 8 April. The sunlit fraction of the surface was illuminated by both directly transmitted solar irradiance and diffuse hemispherical sky radiance, while the shadowed fraction was illuminated by hemispherical sky radiance alone. The sunlit fraction was thus not only brighter, but it had different spectral characteristics than the shadowed fraction due to the differences in spectral characteristics of the two illumination scenarios. The increase in solar elevation angle from 7 March to 8 April decreased the fraction of the visible surface that was in shadow, yielding a change in the effect source illumination spectral characteristics. This would have produced a change in terrain radiance spectral characteristics, even if the reflectance spectra of the terrain material had stayed the same.

Both of these effects, namely the change in relative contribution of terrain and atmospheric radiance and the change in extent of shadowing, were modeled by AASAP using radiative transfer approaches. Their contributions to the observed change were consequently identified and potentially isolated from other changes in the scene.

Other natural changes unrelated to the event were not so easily modeled. These included changes in the density and growth stage of vegetation, changes in sky radiance characteristics due to differences in haze and cloud conditions, changed produced by rain and other weather-related events that may have occurred between scenes, and changes produced by human activity, among others. AASAP included a series of atmospheric and sun angle corrections as enabling components of its scene-to-scene robustness feature. Using header and relevant elevation formation, corrections were generated that attempted to compensate for differences between scenes of: 1) atmospherically scattered solar radiance; 2) atmospheric path attenuation of directly transmitted solar irradiance; 3) diffusely-scattered hemispherical sky radiance; and 4) fractions of directly illuminated vs. shadowed surface. AASAP attempted to bring scenes into environmental equivalence to a reference scene, which was used to derive the signature of a material of interest. For this research, the pre-event (7 March 1991) scene was considered as a reference scene and the post-event (8 April 1991) was brought into environmental equivalence with the reference scene using correction factors generated by AASAP.

The first environmental correction applied was subtraction of AASAP-generated atmospheric radiance components from both scenes. The corrections are listed in Table 7.2.2-1. They were applied by subtracting the listed image plane data number from each pixel in the corresponding scene image plane.

A second environmental correction factor was applied to the post-event scene and attempted to compensate for differences in atmospheric path attenuation, diffusely scattered hemispherical sky

radiance, and shadowing. The AASAP-generated correction is shown in Table 7.2.2-2 and it was applied multiplicatively to the image plane pixel data numbers after subtraction of the Table 7.2.2-1 correction.

Application of the corrections in Tables 7.2.2-1 and 7.2.2-2 brought the 8 April 1991 scene into approximate environmental equivalence to the 7 March 1991 scene. Local scale differences caused by terrain slope, macroscale shadowing, and topographic elevation were not compensated for by these corrections. Differences in atmospheric haze profiles were also not compensated. To compensate partially for these effects, pixels were selected from the pre- and post-event scenes judged to have equivalent terrain slope, minimized macroscale shadowing, and topographic elevation. Selected pixels also avoided vegetated areas to minimize differences caused by variations in vegetation density, growth cycles, and species diversity. Reference pixels were selected from areas judged not likely to be changed by the detonation event to develop a compensation for the differences in atmospheric haze profiles, and other inaccurately compensated environmental factors.

Table 7.2.2-1
Atmospheric Radiance Component
(Image Plane Data Number)

Thematic Mapper Image Plane	7 March 1991 Correction (DN)	8 April 1991 Correction (DN)
1	47	53
2	15	17
3	11	12
4	5	5
5	1	1
7	1	1

Table 7.2.2-2
Sun Angle Corrections
(Unitless Multiplication Factor)

Thematic Mapper Image Plane	7 March 1991 Correction Factor	8 April 1991 Correction Factor
1	—	.8165
2	—	.8125
3	—	.8166
4	—	.8212
5	—	.8198
7	—	.8166

In Table 7.2.2-3 are presented two sets of four pixels each, selected from identical areas (within the accuracy of scene registration) in the pre- and post-event scenes. These were judged to be far enough away from the detonation site so as to be likely unaffected by the detonation. The two sets of pixels were corrected using the factors in Tables 7.2.2-1 and 7.2.2-2. The two sets of corrected pixels were then averaged to create mean reference pixels for the pre- and post-event scenes. The pre-event scene reference pixel was then divided by the post-event scene reference pixel (image plane data number by image plane data number) to derive the haze correction multiplier shown in Table 7.2.2-4. The correction suggested there was a higher atmospheric haze content in the 8 April 1991 post-event scene; although it is uncertain where in the profile the higher haze content occurred. The haze correction factor was applied multiplicatively to the post-event scene.

After all corrections were applied to the post-event data, subscene image statistics were generated for the corrected six TM bands. These are shown in Table 7.2.2-5 together with original pre-event subscene statistics.

Table 7.2.2-3
Reference Pixels

Thematic Mapper Image Plane	7 March 1991 Reference Pixels				8 April 1991 Reference Pixels			
1	114	110	116	120	137	134	139	139
2	64	60	64	67	76	76	73	77
3	100	96	103	108	122	123	126	126
4	91	86	92	98	111	109	113	115
5	155	147	159	167	192	185	194	198
7	98	89	97	99	120	116	116	119

Table 7.2.2-4
Haze Correction

Thematic Mapper Image Plane	7 March 1991 Mean Reference	8 April 1991 Mean Reference	Haze Correction Multiplier
1	68	66	1.03
2	49	49	1.00
3	91	92	.99
4	87	88	.99
5	156	157	.99
7	95	95	1.00

Table 7.2.2-5
Image Statistics for Thematic Mapper (TM) Subscene

Pre-Event Image Statistics

	Band 1	Band 2	Band 3	Band 4	Band 5	Band 7
MIN	59	24	28	30	39	22
MAX	143	78	121	107	177	106
MEAN	77.21	36.57	51.13	53.45	86.41	49.50
STD	12.16	8.11	14.83	10.32	20.76	12.65

Post-Event Image Statistics

	Band 1	Band 2	Band 3	Band 4	Band 5	Band 7
MIN	78	35	45	49	72	41
MAX	175	94	147	129	218	139
MEAN	99.32	48.63	69.89	70.45	120.80	72.88
STD	13.82	9.27	17.06	11.70	22.81	14.41

AAI-Corrected Post-Event Statistics

	Band 1	Band 2	Band 3	Band 4	Band 5	Band 7
MIN	21	14	26	34	58	31
MAX	97	62	109	100	184	110
MEAN	37.25	25.37	45.94	51.72	97.38	57.08
STD	10.59	7.41	13.94	9.72	19.03	11.92

7.2.4   Autometric Multispectral Analyses

Radiometric resolution defines the sensitivity of a detector to differences in signal strength as it records the radiant flux reflected (or emitted) from the terrain. Radiant flux recorded by the TM sensor records data in 8 bits (0 to 255). Using this range, the overwhelming majority of digital image analyses are dependent primarily on the resulting multispectral tones/colors of objects. Usually, these are accomplished using fundamental statistical pattern recognition techniques. Generally, automated devices cannot reliably process elements such as shape, texture, and pattern, let alone the more complex elements of site and association; although advances are being made.

Given a perspective of digital image processing, the goal of the multispectral portion of the research was to utilize the 8-bit radiometric resolution of the pre-event and corrected post-event TM datasets and generate models to detect event-related changes.

The selection of appropriate change detection models was based on several factors. First, the physical characteristics of the study area and type of potential change had to be considered. For instance, in some other unrelated area where change has been dramatic and multitopical, image differencing or ratioing techniques would reveal and help quantify subject classifications (e.g., a topical change from water to land). Any change at BEXAR, however, would not have been such a contrast or multitopical change, and it would have been difficult to differentiate the significance of such slight changes in the arithmetic images. Second, the data to be compared must be registered to a defined registration precision range. Indeed, because of Landsat's predictable orbit, the two TM images were registered to less than 1.0 pixel by determining X and Y tape read parameters; in turn, no directional and/or scale rectifications were needed. Finally, knowledge of the amount of change must be considered on a unitopical basis (e.g., did the chlorophyll absorption level of a given tree change from one date to another?). If a unitopical change had been great enough, a vector change analysis in multidimensional spectral space would have been appropriate. The change af BEXAR, however, was likely not great enough to be detected using this method.

Based on these considerations, the most appropriate models seemed to be those based on investigations of spectral variance. Since these variations from date-to-date would be slight, statistical confidence levels were needed to support any modeling. Three techniques were used to investigate variability and spectral change of BEXAR: 1) a series of comparisons of band pair means (i.e., Band 1 pre- vs. Band 1 corrected post-event, Band 2 pre- vs. Band 2 corrected post-event, etc.) to determine if differences between bands were statistically significant; 2) a one-way analysis of variance (ANOVA) to evaluate differences between all pre- and corrected post-event TM bands; and 3) a posteriori Tukey Honestly Significant Difference (HSD) test to establish a difference matrix for all band means.

On a band-by-band basis (excluding thermal) spectral change observables can be estimated. For instance, Band 1 (0.45 - 0.52 μm (blue)) provided information on water, soil, and vegetation

characteristics. The upper wavelength cutoff was the limit of blue chlorophyll absorption for healthy vegetation. Band 2 (0.52 - 0.60 μm (green)) spanned the region between blue and red chlorophyll absorption and corresponded to green reflectance of healthy vegetation. Band 2 also provided information about water. Band 3 (0.63 - 0.69 μm (red)) was sensitive to the red chlorophyll absorption of healthy vegetation and represented one of the most important bands for vegetation analysis. It also provided soil and geologic boundary information. The 0.69 μm cutoff was significant because it represented the beginning of a spectral range from 0.68 to 0.75 μm where vegetation reflectance crossovers occur. Generally, this range reduces the accuracy of vegetative investigations. Band 4 (0.76 - 0.90 mm (reflected-infrared) was useful for vegetative interpretations as well as soil-vegetation contrasts. Band 5 (1.55 - 1.75 μm (reflected mid-infrared) detected turgidity or the amount of water in vegetation. This was significant for BEXAR because it indicated plant vigor levels. Band 5 also provided geologic typology. Finally, Band 7 (2.08 - 2.35 μm (reflected mid-infrared)), which along with Band 5, had considerable utility for the BEXAR analysis. Band 7 was the best TM band for discriminating geologic changes.

Understanding the utility of each band, statistical models were applied accordingly. The first model involved the testing of band pre- to band corrected post-event pair spectral means, $\overline{X}_{1_{pre}}$ vs. $\overline{X}_{1_{cp}}$ respectively. In all, six band-to-band comparisons (HO: $\mu_{1_{pre}} = \mu_{1_{cp}}$;H1: $\mu_{1_{pre}} \neq \mu_{1_{cp}}$) were made (i = 1 to 5, and 7) using the equation below:

$$\sigma_{\overline{x}_{1_{pre}} - \overline{x}_{1_{cp}}} = \sqrt{\frac{\sigma_{1_{pre}}^2}{n_{1_{pre}}} + \frac{\sigma_{1_{cp}}^2}{n_{1_{cp}}}},$$

where:

$\sigma_{\overline{x}_{1_{pre}} - \overline{x}_{1_{cp}}}$ = standard deviation of the variance $\overline{X}_{1_{pre}} - \overline{X}_{1_{cp}}$;

$\sigma_{\overline{x}_{1_{pre}}}$ and $\sigma_{\overline{x}_{1_{cp}}}$ = standard deviations of band$_{1_{pre}}$ and band$_{1_{cp}}$;

and

$n_{1_{pre}}$ and $n_{1_{cp}}$ = number of observations for bands$_{1_{pre}}$ and$_{1_{cp}}$.

A critical region based on equal tail areas under a normal curve $\overline{X}_{1_{pre}} - \overline{X}_{1_{cp}}$ was chosen for which α = 0.05. With α = 0.05, then, the test of statistical significance was determined based on $1.96 \cdot \sigma_{\overline{x}_{1_{pre}} - \overline{x}_{1_{cp}}}$ = CV$_1$. If $|\overline{X}_{1_{pre}} - \overline{X}_{1_{cp}}|$ was greater than CV$_1$, HO: $\mu_{1_{pre}} = \mu_{1_{cp}}$ was rejected and H1: $\mu_{1_{pre}} \neq \mu_{1_{cp}}$ was accepted. The differences of the spectral means for the corresponding bands, therefore, would be considered statistically significant. The band-by-band results are shown in Table 7.2.3-1.

The results in Table 7.2.3-1 indicated that in each case, the means of the band pairings were significantly different. In each case, some type of spectral change was detected using a 95% confidence level. Although this testing procedure suggested that some change was apparent, the amount of relative change could not be quantified using this method. Other than providing an initial overview of the band comparisons, a comparison of means by itself is not considered statistically rigorous. The spectral comparisons did, however, indicate that further statistical modeling was warranted.

The next model used built upon the findings of the first. Specifically, this second model enabled analysis of the band spectral variance measures using an ANOVA (analysis of variance). In the one-way ANOVA model, the variances of the datasets were used to determine if the spectral means as a group were statistically different. This allowed an assessment of the group differences of the pre- and corrected post-event datasets conjunctively. Such an assessment was important because vegetative and geologic phenomena, as described earlier, are generally sensed by several of the TM bands, and band signature topical overlap needed to be addressed for the BEXAR data.

Table 7.2.3-1
Results of Testing the Differences of Band-to-Band Pair Means
($\alpha = 0.05$, n = 6675)

Bands$_j$	CV$_i$	$\overline{X}_{i_{pre}} - \overline{X}_{i_{cp}}$	Status
1$_{pre}$ vs. 1$_{cp}$	0.39	2.01	Reject H0:; Accept H1:
2$_{pre}$ vs. 2$_{cp}$	0.27	1.21	Reject H0:; Accept H1:
3$_{pre}$ vs. 3$_{cp}$	0.49	2.07	Reject H0:; Accept H1:
4$_{pre}$ vs. 4$_{cp}$	0.33	1.39	Reject H0:; Accept H1:
5$_{pre}$ vs. 5$_{cp}$	0.67	3.74	Reject H0:; Accept H1:
7$_{pre}$ vs. 7$_{cp}$	0.41	2.40	Reject H0:; Accept H1:

In all, 12 spectral means were compared using the hypotheses where H0: $\mu_{1_{pm}} = \mu_{2_{pm}} = ... = \mu_{7_{cp}}$; and H1: $\mu_{1_{pm}} \neq \mu_{2_{pm}} \neq ... \neq \mu_{7_{cp}}$. The results from the ANOVA are given in Table 7.2.3-2.

As indicated in Table 7.2.3-2, the one-way ANOVA yielded an $F_{(11,80088)}$ of 11.04. From the analysis of variance it was inferred that the band means, as a group, differed ($p<0.01$). The accompanying statistical power was estimated to be above 0.99 ($\bullet 0.01$). Similarly, an Fmax test for homogeneity of variance was passed at $p<0.05$.

The ANOVA findings complimented the initial means testing results. The F of 11.04 was well above the indexed F of 2.25; and H0 was rejected, and H1 was accepted. This suggested that there were statistically significant spectral differences associated with the TM BEXAR data. The most compelling aspect of the ANOVA, however, was the high level of statistical power.

By itself, testing for group spectral means did not provide the ultimate solution for determining the amount and type of change. The components of the ANOVA, though, were the foundation for the final model. This last model was accessed to investigate variant signatures on a band-by-band matrices level. This included: individual band pre- to band pre-event differences; individual band pre- to band corrected post-event differences; and individual band corrected post- to band corrected post-event differences.

Table 7.2.3-2
One-Way ANOVA Table

Source	Sum of Squares (SS)	Degrees of Freedom	Mean Square (MS)	F-Ratio
Between	25356068	11	2305.15	11.04*
Within (Error)	16720000	80088	208.77	
Total	47075129	80099		

*$p<0.01$

The examination of spectral differences was accomplished using a posteriori Tukey (HSD) test. The accompanying $\hat{\psi}$ (HSD) critical value was determined using the following equation:

$$\hat{\psi} \text{ (ESD)} = q_{\alpha=0.01;p,v} \cdot \sqrt{MS_E / n} .$$

where:

$q_{\alpha=0.01;p,v}$ = an indexed value based on a studentized range where $\alpha = 0.01$, p = the number of means, and v = degrees of freedom within groups (from ANOVA table);

MS_E = mean square error (from ANOVA table); and

n = number of observations.

With the BEXAR data, $\hat{\psi}$ (HSD) = 0.93, $p<0.01$. This value was then used to evaluate the table of absolute differences among means for the 12 bands of data (Table 7.2.3-3).

As shown in Table 7.2.3-3, all but two differences were significant. As was found in the initial comparison of means, the $band_i$ pre- and $band_i$ corrected post-event differences were once again statistically significant. The greatest differences among band pairings were found in Bands 5 (3.74) and Bands 7 (2.40). Bands 1 (2.01) and Bands 3 (2.07) were also statistically different, but these were less than Bands 5 and 7. Bands 2 (1.21) and Bands 4 (1.38) were significant, but these were only slightly above the $\hat{\psi}$ (HSD) of 0.93. These findings indicated that there were relative vegetative changes from date-to-date; but the increases of reflectivity, based on Bands 1 to 4 comparisons, indicated that the changes were the result of normal cyclical growing patterns. Apparently the BEXAR events, at least as of 8 April 1991, did not damage or alter the normally-increasing Spring chlorophyll absorption pattern of the plants. Indeed, the increased turgidity, as shown by the Bands 5 comparison, indicated that the vegetation was entering the first stage of a new annual growth period. This also was shown by the insignificant Band 4 pre- vs. Band 3 corrected post-event value of 0.25 revealing a shift of healthy vegetative chlorophyll absorption to the slightly shorter wavelengths.

Table 7.2.3-3
Table of Absolute Value of Differences Among Means
$MS_{Error} = 206.77$, n = 6675

	Pre-Event						Corrected Post-Event					
	B1	B2	B3	B4	B5	B7	B1	B2	B3	B4	B5	B7
Pre-Event B1	X	40.05	26.09	23.77	9.18	27.72	2.01	39.44	24.02	22.38	12.92	25.32
B2		X	14.56	16.88	49.83	12.93	42.66	1.21	16.63	18.27	53.57	15.33
B3			X	2.32*	35.27	1.63	28.12	13.35	2.07	3.71	39.01	0.77*
B4				X	32.95	3.95	25.78	15.67	0.25*	1.39	36.69	1.55
B5					X	36.90	7.17	48.62	33.20	31.56	3.74	34.50
B7						X	29.73	11.72	3.70	5.34	40.64	2.40
Corrected Post-Event B1							X	41.45	26.03	24.39	10.91	27.33
B2								X	15.42	17.06	52.36	14.12
B3									X	1.64	36.94	1.30
B4										X	35.30	2.94
B5											X	38.24
B7												X

* < Ψ (HSD) of 0.93, p < 0.01; These were not significant

The findings in Bands 5, however, indicated another apparent difference. Bands 5, together with Bands 7, suggested that the geologic signature of the area had been altered. By reviewing the ground truth information (Annex 1), this was determined to be triggered by a combination of two conditions. First, after the explosion a large dust cloud was seen rising up and moving away from the BEXAR site. In this cloud, smaller particulate matter, which prior to the event was the surface of the site, was removed. After the event and the removal of these smaller particulates, the surface of BEXAR was comprised of larger particulates which were left behind. Furthermore, these larger particulates had been moved around, turned over, and generally disturbed, changing the weathered-particulate signatures. Second, after the event, a large number of cracks appeared on the surface of BEXAR. These cracks, too, suggested two conditions: 1) the cracks and associated shadowing changed the composite geologic spectral signature of BEXAR; and 2) the cracking caused a lateral expansion of BEXAR, and because of this spatial increase, the quantity of TM-sensible geologically-related phenomena was greater in the corrected post-event imagery (this expansion concept is also discussed in Section 7.3).

These findings suggested that a combination of phenomenally- and spatially-related geologic/surface soil changes were attributed to the BEXAR event; and other than natural changes, minimal (if any) BEXAR-related changes were detected in the area vegetation. Furthermore, these changes were detected by statistically modeling the radiometric and spectral resolution characteristics of the Landsat V TM multispectral imagery. Indeed, even with a relatively small number of pixel observations (6675), the discriminating power of TM imagery should not be underestimated from a statistical perspective. It was clear, however, that the exploitation of these discriminating powers was dependent on the validity and reliability of the atmospheric removal processes. Thus, within this multispectral rationale, it can be inferred that Landsat V TM multispectral imagery was successful in monitoring spectral changes attributable to the BEXAR event.

7.2.4   AAI Multispectral Analyses

There are several phenomena associated with the detonation that could potentially have produced measurable changes. Some of these were apparent in the video recording and other ground truth information provided to AAI by Autometric. One was the creation of dust plumes at and around the detonation site. The disturbances which raised the dust may have produced at least two potential observables. One was deposited dust in the vicinity of and down-wind from the dust raising sites (for example on vegetation). The other was the resorting of the particular size distributions at the detonation site and possibly along the lineament disturbance sites. As for the deposited dust, the resorting probably enhanced the relative fractions of fine-grained vs. coarse-grained materials. Exposure over time of mixtures of fine-grained and course-grained materials to wind, rain and vibrational action generally

tends to shift the more mobile fine-grained fractions into cracks, crevices, and other gravitational wells effectively decreasing the fraction of exposed fine-grained material per unit area. The detonation event may have resorted the soil fractions on the spoil pile, enhancing the fraction per unit area of exposed fine-grained materials.

Such an enhancement of fine-grained material (fines) on the spoil pile would have two predicted potential optical effects on the imagery. First, the enhancement of fines would be expected to increase the brightness of the exposed spoil. The fine-grained materials have higher surface area per unit volume than the coarser-grained material, and the single scattering (specular) component of the reflected sunlight would correspondingly be enhanced. Second, the enhancement of fines would change the multispectral characteristics of the material.

The changes in multispectral properties of the spoil due to enhancement of fines are expected as a result of two factors. One factor is that the fines may be compositionally different, either because they are from different source rocks or because they are more weathered. Different source materials will generally have different susceptibilities to physical weathering, the less resistant materials producing correspondingly more fine-grained material than the more resistant source materials. If the fines were derived from the same source rocks as the course materials, the finer-grained fractions would likely be more weathered than coarser-grained fractions, since reduction in particle size is generally a product of weathering. Chemical weathering, which changes composition, generally accompanies physical weathering and the rate of chemical weathering per unit volume is generally proportional to surface area per unit volume. Consequently the finer-grained fraction is typically more chemically weathered than the coarse-grained fraction. The rate of chemical weathering can be fast; therefore, even freshly generated spoil (e.g., less than a week old) can potentially reveal multispectral effects of chemical weathering.

The other factor that produces change in the multispectral properties of spoil due to the enhancement of the fine-grained fraction is the change in effective optical depth-to-grain size ratio. This changes the relation of the single scattering (specular) and multiple scattering (diffuse) components of the reflected radiation. The diffuse component dominates the multispectral optical absorption properties (spectral structure) of the material, while the specular component is dominated by the index of refraction contrast of the material and its environment. By enhancing the fine-grain fraction, the overall reflectance increases due to the increase in specular reflectance (higher surface area per unit volume). The spectral structure will increase or decrease depending on whether the optical depth-to-grain size ratio is closer to or farther from unity in the fine-grained fraction.

It is likely that the spoil material contains iron oxide as an accessory pigmenting mineral; since it is one of the most ubiquitous of weathering products, and it occurs in most soils. Iron oxide has a very small optical depth (strongly absorbing) in the visible portion of the spectrum, and the fine-grain fraction should therefore have enhanced iron oxide spectral structure relative to the more coarse-

grained fraction. If true, a potential observable resulting from a deposit of dust or a resorting of materials following detonation would be a spectral "reddening" of the spoil material. The spoil after detonation would not only be brighter, but the infrared bands would increase in reflectance more than the visible bands in a manner consistent with the spectral structure of iron oxide. The presence of other materials with spectral structure may complicate the change; however, as for most soils that contain low organic content, the spectral "reddening" of the spoil should be the principal observable resulting from an enhancement of the fine-grained fraction, if there was one.

In addition to changes in the spoil pile, the area down-wind of the spoil pile and in the vicinity of the dust-raising lineaments may also have changed. The principal observable would be the modification of the background spectral properties by the addition of deposited dust. Although such a change is potentially observable, the natural changes in the vegetation spectral properties, associated with changes in vegetation density and growth cycle, and in the relative fractions of illuminated vegetation and unvegetated floor material due to changes in sun angle, make detection of change due to added dust unlikely. Spectral "reddening" of the spoil pile is a substantially less ambiguous potential observable related to the production of dust.

Another phenomenon that may have produced an observable was vegetal stress induced by the disruption of the root systems during the event. There are three factors that militate against use of that potential observable in this study, however. First, most of the area directly affected by the detonation was unvegetated spoil material. Although there may have been significant disruption of the surrounding vegetation, the area of greatest disruption was the spoil pile. Whether there was significant disruption of the root systems at distances beyond the spoil pile is uncertain. Second, changes induced by stress can not unambiguously be isolated from changes induced by natural effects unrelated to the event. Third, the four-day time period from the event to the collection of the post-event TM image was short in comparison to the probably longer time scales of stress-induced spectral change (exclusive of severing the water supply).

A third potential observable is measurable expansion of the spoil pile produced by the detonation. Edge expansion could have potentially occurred as a result of subsidence or ballistic expansion. The subpixel detection capability of AASAP potentially makes possible the detection of such change at spatial scales that are smaller than conventional whole pixel techniques, and this potential observable is discussed in more detail in Section 7.3

Other potential observables may have resulted from changes in fracturing of the spoil pile and a variety of other possible effects discussed above. The two principal observables discussed here, enhancement of spoil pile fines and spoil pile edge expansion, were the focus of the subcontractor's search for change. Possible evidence of other change was considered secondarily.

To search for possible evidence of change induced by deposited dust or material resorting, the proposed spoil "reddening" observable was sought in the data. The ground truth photographic data were

used to identify pixels estimated to be at or near the detonation ground zero site. Three pixels were selected in the pre-event image, and the identical (within registration accuracy) pixels were selected in the post-event image. The two sets of pixels are listed in Table 7.2.4-1. The three environmental corrections listed in Tables 7.2.2-1, 7.2.2-2, and 7.2.2-4 were applied to the pixels in Table 7.2.4-1. Each corrected pixel in the post-event scene was divided by the corresponding pixel in the pre-event scene to derive a pixel ratio (post/pre) for each of the three selected pixel locations. These are shown in Table 7.2.4-2. Also included is the average of the three pixel ratios. With the corrections that were applied, these pixel ratios are proportional to the ratios of the image plane reflectances of the after material relative to the before material. The results are generally consistent with enhanced reflectance in the infrared bands in the post- relative to the pre- pixels, compared to the ratios in the visible bands where reflectances are more comparable.

Table 7.2.4-1
Fines Enhancement Pixels
(Data Numbers)

Landsat Thematic Mapper Image Plane	7 March 1991 Pixels (DN)			8 April 1991 Pixels (DN)		
1	117	126	135	150	149	145
2	62	67	72	84	82	80
3	97	106	110	132	129	127
4	81	94	99	111	113	113
5	119	149	149	186	191	192
7	77	89	88	111	118	117

Table 7.2.4-2
Pixel Ratios After Corrections
(Fines Enhancement)

Landsat Thematic Mapper Image Plane	After/Before Pixel Ratios			Average Pixel Ratios
1	1.13	.99	.85	.99
2	1.16	1.02	.90	1.03
3	1.14	1.01	.95	1.03
4	1.15	1.00	.94	1.03
5	1.29	1.05	1.08	1.14
7	1.18	1.09	1.09	1.12

The results are further consistent with imagery of the small ponds near the detonation site. The detonation would be expected to disturb the floor material in the ponds, and as the material settled the fines would settle out later than the coarse-ground material. Some of the silt likely remained suspended in the water following the detonation. The result should be a fines enhancement, and the pixel ratio (post/pre) should similarly show the proposed characteristic "reddening" observable. Pixels from the ponds were selected from the pre- and post-event images, and they are listed in Table 7.2.4-3. The pixels were environmentally corrected and post-/pre-event pixel ratios were calculated directly analogous to the processing of the spoil pixels in Table 7.2.4-1 that led to the results in Table 7.2.4-2. The corresponding results for the spoil pond pixels are shown in Table 7.2.4-4. The reddening was stronger, consistent with the reduced index of refraction contrast within the water. The relatively high Band 7 value also suggested that the silt may have been partially suspended.

Table 7.2.4-3
Spoil Pond Fines Enhancement Pixels
(Data Number)

Landsat Thematic Mapper Image Plane	7 March 1991 Pixels (DN)			8 April 1991 Pixels (DN)		
1	70	79	88	97	96	92
2	47	52	57	67	65	63
3	86	95	99	120	117	115
4	76	89	94	106	108	108
5	118	148	148	185	190	195
7	76	88	87	110	117	116

Table 7.2.4-4
Pixel Ratios
(Pond Fines Enhancement)

Landsat Thematic Mapper Image Plane	After/Before Pixel Ratios			Average Pixel Ratios
1	1.01	1.10	1.19	1.10
2	1.10	1.12	1.15	1.12
3	1.11	1.21	1.15	1.12
4	1.24	1.04	1.15	1.15
5	1.16	1.78	1.53	1.49
7	1.50	1.85	1.55	1.63

The findings appeared to support the proposal that fines enhancement may have been the source of the observed reddening. In particular, the finding that the bright spot (indicative of a local concentration of a fine-grained material) was redder than the average spoil supported the proposal that the fines were redder than the average spoil. The observation that the reddening was enhanced in the pond relative to the open spoil was consistent with the expected enhancement of the diffuse component relative to the specular component of scattered radiation in water vs. air, since the water suppresses the index of refraction contrast between the particles and their environment and hence suppresses the specular component of scattered radiation.

Additional effort is needed to verify whether the observable is a material phenomenon associated with the detonation event, but the results are at least consistent with the proposal that such an observable may be a potential indicator phenomenon.

As mentioned previously in Sections 5.3 and 7.2.4, the BEXAR detonation may have caused changes in the nature and distribution of surface material along the edge of the site's spoil pile that could be detected using subpixel techniques. For instance, a pixel at the edge of the spoil pile might be located so that the spoil covers half of the pixel area. The remaining pixel area might be covered by many non-spoil surface materials including vegetation, dirt, and rocks. A pixel such as this was defined here as a mixed pixel. It contained both subpixel quantities of a material interest or "target" (in this case spoil) and other target background materials. Quantifying the subpixel and the whole pixel target amounts using the pre- to post-event TM data, an examination of the spoil pile edge expansion was conducted.

To search for this subpixel change, the AASAP was used. AASAP provides information about the composition of mixed pixels that can be used to identify and classify change. AAI originally designed AASAP as an automatic target detection algorithm for multispectral image processing. AASAP processes an image on a pixel-by-pixel basis to identify the location of specific materials or targets of interest. For a given pixel, AASAP first estimates the spectral contribution of non-target materials (background) and then removes the background contribution to reveal the presence of target-like materials.

One output of the AASAP background removal process is the K-factor. The K-factor represents the fraction of background removed. It provides a measure of the area of a pixel covered by background material but is more properly defined as the fraction of radiance contributed by background in the original pixel spectrum; the remaining fraction (1-k) is radiance contribution of the target material.

A subpixel change detection technique using the Landsat TM data is described in this section. The AASAP K-factor output was used to show that for select pixels located on the spoil pile edge, the subpixel amounts of spoil material increased in the after image relative to the before image. The subpixel occurrence of more spoil material in the after spoil pile edge pixels indicated the spoil pile expanded after the detonation.

The first step in this technique was to define which pixels were located on the spoil pile edge. Figure 7.3-1 is a Landsat TM image with two spoil piles identified. Spoil pile #1 (BEXAR) is near the center of the image. Spoil pile #2 is in the southwest corner. Spoil pile #2 was from a previous test site, and it was assumed no dimensional change had occurred from the pre- to post-event TM collections. On and around each of the two spoil piles, several 16-pixel windows were selected as samples to develop the spectral data and test for spoil-pile expansion (Figure 7.3-2).
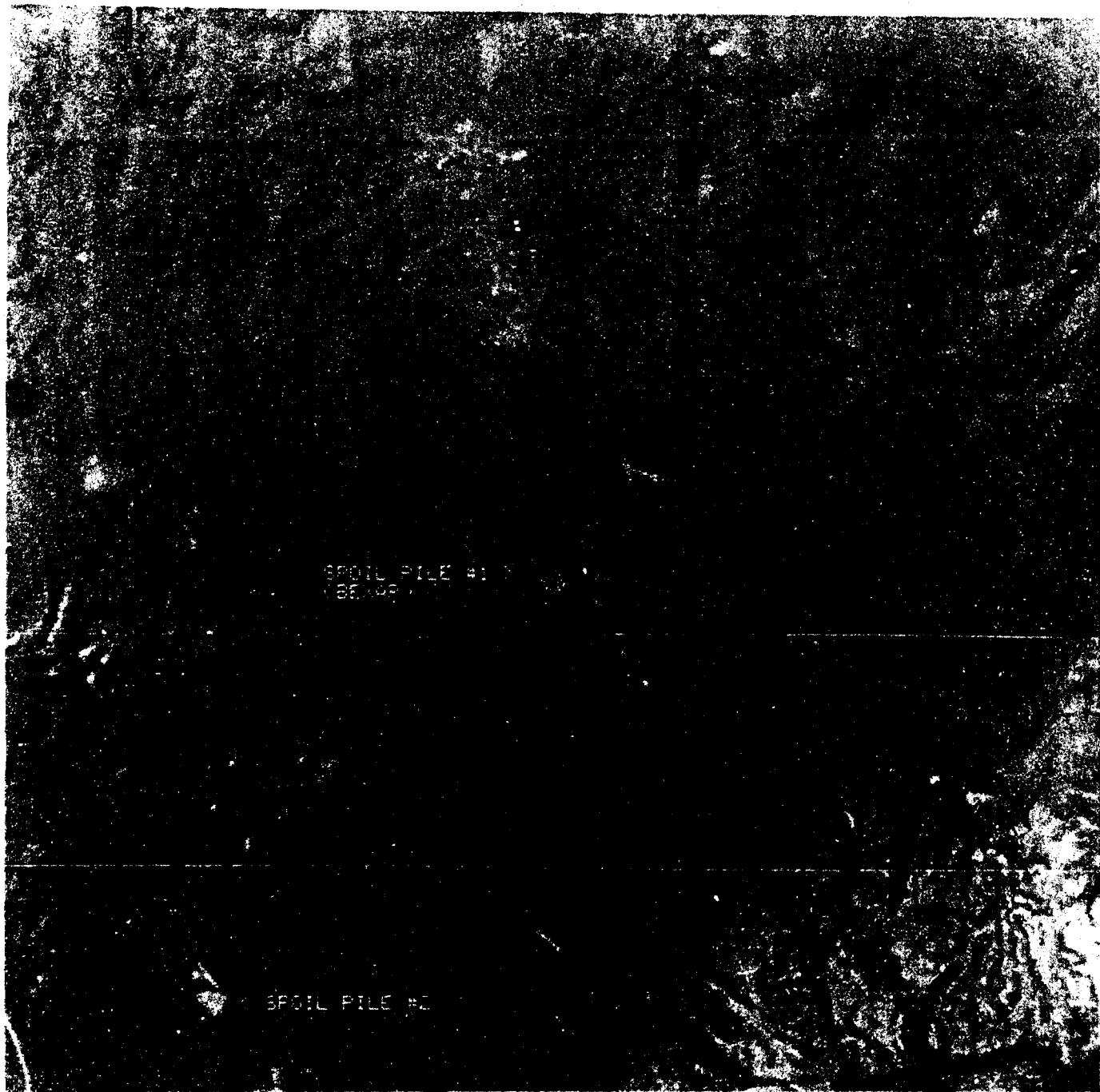
Figure 7.3-1
Landsat Thematic Mapper (TM) Showing Spoil Pile Sites

Figure 7.3-2
Pixel Samples On/Around Spoil File Sites

These patch positions were selected using visual determination of the approximate spoil edge location from displays of the six TM images. Six of the windows were placed over horizontally-oriented edges in the image, and three patches were placed over vertically-oriented edges.

The next step was to identify single pixel locations along the spoil pile edges within each row of the windows (or each column in the case of the three windows on vertical edges). Each row (or column) in the windows represented a single pixel transect across the edge. This was accomplished using AASAP K-factor analyses. Again, the "target" of interest in this case was the spoil material. The K-factor represents the fraction of non-spoil material in the pixel being tested. A large K-factor, for instance 0.70, means a large amount of background (approximately 70% of the spectral energy from the pixel) is present in the pixel. K-factors are provided in Figure 7.3-3 for the windows on spoil pile #1 from the pre-event image (if the background material could not be identified a dash was entered in the corresponding pixel). Note the gradual change in the K-factor from the inner pixels to the outer pixels. For additional discussion, the "yellow" window (top left) from spoil pile # 1 is detailed in Figure 7.3-4.

In the second, third, and fourth row of the patch, the K-factors in the right three columns gradually increased from the inside of the spoil pile to the outside. Moving to the left, the K-factors first increased, indicating that more and more background material had to be removed to indicate the presence of the spoil material. This gradual change in the K-factor was one indication that the spoil material (or spoil-like material) transitioned gradually into the background. At this location it was not a sharp, distinctive spoil/background edge. In rows 3 and 4, the K-factor peaked and then decreased. This indicated the location of an edge. The maximum K-factor along each transect is identified in Figure 7.3-5 by cross hatches.
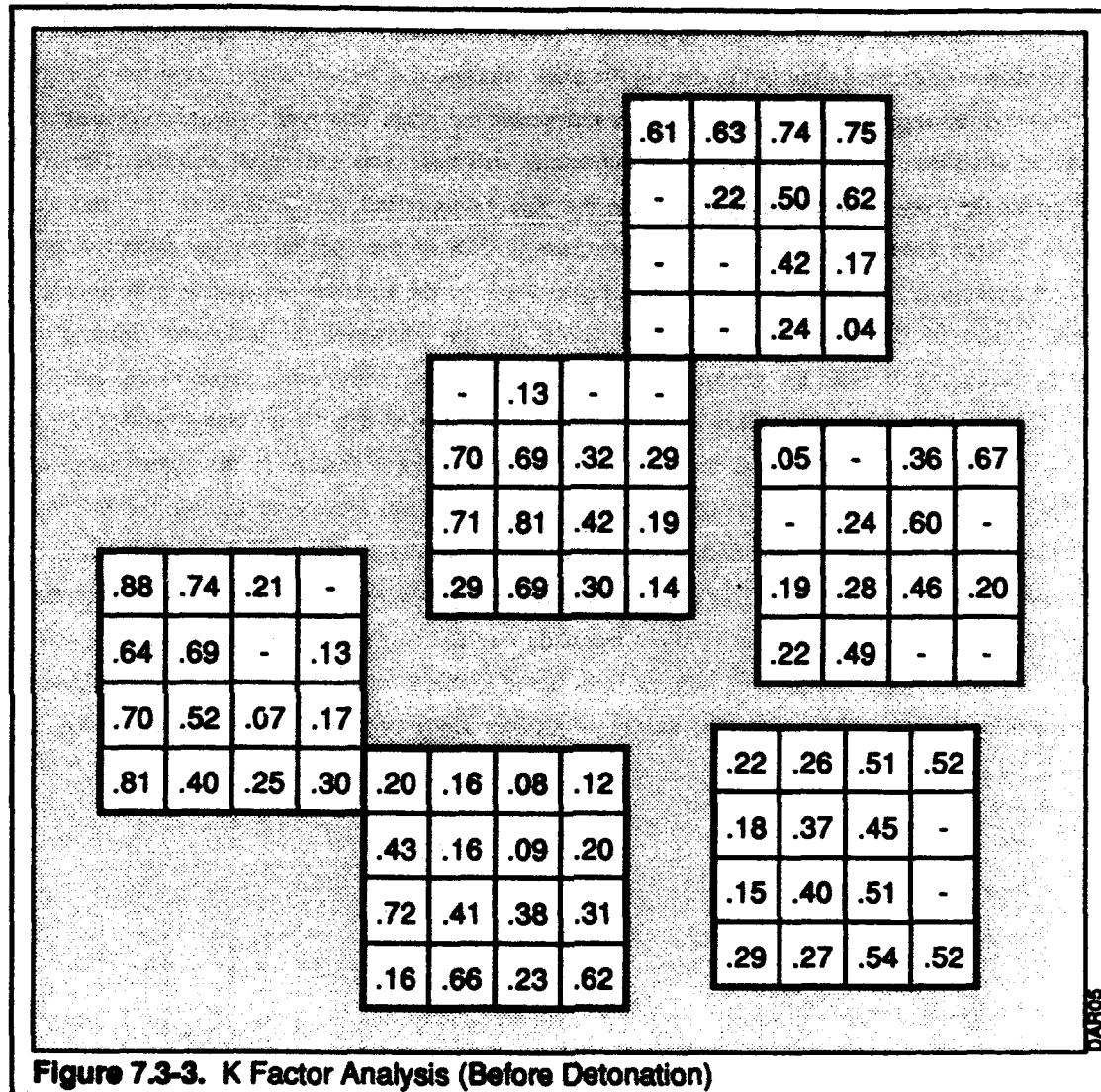
Figure 7.3-3. K Factor Analysis (Before Detonation)

AASAP K-Factors

Edge

Out of Spoil — Inside Spoil

-	.13	-	-
.70	.69	.32	.29
.71	.81	.42	.19
.29	.69	.30	.14

Out of Spoil — Inside Spoil

Edge
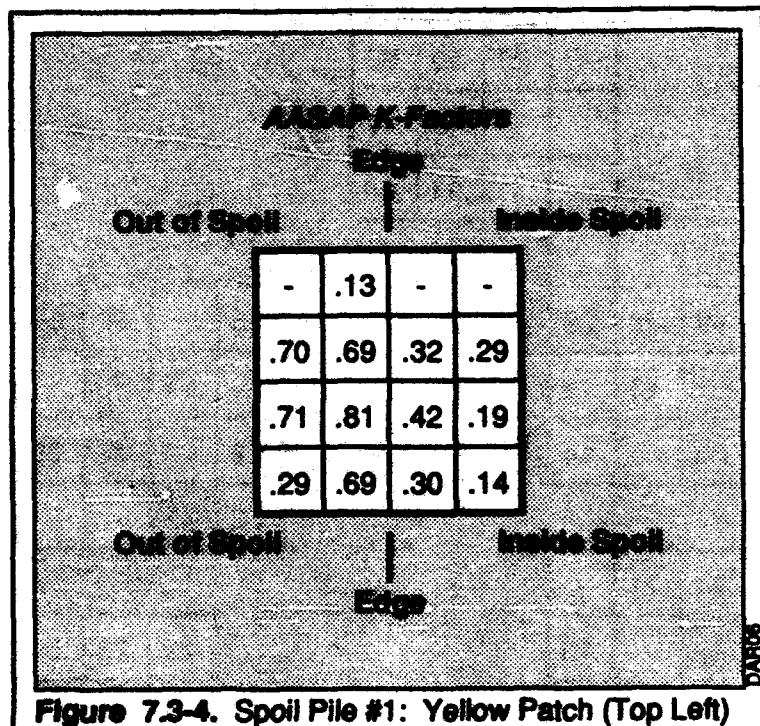
Figure 7.3-4. Spoil Pile #1: Yellow Patch (Top Left)
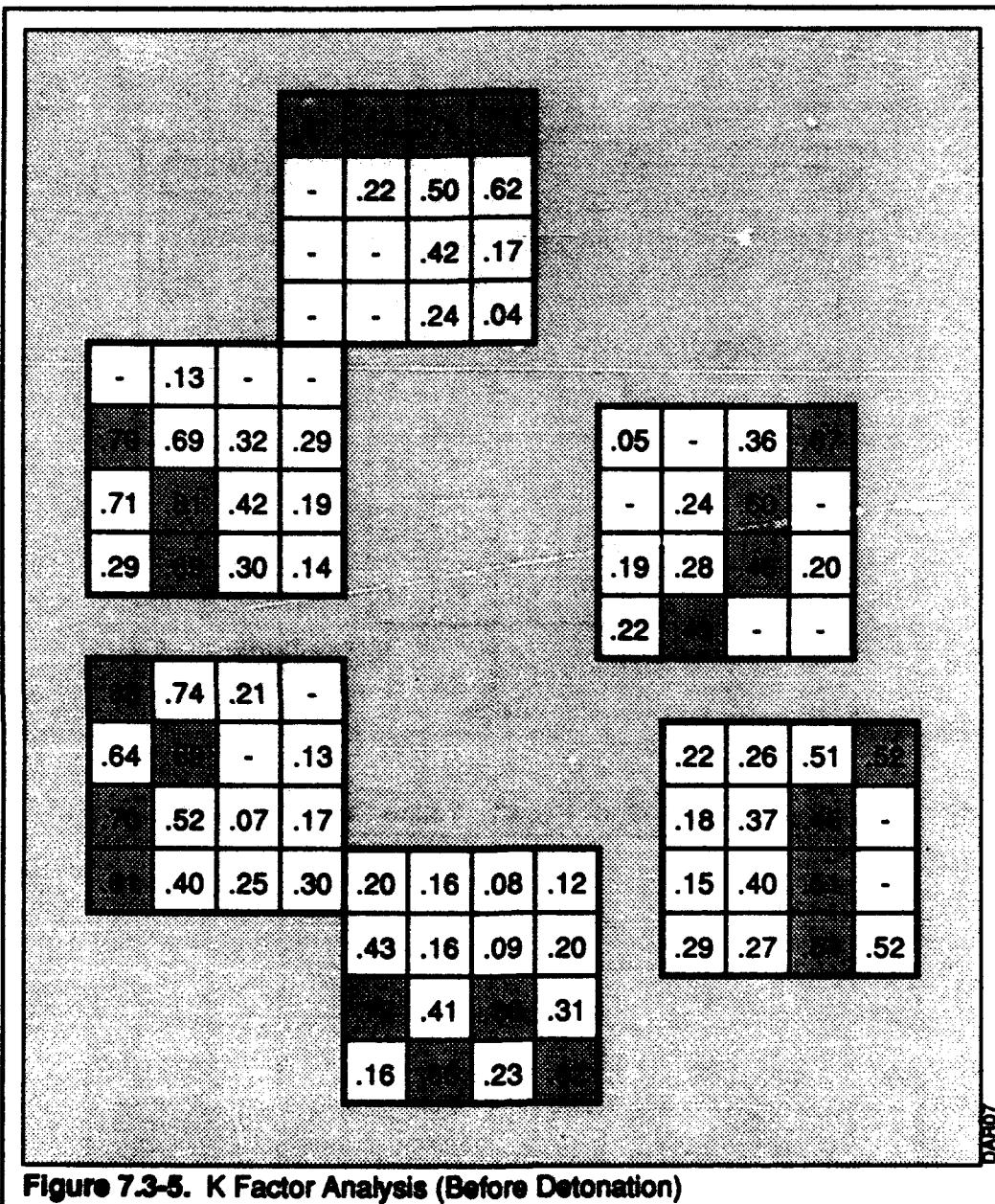
Figure 7.3-5. K Factor Analysis (Before Detonation)

Figure 7.3-5

K-Factor Analysis (Post-Detonation)

The 0.29 K-factor in the bottom left was associated with a relatively poor detection confidence level. The confidence level is determined as an output parameter of AASAP. This low detection confidence value corresponded with a low confidence that spoil material was present. The low detection confidence may have indicated the presence of dirt or some other material that was target-like, but not spoil, and therefore could be overlooked.

Spoil pile expansion may produce a "subpixel" change, where subpixel change is defined as a change in the mixture of materials that combine to produce the multispectral data numbers for a specific pixel. Thus, if the edge of the spoil pile expands, as shown in Figure 7.3-6a, then the fraction of spoil in the pixel will increase as illustrated in Figures 7.3-6b and 7.3-6c. The AASAP K-factors provide a direct measure of the amount of a material of interest in the pixel under evaluation.

The K-factor edge detection technique was used on the top three pixel windows shown in Figure 7.3-2 to identify spoil pile edge expansion near the drill hole in spoil pile #1. As a control, the three pixel windows at the bottom of spoil pile #1 and the three pixel windows at spoil pile #2 were used to demonstrate that the spoil edge did not expand in these control locations.

Figure 7.3-7 provides the K-factor values for the six pixel windows for spoil pile #1 after the detonation, with the maximum K-factors indicated by cross hatches. Figures 7.3-8 and 7.3-9 provide the K-factor values for the pixel windows from spoil #2 before and after detonation, respectively.
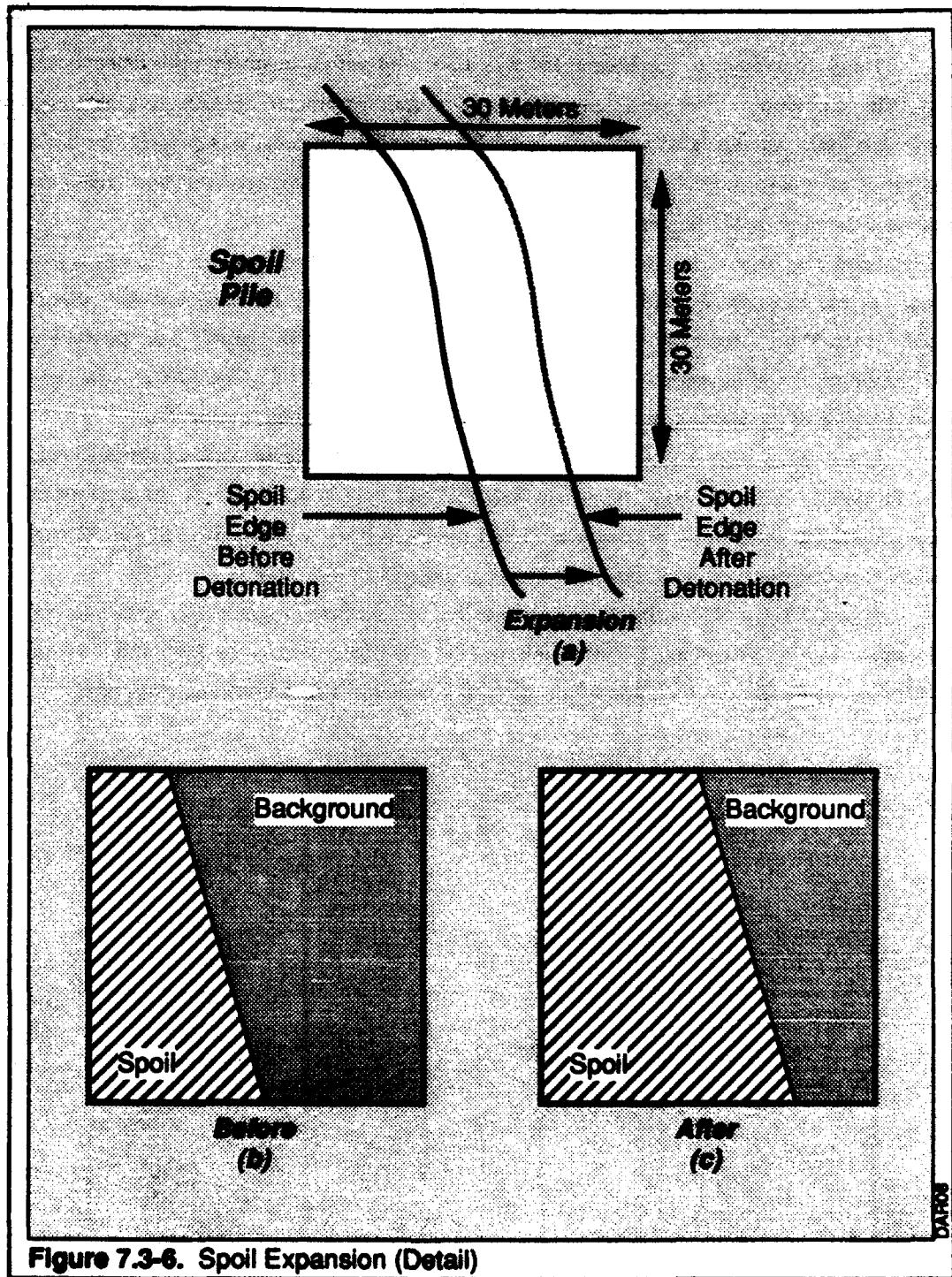
Figure 7.3-6. Spoil Expansion (Detail)

Figure 7.3-6
Spoil Expansion (Detail)
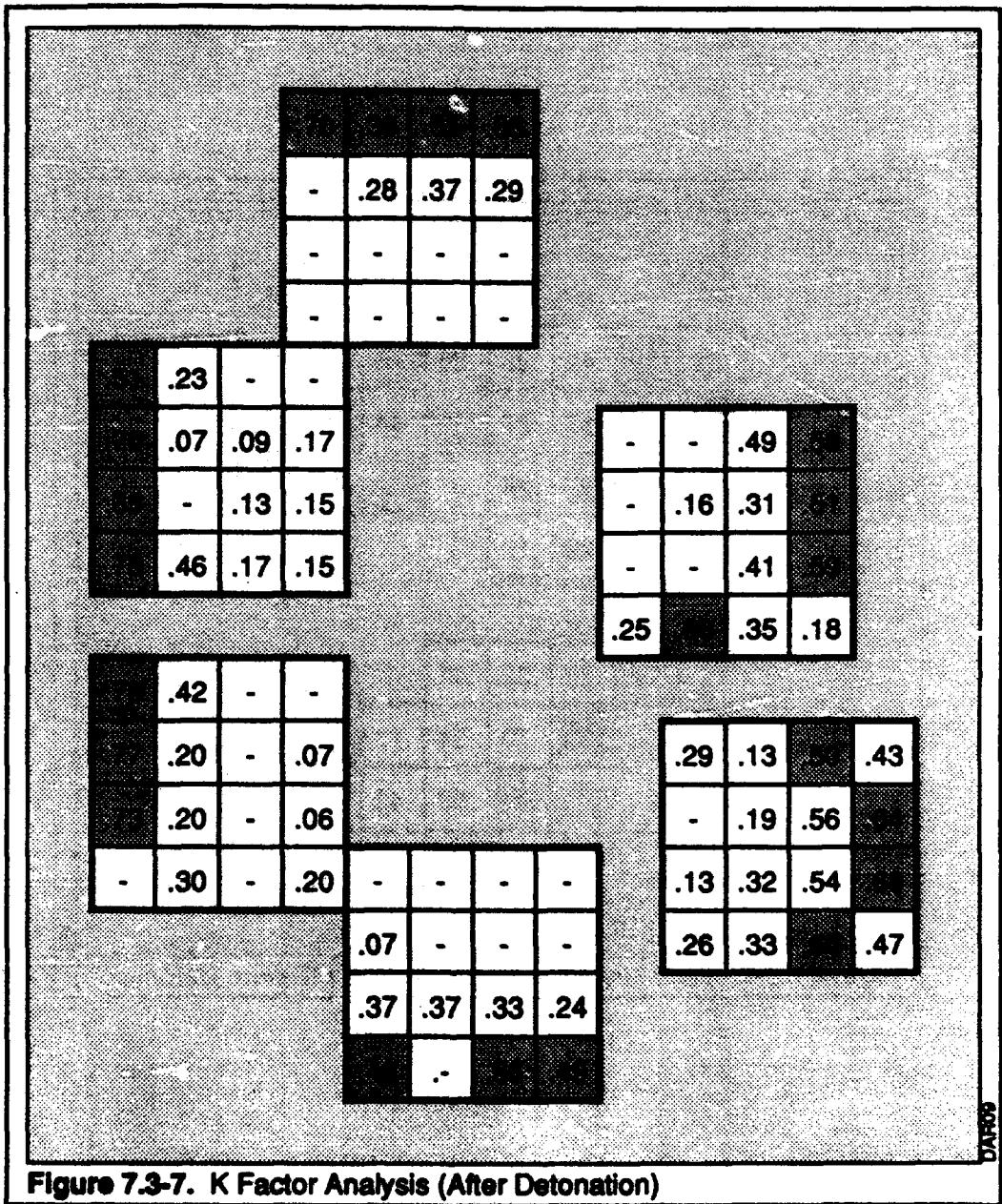
Figure 7.3-7. K Factor Analysis (After Detonation)

Figure 7.3-7

K-Factor Analysis (Post-Detonation)

71
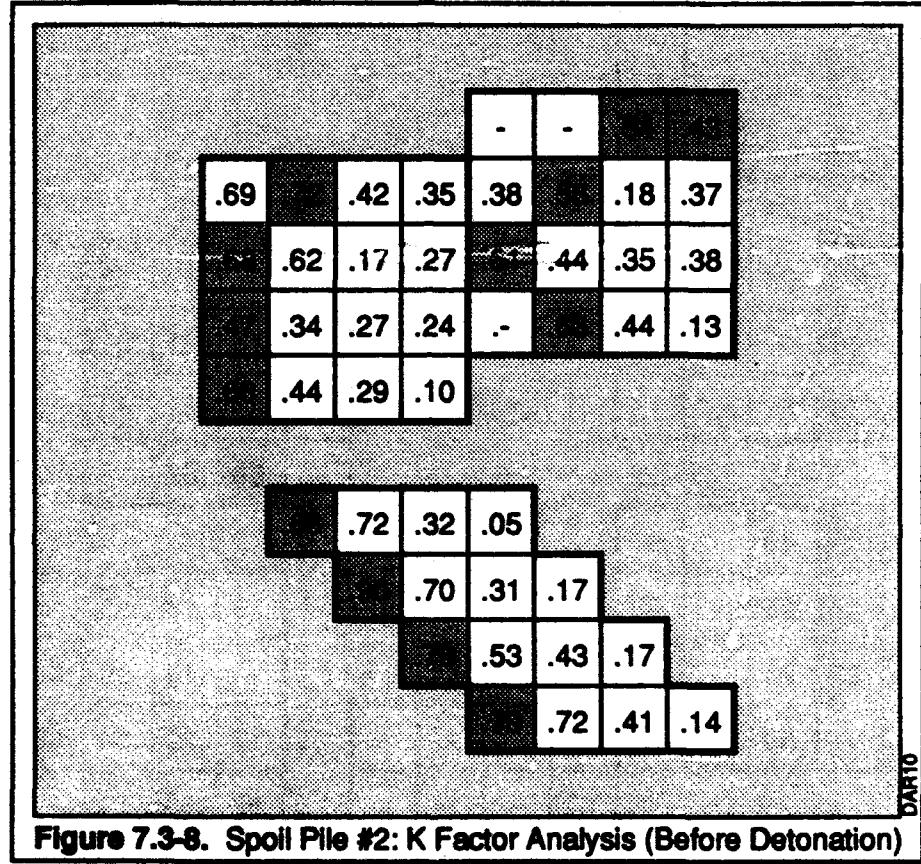
**Figure 7.3-8.** Spoil Pile #2: K Factor Analysis (Before Detonation)

Figure 7.3-8

Spoil Pile #2: K-Factor Analysis (Pre-Detonation)

Figure 7.3-9. Spoil Pile #2: K Factor Analysis (After Detonation)
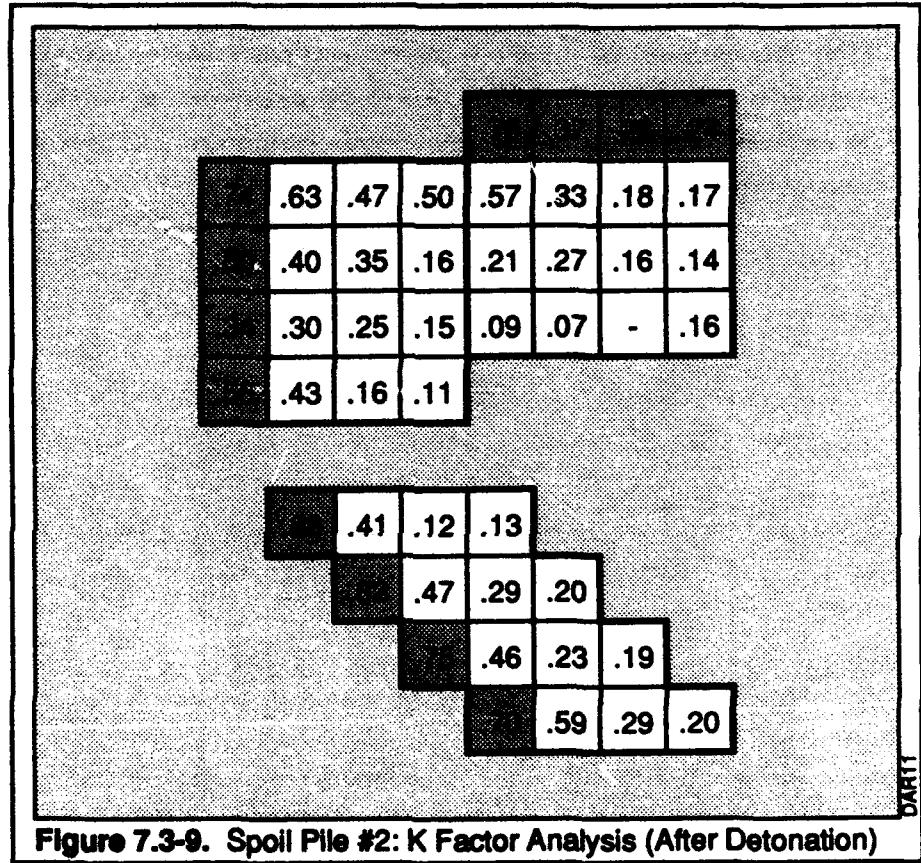
Figure 7.3-9

Spoil Pile #2: K-Factor Analysis (Post-Detonation)

These figures represented the results of the spoil pile edge expansion analysis. By comparing the position of the spoil edge in the pre-event image (the hatched pixels in Figure 7.3-5) to its position in the post-event image (the hatched pixels in Figure 7.3-7), it was concluded that the spoil pile edge expanded outwardly. The pixel locations of the maximum K-factors in the top right and top left pixel windows for spoil pile #1 were shifted outwardly in the post-event image. This indicated an expansion of the spoil pile near the detonation site. No consistent evidence of expansion was apparent in the remaining control pixel patches at the bottom of spoil pile #1 and at spoil pile #2 (Figures 7.3-5, 7.3-7, 7.3-8, and 7.3-9). This supported the hypothesis that the spoil pile expanded near the detonation site. Figure 7.3-10 provides a schematic of spoil pile #1 with the pixel shown in the Figure 7.3-6 (a to c) indicated. The expansion near the top of the spoil is shown schematically and does not correspond to the actual degree of expansion.
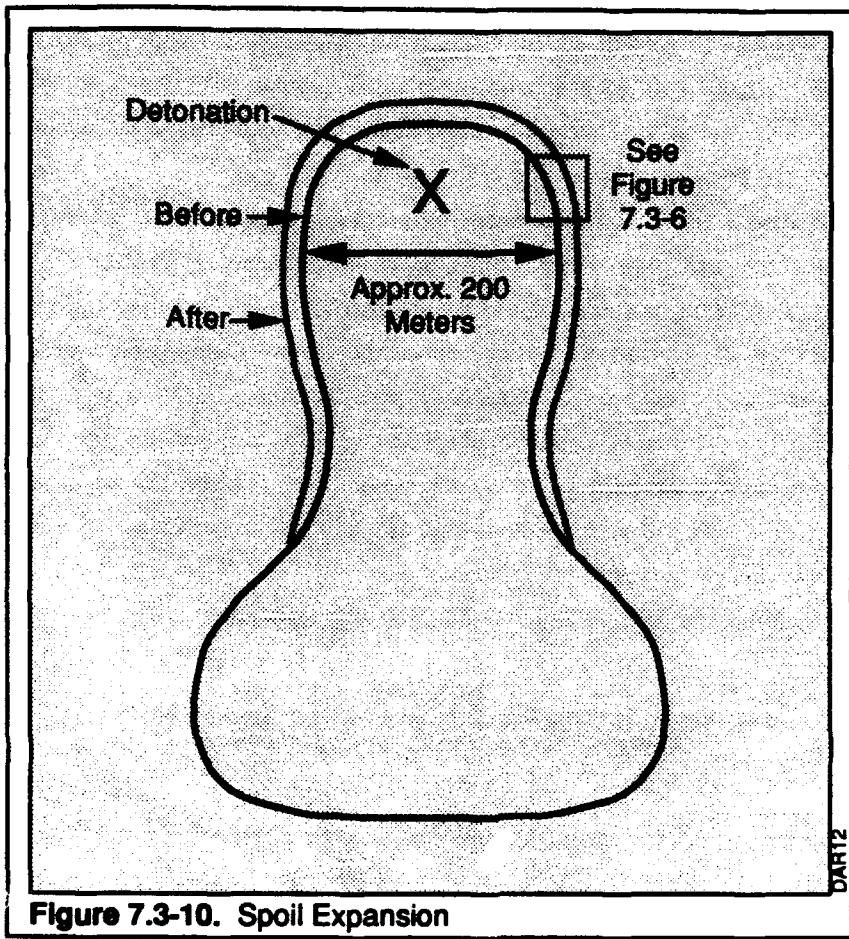
Figure 7.3-10. Spoil Expansion

Figure 7.3-10

Spoil Expansion

7.4 HYPERSPECTRAL ANALYSIS

Th hyperspectral component of the research was accomplished with data collected using the MTL Systems, Inc. 63-band ASIS. As a subcontractor to Autometric, MTL flew the ASIS several times during the first week of April 1991. Specifically, three flights were made before the event on 2 April, and one was made after the event on 4 April.

The 63-band ASIS, flown in a twin-engined Piper Aztec airplane, collects 16-bit electromagnetic energy in the 0.4 to 2.5 μm range. Three grating spectrometers operate in the ASIS. One (a silicon detector) provides 24 bands of data in the 0.4 to 1.0 μm spectral region, and the band width for these 24 is approximately 25 nm. The second spectrometer covers the 1.1 to 1.8 μm region with seven bands, and each of these has an approximate spectral width of 125 nm. The bandwidth of this spectrometer is wider to compensate for lower available signal inputs resulting from atmospheric absorptions. The third spectrometer provides 32 bands in the 2.0 to 2.5 μm region. Each of these has an approximate spectral width of 16 nm. The second and third spectrometers use lead sulfide detectors and are cooled by two-stage thermoelectric cooling devices.

Summaries of the four ASIS collections of BEXAR are provided in Table 7.4-1.

Table 7.4-1
Airborne Spectroradiometric Imaging System (ASIS)
BEXAR Image Collection Summaries

Date	Time (local)	MTL-derived filename	Altitude	Spatial Resolution
2 April 1991	11:30	BEXAR 2	13,000	6 by 6 m*
2 April 1991	11:40	BEXAR 4	13,000	6 by 6 m
2 April 1991	11:55	BEXAR 1	17,000	10 by 10 m
4 April 1991	14:45	BEXAR 5	13,000	6 by 6 m*

*Sent to AAI (see Section 7.4.2)

As with the Landsat TM imagery, both Autometric and AAI analyzed the ASIS data. Accordingly, these analyses have been reported separately and are provided in the following Sections 7.4.1 and 7.4.2, respectively.

7.4.1   Autometric Hyperspectral Analyses

Airborne spectroscopic devices were originally designed to satisfy discriminate analytical requirements. The narrow-band discrimination capability provided by the systems compliment statistically-driven multispectral imagery (e.g., Multispectral Scanner and TM) methodologies. Discriminate techniques (mainly spectral response curve investigations) are commonly used by analysts reviewing the voluminous data; indeed, statistical models built with 50 to 200+ spectroscopic bands (input variables) are difficult to apply. Accordingly, for this portion of the research, discriminate spectral curve analyses were performed on pre- and post-event ASIS hyperspectral data for studying event-related changes.

Before the spectral data could be compared, several preparatory steps were required. For instance, the original ASIS imagery was collected as 16-bit data. The display devices at the Autometric image processing laboratory, however, being standard 8-bit black and white and 24- and 32-bit color displays, were not compatible with the raw 16-bit data. The first step in the ASIS processing, therefore, was a reduction of the 16-bit (0 to 65535) imagery to 8-bit (0-255). This was performed separately on each band using the band-unique statistical profile information. For a given 16-bit band, minimum and maximum values were declared at 2σ about the mean (i.e., approximately 95% of the data). These were divided by 256, and the resulting values became the absolute minimum and maximum for the output band. The remaining pixels, starting with the declared minimum value, were density sliced into brightness level interval classes, each having a 16-bit range of 256. The last class was comprised of a remainder amount. In turn, these interval classes were used to remap each 16-bit pixel to an 8-bit scale. Although this process reduced the original radiometric range, the output 8-bit bands nevertheless retained the overall 16-bit histogram profile as well as vital relative band spectral integrity. This conversion was performed for each of the four 63-band ASIS datasets.

After being converted to 8-bit imagery, the four ASIS sets were reviewed for image qualities. An example of Band 10 for each collection is shown in Figure 7.4.1-1. (BEXAR 3 was a null scene due to sensor malfunctions, hence the numbering BEXAR 1, 2, 4, and 5.) Specifically, keeping in mind the goal of this analysis was to detect spectral changes caused by the BEXAR event, these four datasets were analyzed to determine which two would be most appropriate for making pre-to-post-event discriminations. There was no choice for the after image; BEXAR 5 was the only post-event image. For the pre-event scene, though, there were three potential choices. BEXAR 4 was eliminated because a large cloud shadow obscured the general test site area. Considering BEXAR 5 had a spatial resolution of 6m, it was decided that BEXAR 2 — also at 6m and approximately the same geometric orientation as BEXAR 5 — would serve as the pre-event data. BEXAR 1, at 10m and skewed badly, would have required substantial rectification, and this would have significantly degraded the spectral integrity of the data
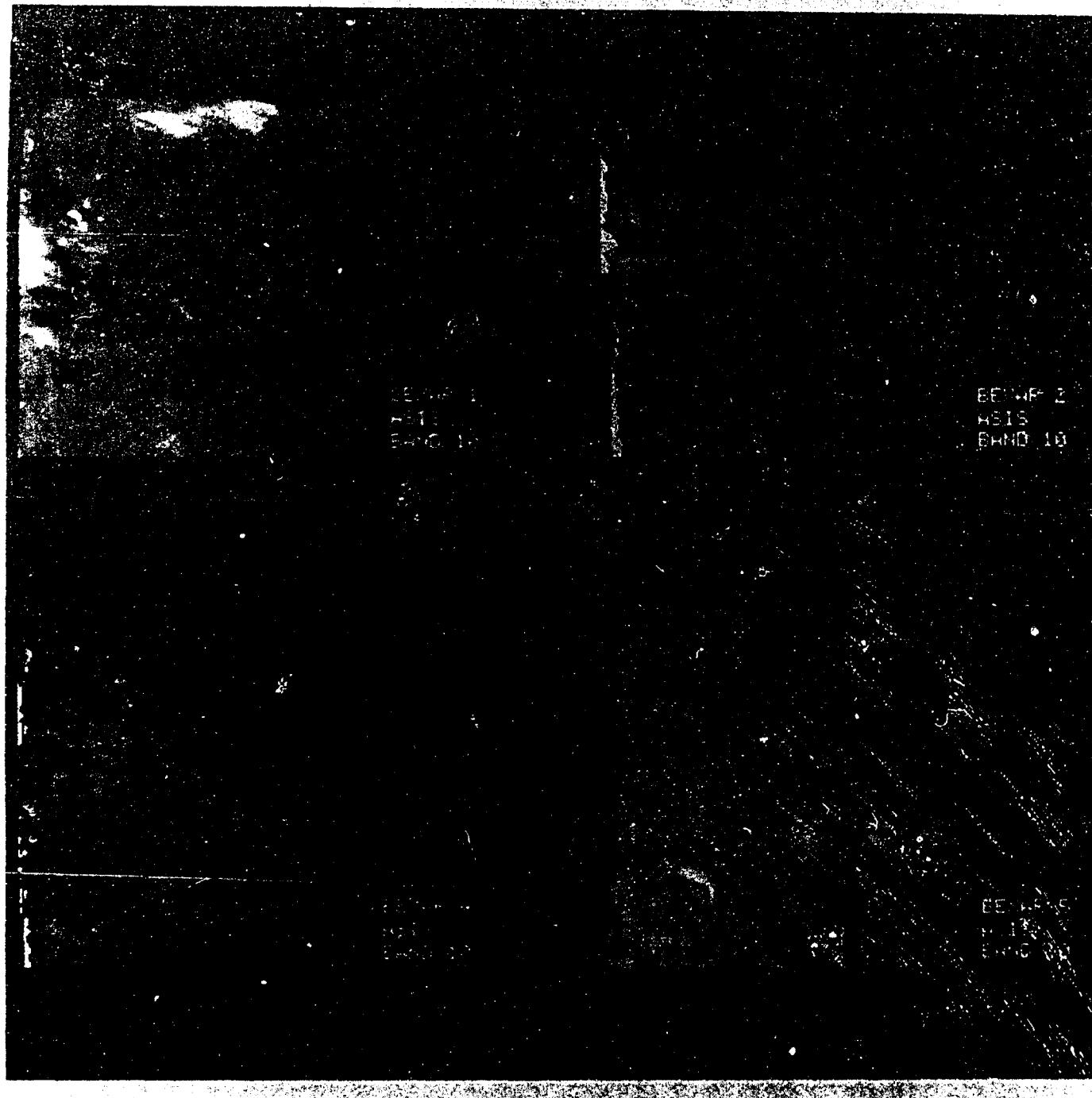
Figure 7.4.1-1
Four Airborne Spectroradiometric Imaging System (ASIS) Band 10 Examples

As shown in Figure 7.4.1-1, BEXAR 2 did contain a series of scanline dropouts, but these were not over the BEXAR site. Consequently, they were ignored.

Once the pre- (BEXAR 2) and post-event (BEXAR 5) data were chosen, the image sets were registered. This ensured for a given ground location (X,Y) in the pre-event image, the same specific ground location (X,Y) could be located in the post-event image. The specific method of registration was discussed in Section 7.1; with the ASIS data, however, the pre-event imagery served as the geometric ground truth (instead of a map as in the multisensor registrations). In turn, the post-event imagery was registered to the pre-event base image. To achieve this, 12 GCPs were selected from the general test area, and using them in the rectification model, an RMS error of <1.50 pixels was obtained.

In reviewing the 63 bands of each data set, it became apparent that the ASIS sensor gains were set differently from collection-to-collection. Upon follow-up, the MTL sensor operator reported these different gain settings were an effort to boost the input signal during the post-event collection. Apparently, this was done to compensate for thin upper-atmospheric clouds on the afternoon of 4 April which absorbed significant portions of near- and mid-infrared energy. Thus, the post-event data were much brighter relative to the pre-event. To remove these impacts from sensor-related differences, two calibration sites were chosen away from the immediate BEXAR site. One was a vegetation sample, and the second was a bare soil sample. Gain offsets were then determined for each band, and these values were used to calibrate the post-event data to a pre-event baseline.

Results from the data rectification and calibration preparatory functions are shown in Figure 7.4.1-2 using another Band 10 example.

To analyze the discriminate signature features of the pre- and post-event ASIS data, nine ground locations were determined from the registered imagery. Samples consisting of both "soil" and "vegetative" areas were taken from the BEXAR site and surrounding areas. These are shown in Figure 7.4.1-3. One of the test samples (site 6) was under the leading edge of a cloud shadow on the pre-event imagery and was not included. Hence, a total of eight valid samples as used for the discriminate signature evaluations.
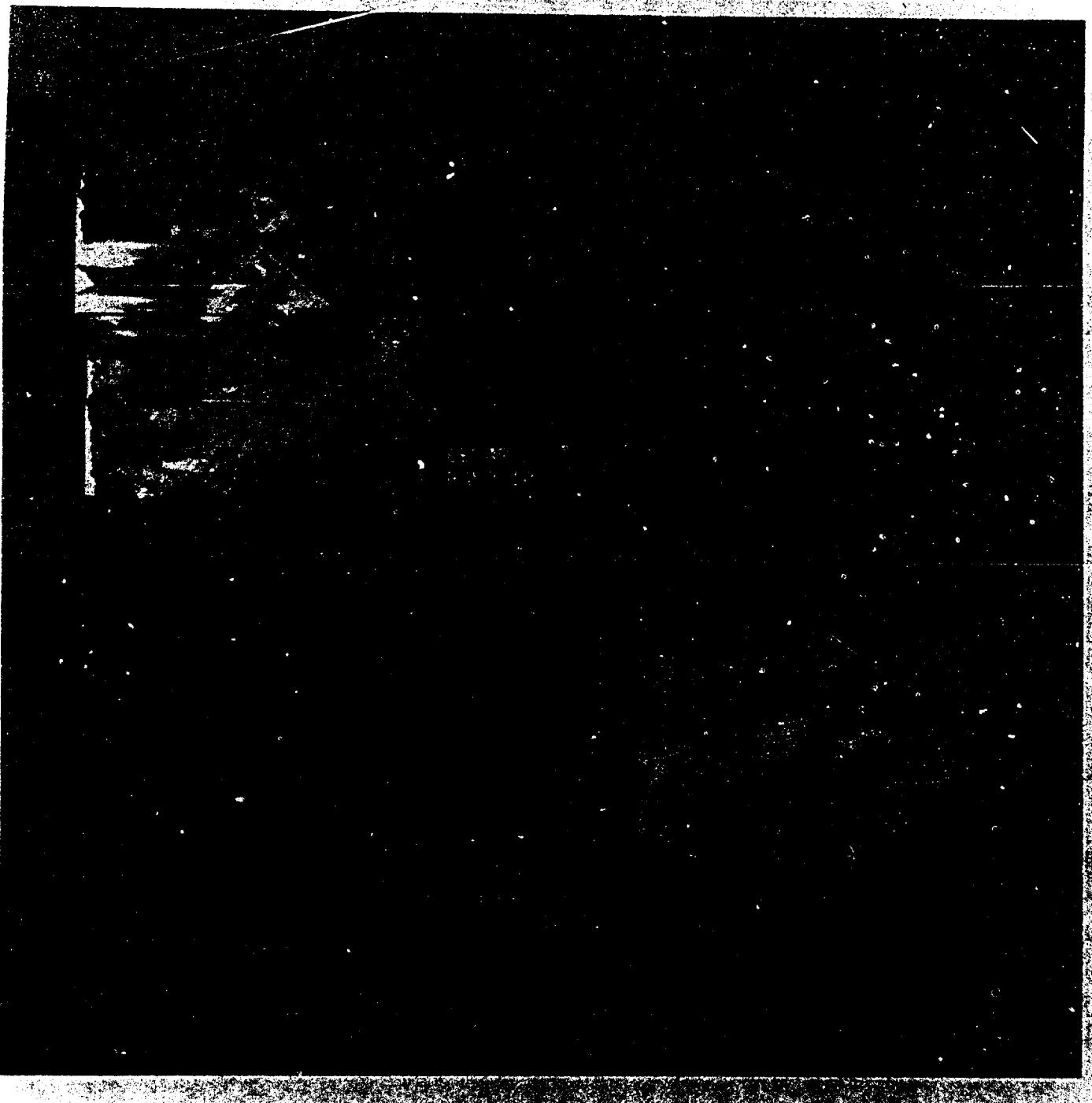
Figure 7.4.1-2
Rectified and Calibrated
Airborne Spectroradiometric Imaging System (ASIS) Band 10 Examples
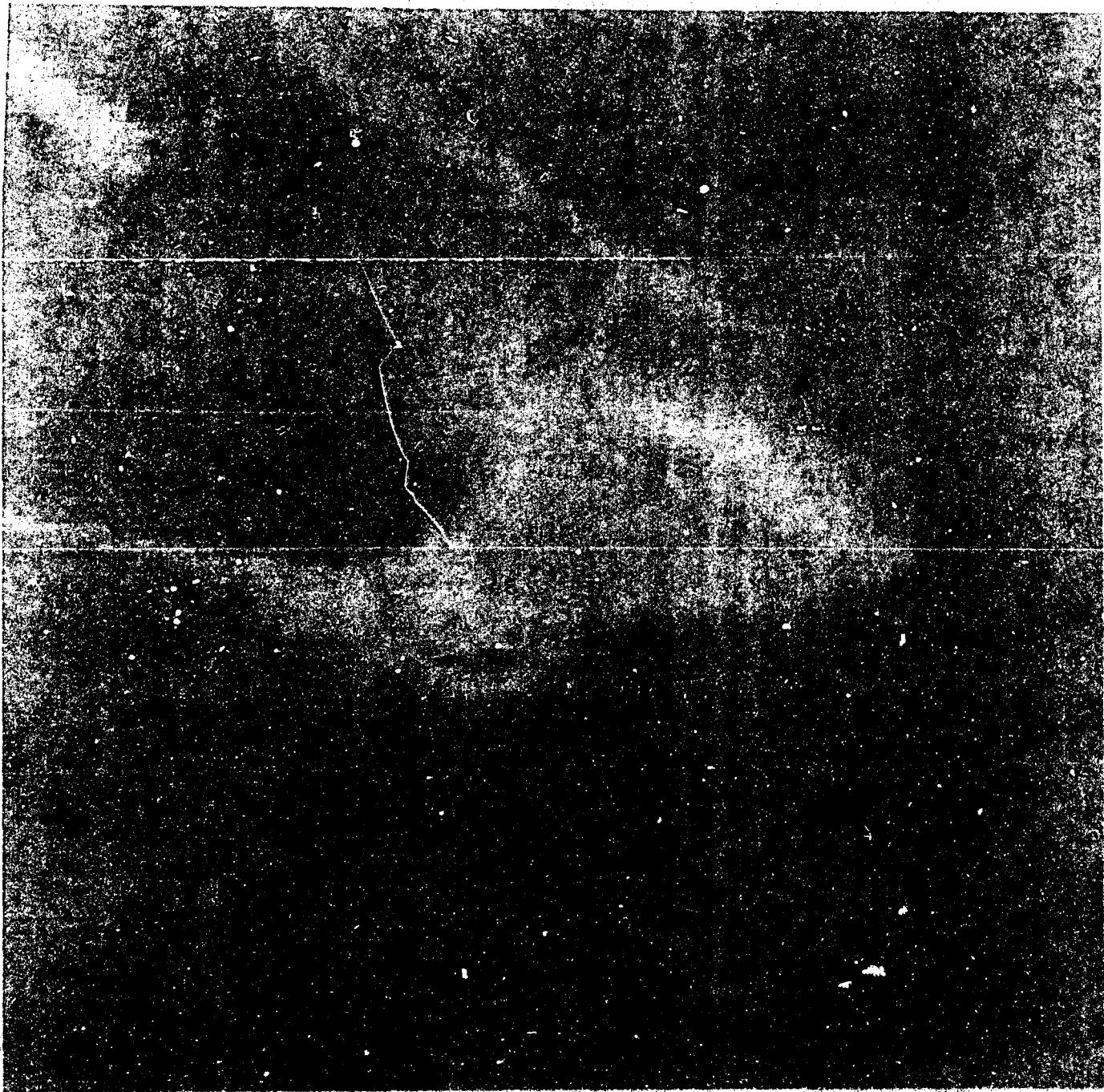
Figure 7.4.1-3
Soil and Vegetation Sample Areas

Complementing previous study results, an analysis of the soil and vegetative sample spectral curves from the two collections revealed the detection of apparent event-related and event-unrelated changes. Unfortunately, the spectra suggested the ASIS sensor was not functioning at full capacity. Specifically, in all sample cases Bands 32 to 63 had extremely low brightness value counts; they were also highly correlated (>95%). Bands 32 to 63 were collected by the third spectrometer, and their corresponding minimal utility indicated: 1) spectrometer three was not functioning properly; 2) spectrometer three was functioning as designed, but it was not sensitive enough to detect the variant spectral information resident in the 2.0 to 2.5 µm spectral region; or 3) the upper-atmosphere clouds absorbed too much of the near- and mid-infrared energy, and not enough energy was reaching the sensor. Consequently, considerable amounts of data on the geologic surface composition were not available. Comparatively, ASIS spectrometers one and two apparently functioned normally. They produced valuable data from 0.4 to 1.0 µm and, more importantly, in the 1.1 to 1.8 µm range.

With regard to the detection of change, two example plots are shown in Figures 7.4.1-4 (site 7 - vegetation) and 7.4.1-5 (site 5 - soil). Figure 7.4.1-4, together with other plots not shown, indicated no apparent change could be detected from 0.4 to 1.0 µm. This suggested the chlorophyll absorption levels remained constant from the 2 to 4 April collection dates. Slight spectral changes were observed, but these were not considered significant. In contrast, change in the 1.1 to 1.8 µm portion was noticed. Specifically, a slight increase in the corrected post-event data indicated a small increase in turgidity. The greater turgidity level was likely the combined result of a continuing seasonal natural increase and also the later time-of-day sensing on 4 April. Because of the lack of data in the 2.0 to 2.5 µm range, however, no reliable assessment of the spectral impact of the detonation shock dust cloud could be made. Indeed, some increase in reflectivity from the post-event collection in the 1.1 to 1.8 µm range could have been attributed to particulate deposits on the vegetation (especially for sites 7 and 8), but none was detected. (Given the high wind velocity at the site, the dust coating had probably been blown off the surface of the evergreen vegetation soon after the test.)

Although natural change was noticed, no event-related changes were detected using the vegetation sample sites. These results agree with the findings from the multispectral analyses (Section 7.2).

For the soil sites, the data seemed to contradict results from previous analyses. In particular, post-event brightness values in the 1.1 to 1.8 µm range were less than values in the pre-event imagery. Again, though, the 2.0 to 2.5 um range was not usable for comparison. Referring to Sections 7.2 and 7.3 and Annex 1, however, three physical changes to the test site were detected previously: 1) expansion of the test site surface (as shown in TM Band 7 increases in the ANOVA and Tukey HSD tests and the subpixel processing); 2) the alteration of the surface particulate material (as shown by the spectral reddening in TM Bands 5 and 7); and 3) the formation of a series of surface cracks after the explosion.

Figure 7.4.1-4. Site 7 - Vegetation
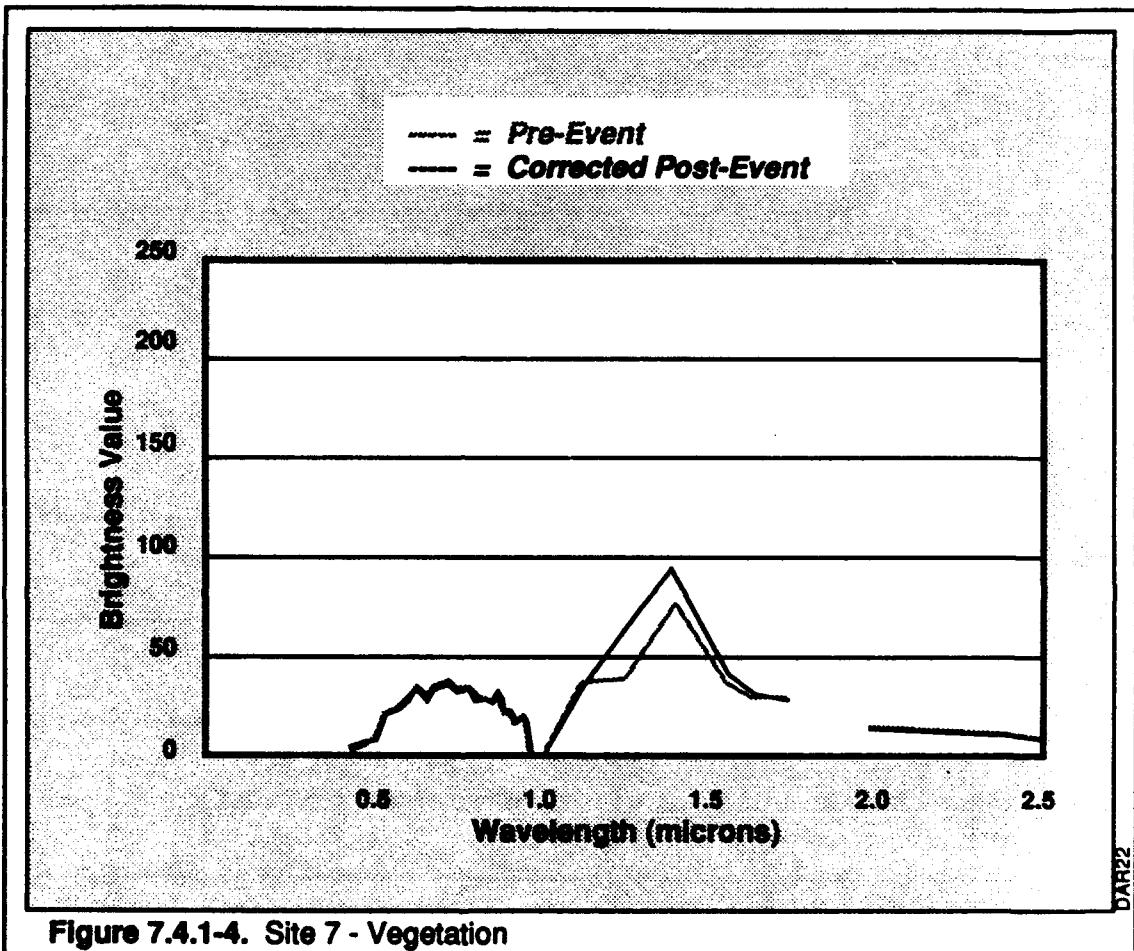
Figure 7.4.1-4
Site 7 - Vegetation
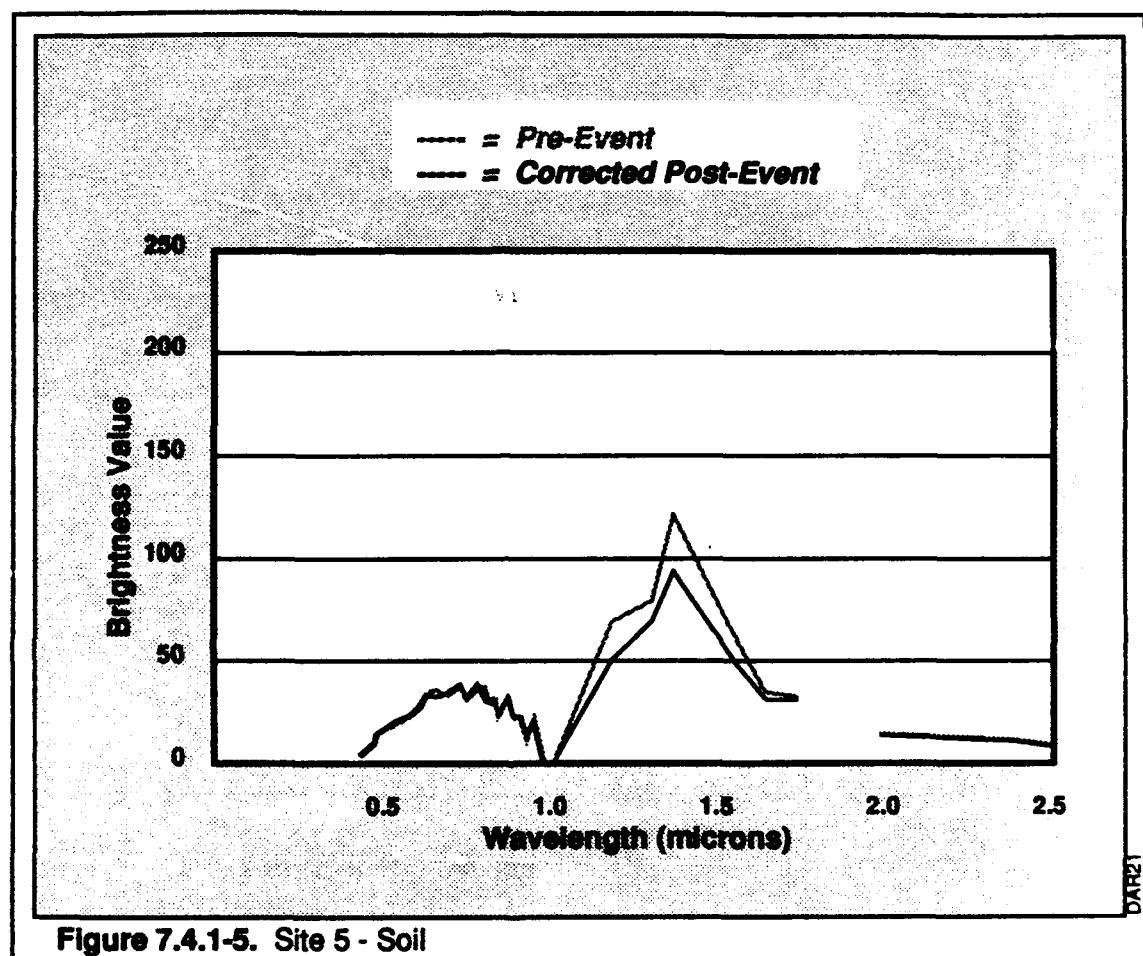
Figure 7.4.1-5. Site 5 - Soil

Figure 7.4.1-5
Site 5 - Soil

The ASIS data had a spatial resolution of 6m, and this was much higher than the 30m of the TM imagery. Compared to the TM imagery, with this increased resolution the cracks and accompanying shadow features comprised more of an ASIS composite pixel signature. In the 6m ASIS imagery, these changed states reduced considerably the level of sensed energy during the post-event collection. Furthermore, the shadowing effect was also amplified by the low sun position during the 14:45 (local) collection time.

Based on these results, it was inferred that data from the ASIS did detect specific changes related to the underground detonation. The greater spectral resolution of the ASIS data, however, did not provide substantially more information compared to the six-band Landsat TM imagery. This may not have been the case had spectrometer three provided usable data. Also, some information was lost during the 16-bit to 8-bit conversions, as well as the rectifications. In contrast, the considerable spatial resolution increase did detect the cracking and associated shadowing, and these features were not isolated using the TM data.

Perhaps additional processing methodologies should be considered to utilize fully an ASIS or other spectroscopic data set. Indeed, a combination of 16-bit stochastic time- and frequency-domain modeling techniques with conjunctive 8-bit discriminate and limited statistical image processings may provide a more rigorous analytical approach. In general, though, the results from the 8-bit discriminate methods used here agreed with the findings from the other components of the research: spectral changes related to the underground detonation were detected using remotely-sensed data together with ground truth data.

7.4.2 AAI Hyperspectral Analyses

Complimenting the multispectral (Section 7.2) and subpixel (Section 7.3) analyses, AAI sought another line of evidence for potential fines enhancement using the ASIS data. As indicated, the ASIS data had higher spectral and spatial resolutions than the Landsat imagery.

Not all of the ASIS data was found to be usable as illustrated in Figure 7.4.2-1. In the figure the data number ranges for the pre-event 2 April 1991 and post-event 4 April 1991 images are shown. Unfortunately, many of the bands from spectrometer could not be used.

In Figure 7.4.2-2 are shown the averages of 18 pixels (6x3 grids) spectra for a spot on an unvegetated road area away and upwind from the spoil pile. Two sets of 18 pixels were obtained, one set from the pre-event image and the other from the post-event image. It was attempted to extract the pixels from the identical locations on the road in the two images. It was apparent from the imagery and from Figure 7.4.2-1 that the two sets of data had different sets of sensor gain settings, in addition to other environmental differences. It was assumed that the materials were relatively unchanged, however. In Figure 7.4.2-2 is also shown the ratio of the post- to the pre-event "road" pixels, which divided out that which was common to the two scenes. The resultant pixel ratio (ratio spectrum) provided a correction factor to compensate for differences in sensor gain factors, sun angle effects, atmospheric path attenuation effects, and diffuse hemispherical sky radiance effects. Spectral differences between the road and spoil are also included, but they were assumed to be minimal relative to the other factors.

Pixels were next selected from spoil pile water ponds in the pre- and post-event scenes. Averages of nine pixel grids were generated from as close as possible to the identical water pond locations in the two images. The averaged pixel spectra and the ratio of the two spectra are shown in Figure 7.4.2-3.
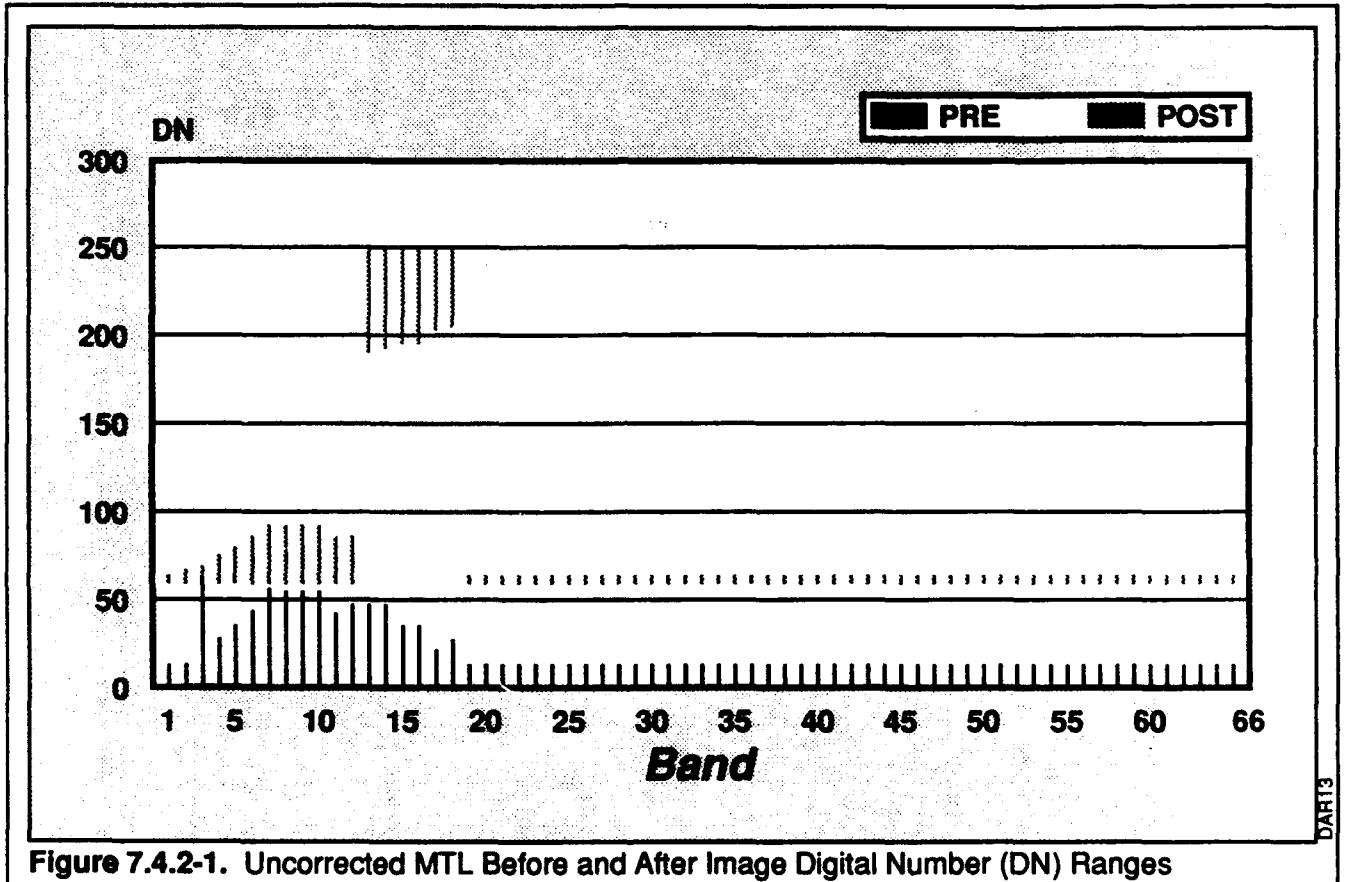
Figure 7.4.2-1. Uncorrected MTL Before and After Image Digital Number (DN) Ranges
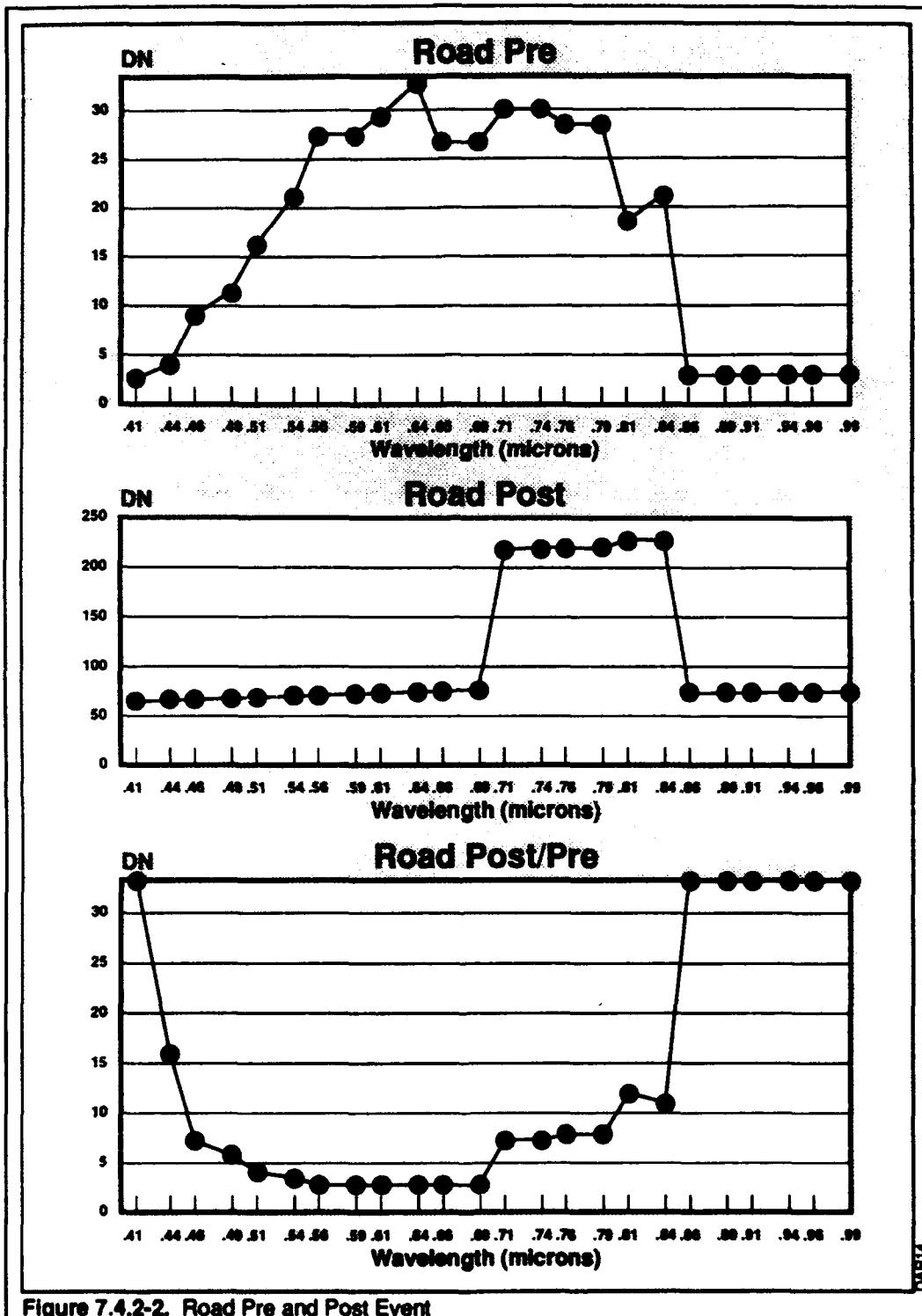
**Figure 7.4.2-2.** Road Pre and Post Event

Figure 7.4.2-2
**Road Pre- and Post- Event**

88
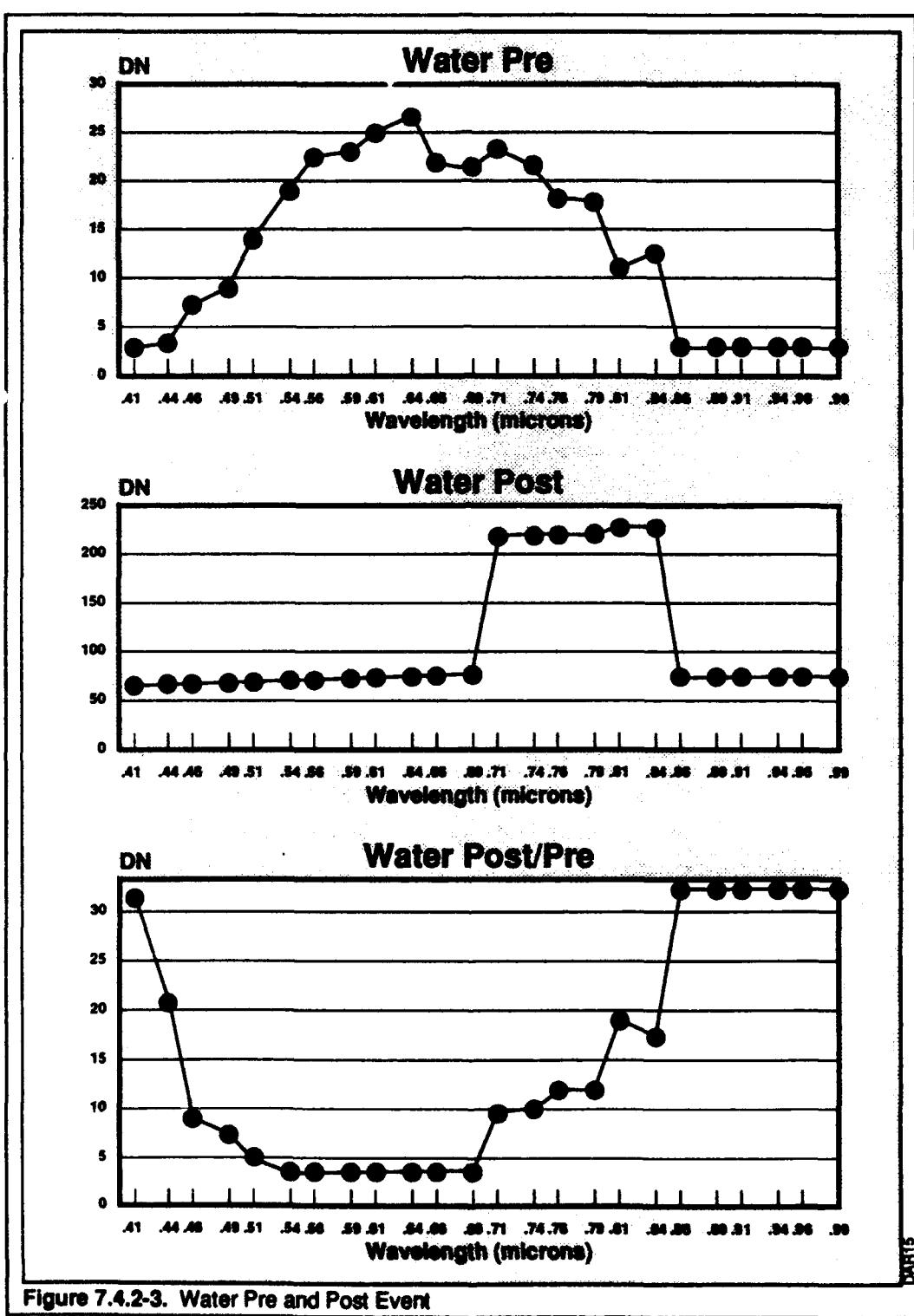
Figure 7.4.2-3. Water Pre and Post Event

Figure 7.4.2-3
Water Pre- and Post- Event

89

Before dealing further with the Figure 7.4.2-3 spectra of the spoil pile water pond, additional spectra are presented in Figures 7.4.2-4 and 7.4.2-5. In Figure 7.4.2-4 are average spectra of pixels from an area of the spoil pile, relatively homogeneous, away from the ground zero detonation site and away from the cables and vehicles. In Figure 7.4.2-5 are average spectra of a bright spot, assumed to be a concentration of the fine-grained fraction, at or close to the ground zero. This spot was evident in the post-event image but not as evident in the pre-event image.

To remove the spectral structures associated with the sensor gain factors and environmental factors, the three ratio spectra (water pond, general spoil, and bright spot) shown in the bottoms of Figures 7.4.2-3, 7.4.2-4, and 7.4.2-5 were divided by the ratio spectrum in Figure 7.4.2-2 (the road ratio spectrum which was used here as a standard). The resultant divided spectra are shown in Figure 7.4.2-6. Examination of the spectra revealed unrealistic discontinuities in the spectra near 0.44 μm and 0.84 μm. The discontinuities suggested the data may have been bad outside of the 0.46 to 0.80 μm wavelength range. Truncated versions of the spectra in Figure 7.4.2-6 are shown in Figure 7.4.2-7. The spectra in Figure 7.4.2-7 represent the post-/pre-event pixel ratios for the spoil pile pond water, the bright spot, and the spoil. Dividing the original (water, bright, spoil) post-/pre-event spectral by the original road post-/pre-event (the standard) removed the gain factors and environment factors which were common to both spectra and produced the spectra in Figure 7.4.2-7, which more accurately represented the "true" water, bright and spoil post-/pre-event spectra.

An additional ratio spectrum is shown in Figure 7.4.2-8 which represented the ratio of bright spot material with any residual road contribution removed. Note both the spoil pile pond water ratio spectrum (Figure 7.4.2-7, top) and the bright spot vs. general spoil ratio spectrum (Figure 7.4.2-8) revealed similar spectral "reddening" to that observed in the Landsat TM data (Section 7.2).

The observation that the reddening occurred in both the ASIS and TM imagery, and that the pond reddening was stronger than the open soil reddening in both datasets further supported the possibility that the observed reddening was a substantive phenomenon.
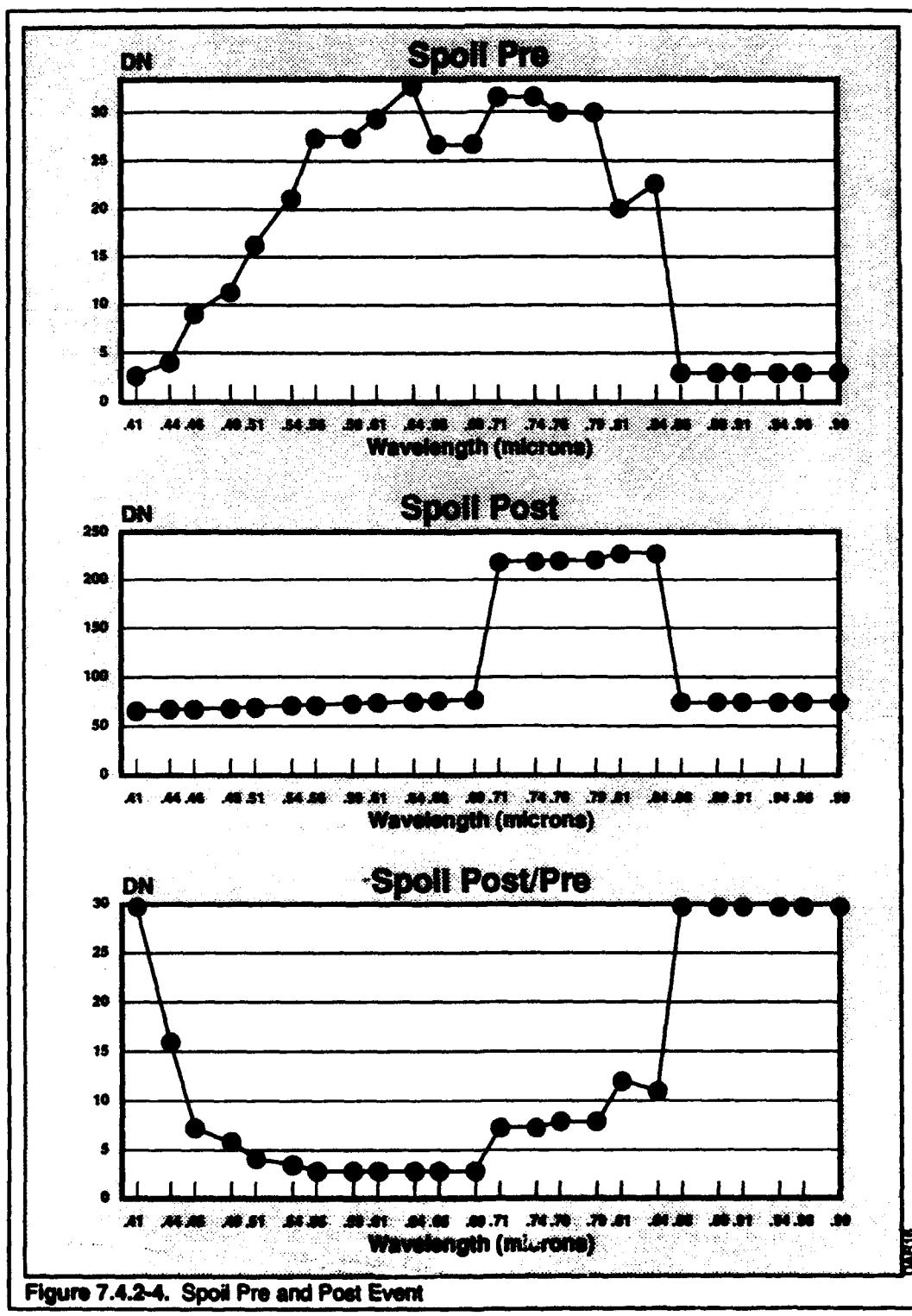
Figure 7.4.2-4. Spoil Pre and Post Event

Figure 7.4.2-4
Spoil Pre- and Post- Event
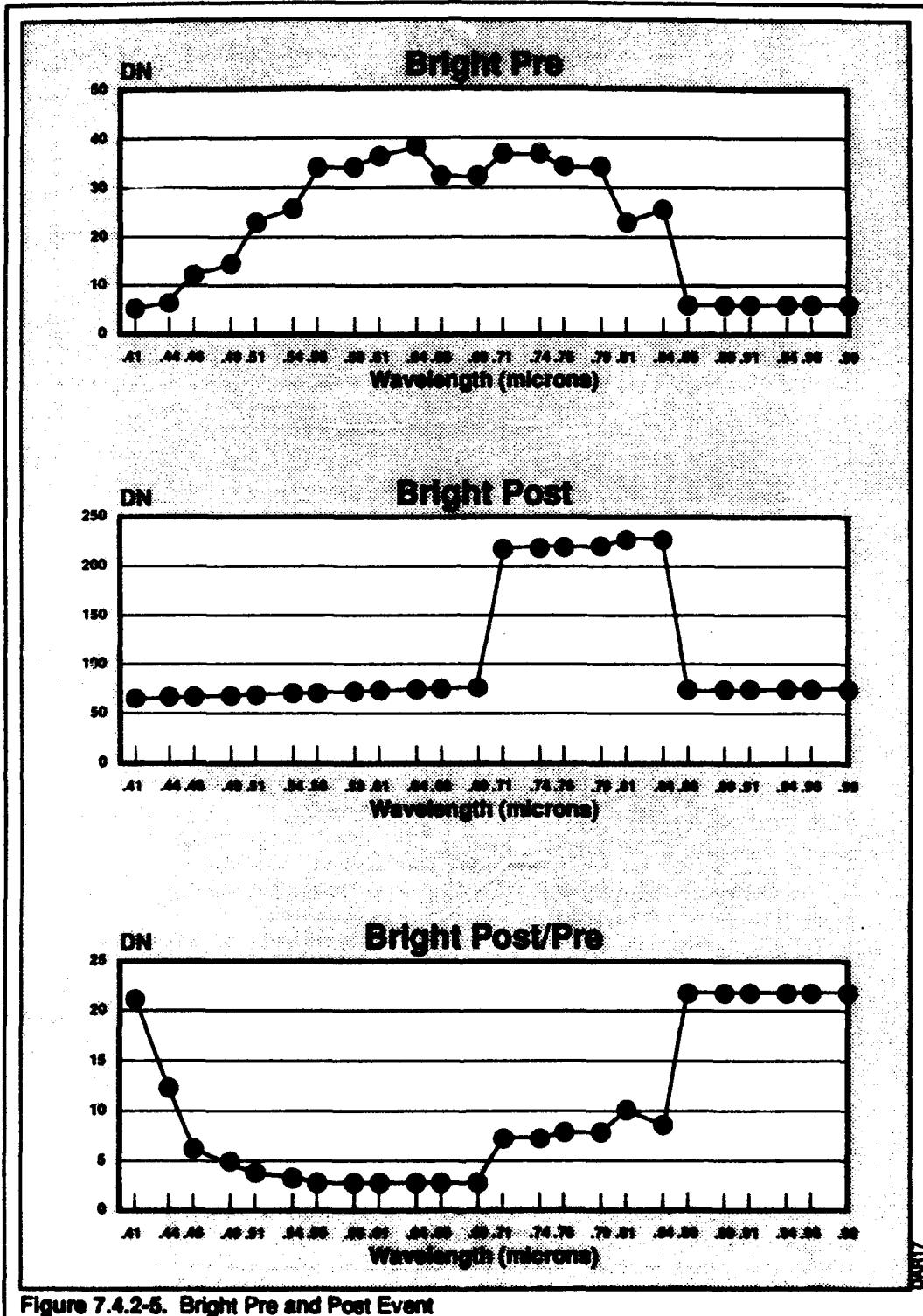
Figure 7.4.2-5. Bright Pre and Post Event

Figure 7.4.2-5
Bright Pre- and Post- Event

Figure 7.4.2-6. Water, Bright, Spoil/Road Pre and Post Event

Figure 7.4.2-6
**Water, Bright, Spoil/Road Pre- and Post- Event**

93
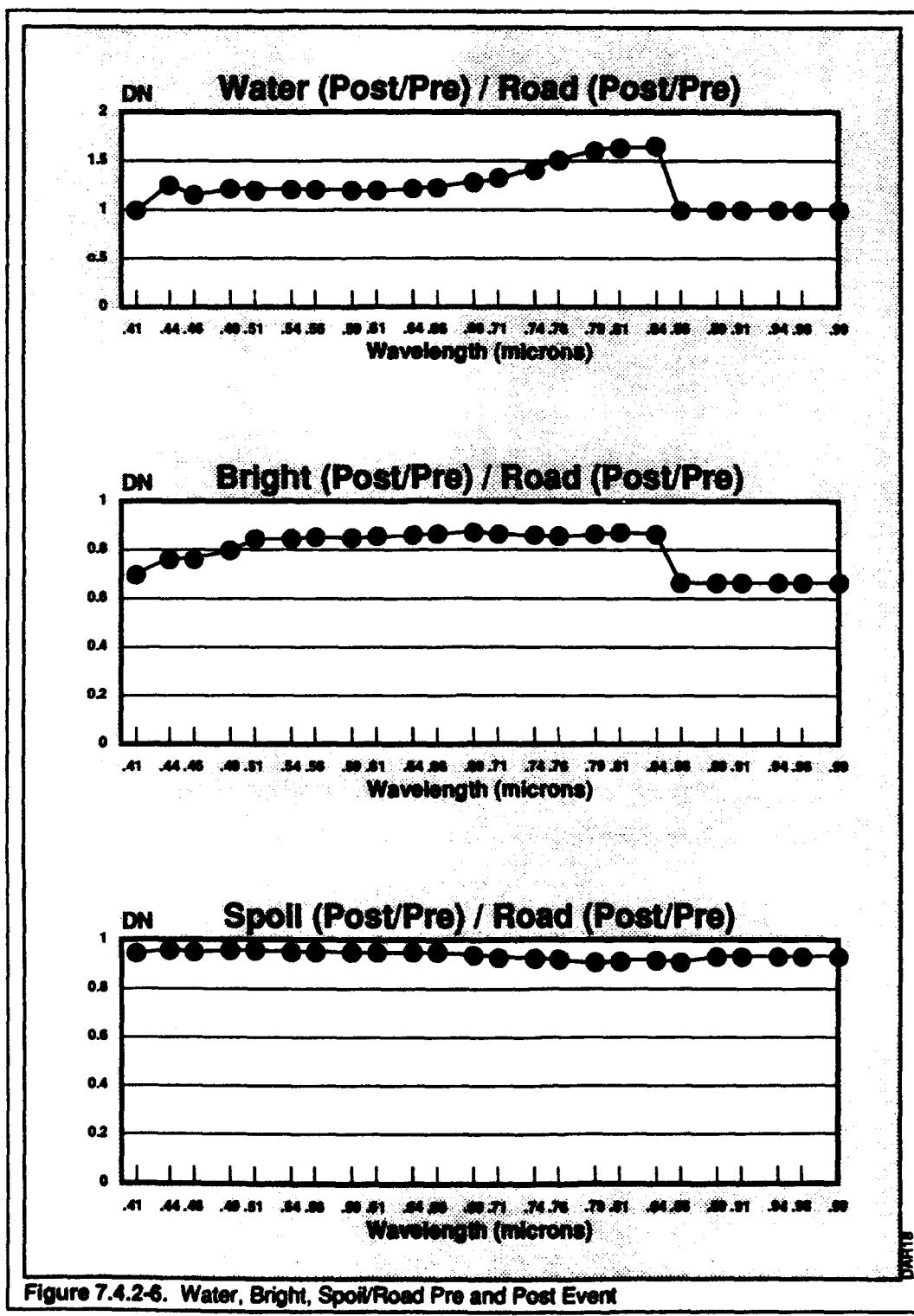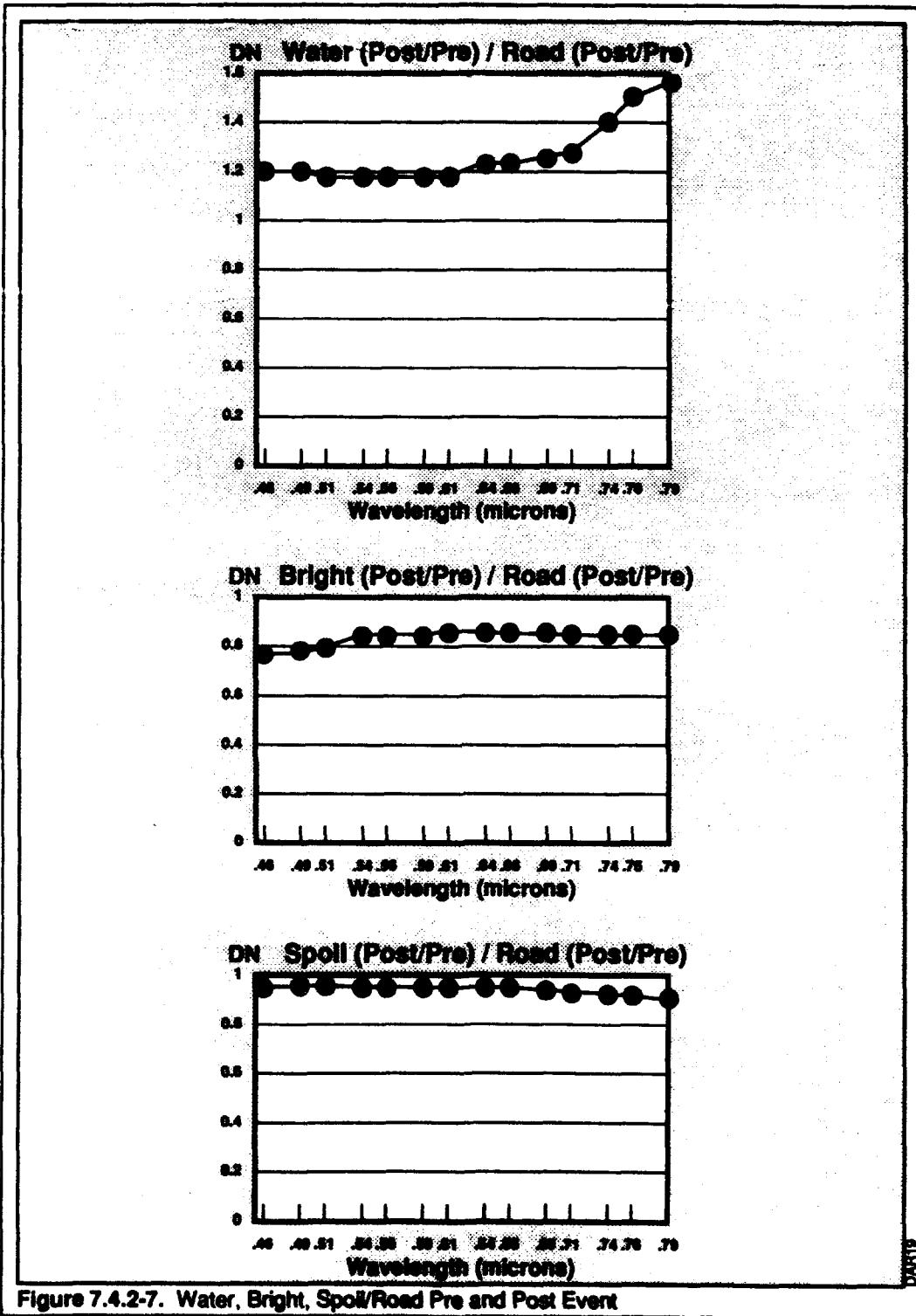
Figure 7.4.2-7. Water, Bright, Spoil/Road Pre and Post Event

Figure 7.4.2-7
Water, Bright, Spoil/Road Pre- and Post- Event

DN   (Bright/Road) / (Spoil/Road)

Wavelength (microns)

DAR20
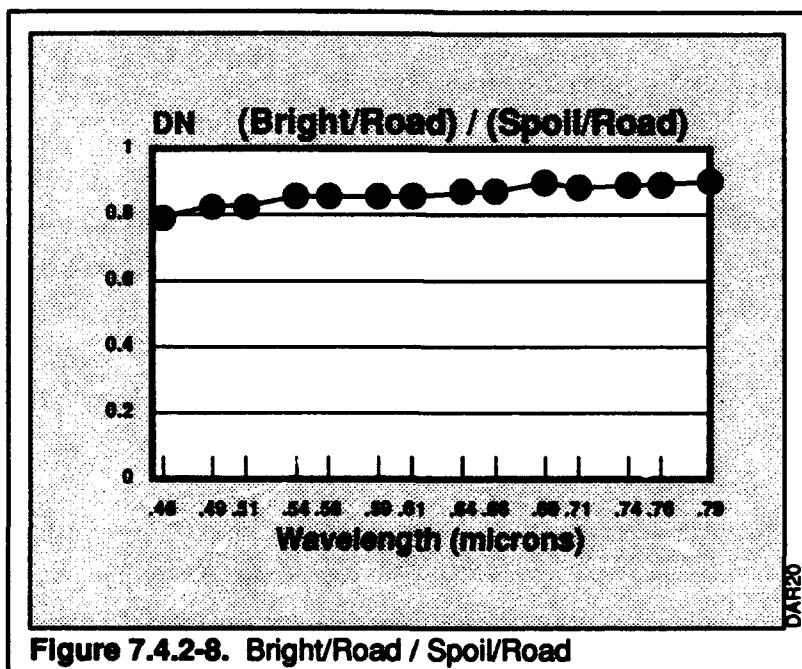
Figure 7.4.2-8. Bright/Road / Spoil/Road

Figure 7.4.2-8
Bright/Road - Spoil/Road

Another relevant finding was there were minimal fine scale spectra structures in the ASIS data, and the large number of spectral bands did not add apparent value compared to the six-band Landsat TM data for this observable. While high spectral resolutions may add value for many applications, there was no apparent advantage here. For this particular study site, and this particular observable, the spectral resolution of Landsat TM revealed approximately the same level of information as the ASIS data.

7.5   THREE-DIMENSIONAL DIGITAL MODELING

For remote sensing projects, the use of three-dimensional digital imagery models has become increasingly common. These models assist analysts by providing "three-dimensional" portrayals of a given study area; these models, however, are displayed in two-dimensional image space. As a result, subtle terrain and thematic features are shown in their X and Y and relative Z (elevation) positions.

The first step in creating a three-dimensional digital image is to generate a digital elevation model. Usually, this is accomplished using digital stereo imagery. Once these elevation (Z) data have been generated, two-dimensional (X and Y) imagery is registered to the elevation file. When displayed, the incorporated results appear as a three-dimensional image.

To generate the elevation data of BEXAR, stereo 10m SPOT panchromatic images were processed using the Autometric-developed PEGASUS™ digital photogrammetric processing workstation. To utilize the inherent spatial resolution of the SPOT data, elevation models were generated at three posting resolutions. These were established at 10, 20, and 30m, respectively.

An evaluation of the resultant models suggested the 30m model, as expected, was too coarse. In turn, the NTS elevation features were smoothed significantly, and the mesa containing the BEXAR site was not discernible. Compared to the 30m generation, the 20m model provided substantially better definition of the mesa, and generally, the terrain shapes were distinguishable. Unfortunately, the 20m generation represented a resolution threshold of the modeling process. Specifically, the 10m elevation data did not have an acceptable elevation error component. These findings were significant because they indicated the 10m (X and Y) digital data could not produce 10m elevation data. Rather, the elevation posting resolutions were dependent upon other modeling factors such as base-to-height ratios and relative off-nadir locations of BEXAR in the two SPOT scenes.

The next step in the modeling process involved registering a two-dimensional image to the elevation data. Both Landsat TM and SPOT panchromatic images were accessed for this purpose. Upon displaying the resultant three-dimensional generation, however, it was apparent the 20m elevation model was not sufficient for analyzing the BEXAR event. In particular, although the mesa was represented well in the elevation data, the BEXAR site — spatially comprising a portion of the mesa — lost significant image detail. Thus, while the general terrain of NTS was shown well using the three-

dimensional image model, BEXAR, being a site-specific feature, was not portrayed sufficiently. Because of these results, no other three-dimensional analyses were conducted using the SPOT elevation model.

In short, three-dimensional imagery models have proven their utility in past remote sensing research activities. Accordingly, while the 20m elevation model did not produce adequate detail of BEXAR, a model with smaller posting resolutions would likely support site-specific imagery investigations such as the detection and monitoring of underground detonations.

7.6   THERMAL ANALYSES

Thermal analyses of the BEXAR event were conducted using Landsat TM Band 6 imagery. In general, Band 6 (10.4 to 12.5 μm) measures the amount of infrared radiant flux emitted from surfaces. Apparent temperature is a function of the emissivity and true kinetic temperature of a given surface. Initially, the thermal data, collected before and after the event, were to be analyzed for detections of event-related change. Upon displaying the thermal imagery, however, it was unfortunately apparent the 120m spatial resolution of Band 6 was not adequate for interpreting change. In short, while generalized NTS seasonal thermal changes were observed, because of the poor spatial resolution, no site-specific thermal change related to the BEXAR event was found.

Surface thermal change remains a potential observable for the detection and monitoring of underground detonations. For such change to be observed, though, the thermal imagery must have significantly higher spatial resolutions than that provided by the 120m TM Band 6 data. Likely, spatial resolutions in the 10m range would be required.

SECTION 8
INTRODUCTION/BACKGROUND

8.1   INTRODUCTION

The purpose of this portion of the research was to define an integrated workstation concept addressing the requirements for economical, timely, reliable, and versatile exploitation. Indeed, the increasing capabilities of medium- to low-cost workstations has allowed "commercial-off-the-shelf", or COTS, technologies and standards to be applied to newly-emerging analytical areas. A system was required to support end-to-end solutions (i.e., data import, processing, and output) and be designed based on industry standards (e.g., UNIX, C, W-Windows). The combination of UNIX, C, W-Windows, standardized bus architectures, and general purpose processors (GP) provides an analyst with a processing platform commonly referred to as an open system. The open system concept is discussed here for its role in detecting, monitoring, and analyzing underground nuclear tests and associated test facilities.

The consolidation and stabilization of operating systems, software development languages, and graphical user interfaces has allowed software development activities to focus on the development of more modular and sophisticated software packages. Database generation and maintenance activity is required for many applications, and because of this, it can be considered an enabling technology (those portions of software that application developers use as part of their total solution). In contrast, applications provide a total solution to a user's problem, such as nuclear test monitoring, targeting, indications and warning, mission rehearsal, cross-country mobility analysis, etc.

8.2   SYSTEM FUNCTIONING

The fusion of multiple products to produce a working display for detecting and monitoring test facilities will demand unique software and dedicated equipment. Fundamental to solving the data fusion problem will be the ability to bring multisensor imagery having different viewing geometries into a common and accurate coordinate system. Disparate datasets can be registered to each other directly or indirectly by being first tied to geo-coordinates of the earth. Once a merged data set has been generated, many analysis options become possible. For nuclear test detection and monitoring scenarios, three applications were considered as important: stereo viewing and mensuration, three-dimensional terrain visualization and analysis, and multispectral/hyperspectral analysis. Specifically, the exploitation concept provided includes the following capabilities:

Digitizing hardcopy data;

Abilities to fuse various data types;

Base image enhancement;

Multispectral/Hyperspectral analysis;

Precise Mensuration;

Stereo viewing;

Three-dimensional perspective scene generation; and

High-quality hardcopy output.

Figure 8.2-1 illustrates the major functional components of a digital exploitation workstation. There are two basic components to the architecture. The first component (shown on the left portion of Figure 8.2-1) is Database Generation and Maintenance; this includes: (1) the importation of digital and hardcopy datasets (input functions); and (2) generation of merged datasets using a variety of photogrammetric techniques. Rectified imagery can be used to generate enhancements to the database such as feature data, digital elevation models, or orthorectified images. These data can be used for applications (second basic component) shown on the right of Figure 8.2-1. By keeping the data preparation software separate from the applications software, duplication of an overlap between software functions is reduced. This also enables rapid prototyping of new applications oriented to specific analytical requirements. The various system components are discussed separately in the following sections.

8.3   DATABASE GENERATION AND MAINTENANCE

8.3.1   Hardcopy Data Import

Hardcopy data must be converted to a digital format to be utilized by a digital exploitation system. This usually is accomplished with a digitizer (also known as a scanner). The type of digitizer required for hardcopy input is defined, in large part, by the type of hardcopy data being imported to the image processing system. If map data are to be incorporated, an inexpensive flatbed scanner with a resolution of 300 dots/inch (dpi) can be used (approximate cost is $7,000). If imagery is to be digitized, a higher resolution system is usually required such as an Eikonix 1412 digitizing camera with a Gordon Instruments digitizing workstation. These can digitize 4000-by-4000-pixel scenes from black and white or color prints and transparencies at a resolution of up to 20 micrometers (approximate cost is $30,000). A high-end option exists where a high-resolution digitizing capability is required over large areas. In this scenario, a digitizer with a movable stage is used to move accurately around large images and digitize smaller patches. These are then mosaicked together (approximate cost is $60,000).
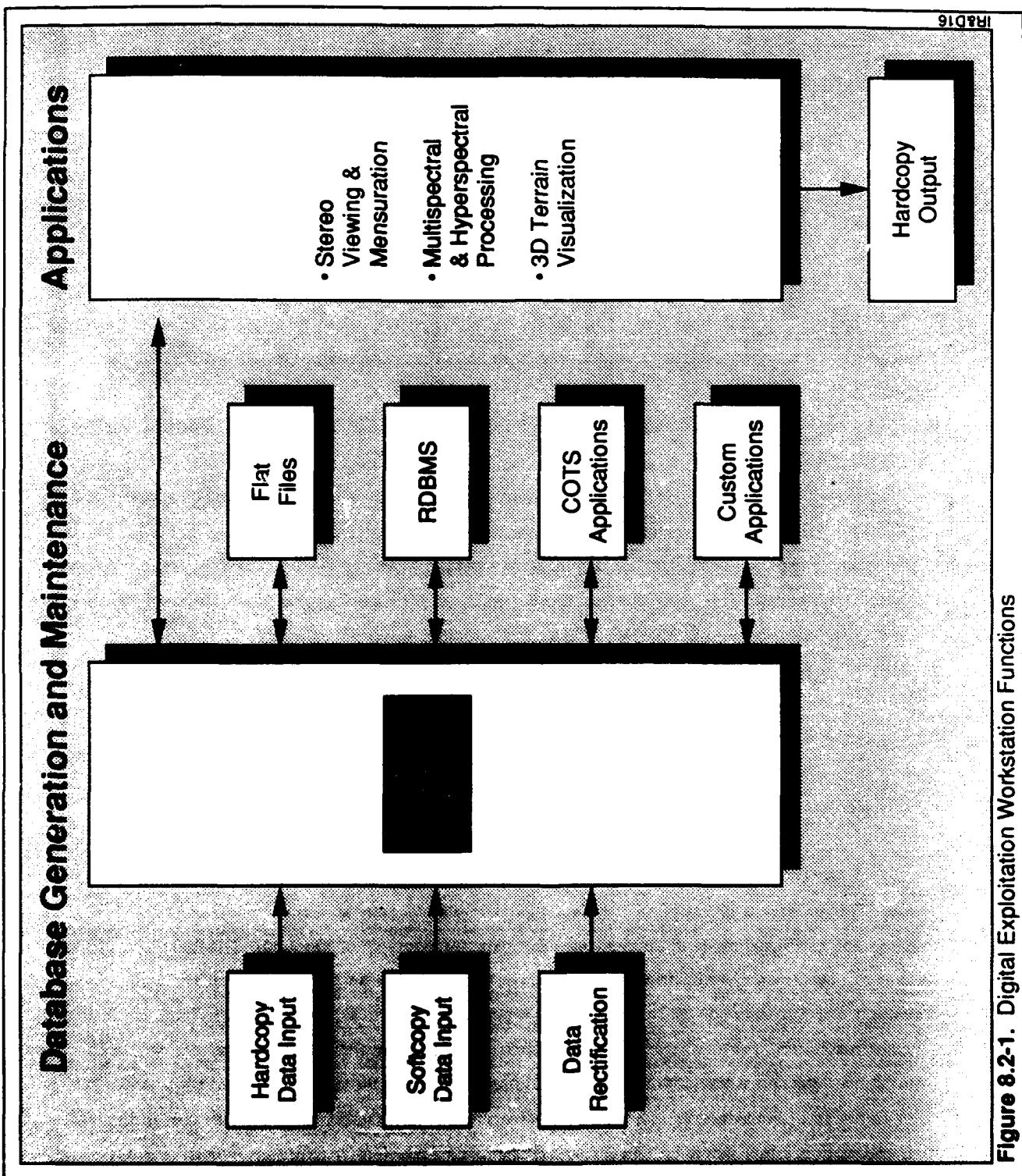
Figure 8.2-1. Digital Exploitation Workstation Functions

8.3.2 Softcopy Data Import

There are an increasing number of ways to import digital data to digital exploitation systems. Most digital imagery is stored on magnetic tape media. Tape formats include: 150 Mbyte SCSI cassettes, common on many engineering workstations; 9-track tapes which hold approximately the same amount of data as SCSI cassettes; and a recently-developed and inexpensive tape storage capability using 8mm tapes (5Gbytes).

Another recently introduced format and media, which are becoming increasingly popular to users, are CD-ROMs produced by the Defense Mapping Agency (DMA). The disks are similar to CDs commonly used in home stereos, and these can hold large amounts of data (650 Mbytes.). DMA currently distributes a number of data types on CD-ROMs including Arc Digital Raster Graphic (ADRG) data (digital maps), Digital Terrain Elevation Data (DTED), and some vector datasets such as World Vector Shoreline (WVS). The capability to read these new datasets is critical to an imagery exploitation system.

8.3.3 Data Storage

The various data utilized by digital exploitation systems require large amounts of data storage. Data storage remains a significant problem for digital exploitation systems. A standard three-color 9- by 9-inch aerial image, digitized at 100 dpi resolution, contains approximately $2.45 \cdot 10^8$ pixels. Most remote sensing projects contain many such large images which must be stored in a system during the compilation process. If they can be read into the system from magnetic tape, the tape reading itself takes considerable time.

Generally hardware vendors have not yet provided data storage devices to hold several gigabytes of information cost-effectively. Tape cartridge storage is inexpensive but requires significant seek and transfer time (more than ten minutes to locate one-gigabyte images). While data storage costs are continuously dropping, data storage will remain a major bottleneck in projects using large volumes of softcopy imagery.

With regard to format considerations as much as possible, common data formats should be used. For instance, the data file format may be a generic "flat file" with neither header information nor proprietary formatting. Alternatively, it may be in a proprietary format of some commercial relational database management system (RDBMS). Other proprietary or special formats may be required to support COTS or custom application software packages.

If multiple formats exist, to manage the data files shared between the various software applications and the workstations the ideal solution would be a virtual database interface (VDI). The VDI serves as the clearinghouse for all data exchange. Autometric is striving toward developing such a

solution; however, it is not a COTS solution at this time. If a VDI is not available, software utilities should be generated to convert between the various data formats required by the many applications.

8.4 APPLICATIONS

8.4.1 Data Rectification

Without a method for registration of imagery to a geographic coordinate system or other images in a rigorous, accurate manner, mensuration capabilities are in doubt. Often vector overlay data and elevation data are tied to the earth; and without knowledge of where images are located on the earth, it is difficult, if not impossible, to fuse the datasets.

Over the last 30 years, Autometric has based a significant portion of its business on its often unique capability to relate imagery to accurate geo-positions. The heart of this capability is the use of rigorous and accurate imaging sensor models that provide for simultaneous registrations of up to ten overlapping or independent images to ground control. Autometric has emphasized accuracy of mathematical models and data integrity in the development of its data fusion and mensuration capabilities (particularly since much of Autometric's work has involved defense mapping, military targeting, and intelligence exploitation). Military sensors frequently have highly complex imaging characteristics which require rigorous adherence to the modeling of the physical phenomena of the imaging event to ensure the mathematical models correctly represent the sensor. The mathematical models present in the Autometric-developed photogrammetric software preserve the metric accuracies inherent in these complex imaging systems.

Once a rectified imagery database has been constructed, the mensuration functionality is not complicated. Using polynomials generated by the sensor models, geographic coordinates can be determined for any point in the image allowing distances, azimuths, and areas to be calculated simply and accurately.

8.4.2 Multispectral and Hyperspectral Image Processing

The most important hardware consideration when processing multispectral data is the display device; 24-bit color is an option on most systems but not necessarily a standard configuration. Additionally, if imagery is to be scrolled or three-dimensional images are to be manipulated, a double buffering capability may be necessary, and this requires 48-bits of color.

As for the software, basic multispectral analysis capabilities are readily available on a wide variety of hardware configurations. It is important, however, to determine that the software package

selected can accept and process the expected input data. For example, hyperspectral analysis capabilities are not as common.

Besides COTS solutions, there are also custom processing techniques available which hold great promise for analyses of multispectral and hyperspectral imagery (e.g., subpixel analyses).

Given the map-like quality of commercial multispectral imagery, users often perform analyses on these data using other non-imagery data such as elevation data and thematic (map) data. These capabilities are provided in geographic information systems (GIS). Containing data management functions, these are slightly more complex than standard multispectral image processing packages. It is important that the image processing and GIS software (usually separate packages) utilized allows for exchange of data between these two functional areas.

8.4.3 Stereo Viewing and Mensuration

With certain sensors (e.g., SPOT), stereo pair images can be acquired. Using stereo viewing techniques, the terrain is depicted in three dimensions which is extremely useful for terrain, topographic, and microchromatological analyses. Prior to viewing, the stereo pairs must be prepared using rectification procedures.

In addition to viewing in stereo, a complimentary capability is the ability to mensurate accurately in three dimensions. If the imagery has been tied to the earth's surface, the latitude, longitude, and elevation (or similar coordinates) can be determined for any point in the image. This is an important capability when measuring locations, aerial extent, and volumes of various features found in the imagery.

8.4.4 Three-Dimensional Terrain Visualization

Stereo imagery may not always be available for an area of interest. Alternatively, the terrain can still be modeled in three dimensions if imagery and elevation data (e.g., DTED data) are both available. Using perspective transformation techniques, an accurate representation of the terrain can be created. On some hardware platforms, such as most Silicon Graphics workstations, perspective scenes can be built quickly and can be manipulated interactively.

8.4.5 Applications Development Environment

In addition to using COTS software packages, a digital exploitation workstation should provide an applications development environment. Industry standards such X-Windows, UNIX, MOTIF, and C should be supported. When available, development options should be acquired for the COTS

applications. These options usually consist of libraries of software functions that can be used to add functionality to the COTS software or to build separate applications.

8.5   HARDCOPY OUTPUT

The majority of analyses of digital imagery will be accomplished in softcopy; however, there is always a need for the production of hardcopy output. Hardcopy output is necessary to record images as displayed on a high-resolution computer display. Hardcopy devices can produce output that contains a larger image area than can be displayed on a computer display screen. Printed output can be used as a storage medium and can be easily utilized by many people without specialized computer equipment. For this reason, and others, results from softcopy analyses are often presented in a hardcopy format.

When working with multispectral image data, it is important that the printing device be capable of 24-bit "true-color" printing. In many cases, three image spectral bands are combined and printed as a red-green-blue (RGB) image. Color printers are capable of printing black and white images by repeating the same data to the three RGB channels of the printer. However, sometimes this method produces black and white images that have a color cast to them (e.g., bluish tinge). If only black and white images are to be produced, then a black and white printer should be used or the color printer should be adjusted accordingly. Depending on the type of printing process, this adjustment might include using a black and white ribbon (thermal dye printer) or black ink exclusively (ink-jet printer).

There are numerous hardcopy output options available. The one selected depends on the hardcopy output needs. If high quality output is desired (photographic quality), a continuous-tone process should be used. The 3M Color Laser Imager (CLI) utilizes a wet photographic process that produces extremely high-quality color output at 300 pixels/inch resolution. Its output size is limited to 12 by 18 inches. This printer is a high-throughput model that costs approximately $133,000. For lower quantity and smaller format printing, the Kodak XL7700 printer is a good alternative. Its image quality is not as high as the CLI since it records at 200 pixels/inch. It utilizes a thermal dye process, and its throughput is not as high as the CLI. The XL7700 output is limited to 11 by 11 inches. The cost of a color XL7700 is approximately $20,000.

If larger format output is desired, continuous tone printing is not viable; however, there are three options available. The first option is photographic enlargement. This process is expensive, and if geometric accuracy of the data is to be preserved, this is not a realistic option. Lithographic printing can be done, but its cost is only justified when large numbers of prints are to be produced (minimum of 500). The lithographic process utilizes much specialized equipment, and the image quality is inferior to continuous tone printing since half-tones are used. The cost of a medium-format lithographic image setter and pre-press equipment would be approximately $130,000, and this would not include printing press plate production equipment. The third large format option is the IRIS Graphics 3024 or 3047

printer. These two printers are ink-jet printers that offer exceptional image quality at 300 pixels/inch resolution. To the unaided eye, the output appears to be a continuous tone; however, these printers actually utilize fine resolution half-tones. For most purposes, these half-tones are not a hindrance, unless the image data are to be analyzed under magnification. The output sizes for these two printers is 24 by 24 inches for the 3024 and 34 by 47 inches for the 3047. Therefore, high-quality full-size image maps can be produced on the 3047. The 3047 printer sells for $130,000 and the 3024 for $84,500.

8.6   SYSTEM CONCEPT

The rationale used for the analysis system is to develop an open system built using COTS solutions as much as possible: this includes both hardware and software. The major advantage to this approach is that it greatly reduces costs (both initial and maintenance). A typical digital exploitation workstation is shown in Figure 8.6-1.

The suggested host computer is a Silicon Graphics 4D/35TG workstation. The UNIX-based workstation has a COTS general purpose 36 Mhz RISC cpu. It utilizes COTS graphics boards that enable 24-bit color display of imagery and also double-buffering of 12-bit data. It easily handles large image datasets quickly. The workstation can also support a hardcopy digitizer and hardcopy printer. The Silicon Graphics is a COTS hardware solution that supports industry standards for software development with UNIX, X-Windows, MOTIF, and C, to name a few.
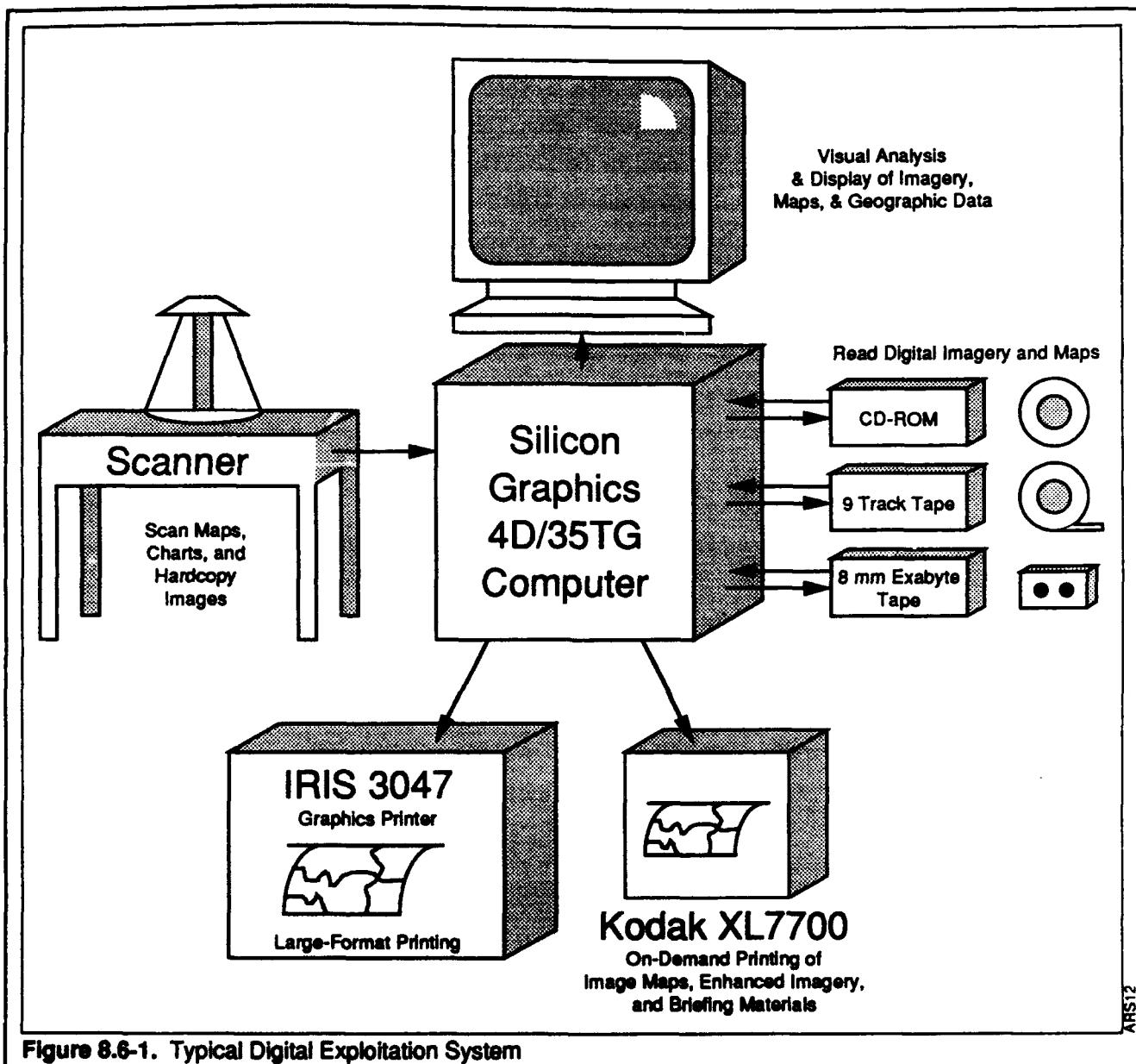
Figure 8.6-1. Typical Digital Exploitation System

Since the Silicon Graphics computer is a COTS solution, there is a variety of COTS software available to support this platform. There are various options to consider for both image processing, GIS, terrain visualization, and photogrammetric (rectification and mensuration) functionality. As an analysis laboratory grows in size, additional workstations can be added via a Local Area Network (LAN), and the data files can shared.

For hardcopy digitization, the Eikonix 1412 scanner is suggested. This scanner along with the Gordon Instruments transmissive/reflective workstation will provide capability to digitize black and white and color paper and transparent imagery.

The most viable solution for small-format, high-quality printing is the Kodak XL7700 printer. This printer is easy to use and can make both black and white and color prints (separate ribbons). An additional printer may be desired depending on the required type of output. A decision should be made between a high-throughput CLI that produces 12 by 18 inch output or a large format printer such as the IRIS Graphics 3047 (which may take an hour to produce a 34 inch by 47 inch color print).

8.7   COSTS

Costs are provided for workstation components discussed in Section 8.6. These are approximate costs; no discounts have been considered.

Silicon Graphics 4D/35TG Workstations	$54,000
48 Mb RAM	
1.2 Gbyte hard disk	
9-track tape drive	
8 mm cassette drive	
CD-ROM drive	
Eikonix 1412 Digitizer and Gordon	
Instruments Digitizing Workstation	$30,000
Application Software Packages	
(including GIS, image processing,	
photogrammetry, terrain visualization)	$90,000
Kodak XL7700 Color Printer	$20,000
Printer Options:	
IRIS Graphics 3024 Printer	$84,500
IRIS Graphics 3047 Printer	$130,000
3M Color Laser Imager	$133,000

SECTION 9
CONCLUSIONS

9.1 STUDY CONCLUSIONS

Based upon the analyses conducted under this two phase research study, the following conclusions are documented:

9.1.1 General

- With the dissolution of the Soviet Union and proliferation of nuclear technology, the requirement for global search, detection and monitoring of current and pending nuclear test facilities increases in priority.

- The use of current and planned national and international civil and commercial imaging satellites, combined with National assets, provide a reliable means for detecting and monitoring worldwide underground nuclear test preparations and detonations, whether covert or under arms control treaties.

- The large area coverage and wide area search capabilities of multispectral satellite systems such as Landsat and SPOT would aid in establishing whether nuclear weapons development has advanced beyond the laboratory, by providing important information on test site activities.

- The stability of spaceborne platforms for imaging systems is far superior to that of aircraft platforms which, and when combined with their synoptic, repetitive, wide area coverage parameters, results in the conclusion that spaceborne platforms enhance exploitation and, in particular, the registration of scenes for change detection.

9.1.2 Database Management

- Establishing a database of remote sensor/reconnaissance imagery, both hard and softcopy, is a key component for monitoring worldwide underground nuclear development and testing.

- Once an area becomes suspect, all source historical data of that area should be gathered to establish a comprehensive database that will support collection planning and product exploitation.

- The collation of both imaging sensor products and collateral data such as maps and schematics into a common digital media is the most efficient means for exploiting the multiple data sets.

- Generic test preparation chronological timelines can be documented through the use of commercial imaging satellites, and can provide a reliable means for monitoring the progress and eventual success of future underground tests.

9.1.3   Collection Management

- "Smart" all-source imagery collection planning is mandatory, both in terms of global and directed search strategies and in selective multiple sensor/multispectral collections, once a suspicious area is delineated.
- Periodic and point target tasking of imaging sensors should begin at the inception of a test and continue past the day of the final event.
- Collection management and tasking of imaging sensors should be coordinated with other intelligence and verification sources, including seismic monitoring.

9.1.4   Data Processing/Exploitation

- The combined use of various imaging systems and the correlation of multiple sensor/multispectral imagery with collateral data demands the use of a computer based digital image processing, exploitation and fusion system.
- A test bed digital workstation designed and dedicated to the requirements for detecting and monitoring underground tests should be developed and installed within the DARPA and eventually deployed operationally.
- The 30m spatial resolution of the Landsat TM is marginal in terms of detecting activity at a site. The 15m spatial resolution of the pending Landsat 6 panchromatic band will allow the detection of heavy equipment and trailers at a site.
- Ground scarring and terrain changes can best be analyzed using the Landsat TM Band 5 and 7 spectral windows whereas vegetative changes are emphasized by using the visible and near infrared bands.
- Tools have been developed and tested in this study that will allow the isolation of changes that occur due to testing from those that result from nominal atmospheric or vegetative changes.
- A precise digital three-dimensional perspective view of an identified test area should be produced to support analyses of the site, the future tasking of collection assets, and a readily understood vehicle for decisionmakers.

9.2   BEXAR TEST CONCLUSIONS

9.2.1 General

- For a given test having a spoil pile at or near ground-zero, the detonation should change the pile predictably. Phenomenologically, the detonation event should produce a variety of observables. From the research, these changes were categorized as either spectral changes (e.g., reddening, cracking and shadowing, particulate shifts) and/or spatial changes (e.g., lateral expansion). The usefulness of these indicators, however, would likely be dependent on the size and depth of the spoil pile, depth of the detonation, and the characteristics of the overburden.

9.2.2 Multispectral

- BEXAR-related changes were found using the multispectral TM data, and these were detected using statistical techniques to model the spectral variance measures. For detonation conditions comparable to those of BEXAR, the results suggested Landsat TM, at 30m, provided adequate spatial resolution capabilities for detecting event-related changes. Furthermore, the statistical techniques required minimal complementary visual analyses of the data.
- Soil and geologic changes detected were attributed to the BEXAR event.
- Vegetation changes were due to naturally-occurring plant cyclical states and were not attributed to the BEXAR event.
- Originally, the TM spectral band positions and the bandwidths were designed to be effective for a multitude of diverse earth resource monitoring tasks. These spectral bands were sufficient for underground detonation detections because they addressed the diverse observables associated with the test.
- A space borne platform, such as Landsat, is best for detecting change because of its orbital stability. Images can be acquired repeatedly of the same area from approximately the same position in space. In particular, the stability of Landsat is superior to that of an airborne platform subject to pitch, yaw, and roll distortions.

9.2.3 Subpixel

- BEXAR-related changes were found using the subpixel technique. Specifically, the process revealed the occurrence of lateral expansions of the BEXAR site's surface.
- Vegetative changes were detected, but none of these were attributed to the BEXAR event.
- The surface expansion was defined better using the subpixel technique compared to the whole-pixel analysis of spectral variance methods; and accordingly, the subpixel process complimented well the multispectral techniques.

- Post-event spectral reddening of the site-specific iron oxide found using the whole-pixel multispectral analyses was also found using the subpixel analyses technique.

9.2.4   Hyperspectral

- BEXAR-related changes were found using the ASIS hyperspectral data. Specifically, discriminate soil/surface changes (non-statistical) were attributed to the BEXAR event; however, no event-related vegetative changes were found.
- Due to specific sensor malfunctions (in the ASIS spectrometer number three), the greater spectral resolution provided by ASIS did not provide substantially more information vs. the six-band TM data; greater spatial resolutions, however, did allow for detection of change not found using the TM.
- From an imagery perspective, the ASIS data were not used in their original 16-bit radiometric range, and subsequently, information was lost.
- For small, site-specific applications, the utility of airborne sensor data, such as ASIS, is limited due to significant impacts of aircraft pitch, roll, and yaw distortions.

9.2.5   Thermal

- Due to the poor spatial resolution of the TM Band 6 (120 by 120m), no thermal changes attributable to the BEXAR event were found.

9.2.6   Digital Three-Dimensional Modeling

- Digital elevation data generated using 10m SPOT stereo imagery did not provide sufficient spatial definition clarity for small-area site-specific modelings of the BEXAR site.

SECTION 10

RECOMMENDATIONS

10.1   STUDY RECOMMENDATIONS

10.1.1   General

- An ideal sensor configuration and acquisition strategy should be considered for detecting test-site potential and actual observables. It is recommended that observables at NTS and other test sites be evaluated further before specific sensor and sensor parameters are declared. Indeed, other observables should be verified as representative of event-related change phenomena. Detectabilities of these additional observables using Landsat or other airborne sensors must be determined.

- Many of the environmental changes due to the BEXAR blast were subtle. Some of the changes were evident immediately after the blast whereas other changes were seemingly not apparent for days. Other potential changes could take weeks or months to occur (such as vegetation stress). For these reasons, an image collection rate of approximately once every seven days would be desirable for a given test site. The seven-day rate would also help quantify natural rates of environmental change. (These can be quite rapid depending on the growth season status.)

- An economical digital workstation should be developed that could be tested and deployed to field sites to support treaty verification and site monitoring.

10.1.2   Multispectral

- Landsat TM should be considered as a primary sensor for monitoring and detecting underground explosions. This is due to Landsat's collection-to-collection geometric fidelity. Thus, Landsat is not only capable of sensing event-related changes, but the TM data could serve as the geometrically-accurate registration base for subsequent multisensor fusions (particularly when adequate map data are not available).

- Research should be focused on the potential utility of added spatial resolution capabilities of future Landsat's (i.e., 6, 7, and 8)

- To provide more quantifications of change, analysis of variance techniques should be used in conjunction with advanced regression techniques (e.g., LISREL) to measure latent ("unmeasured") variables of a given site.

10.1.3 Subpixel

• Since the subpixel process can detect objects comprising as little as 20% of a spatial pixel, the utility of the technique should be researched in conjunction with the spatial resolution changes of pending multispectral systems.

• Since the subpixel process requires at least five multispectral bands and accuracy increases when more bands are available, the utility of the technique should be researched in conjunction with the spectral resolution changes of pending multispectral systems.

• Other advanced subpixel techniques exist, and their validities and reliabilities should be evaluated for purposes of detecting and monitoring underground tests.

• Due to the computational demands of subpixel processings, high-end computing devices — such as the NIDL Princeton Engine — should be evaluated for their potential application and testing roles.

10.1.4 Hyperspectral

• Hyperspectral data must be analyzed both as image data and non-image data; specifically, 16-bit time-series and frequency-domain stochastic modeling techniques should be considered as complements to 8-bit discriminate imagery processing.

• If aircraft hyperspectral data are to be used, collection management parameters must be strictly controlled.

• As other hyperspectral and ultraspectral systems evolve, their comparative utilities for detecting and monitoring underground tests must be considered.

10.1.5 Thermal

• The spatial resolution of the thermal data must be significantly better than the 120m Landsat TM thermal imagery. Likely, a spatial resolution in the 10m range would be needed if thermal data are to detect event-related changes.

• As multiband thermal systems evolve, their comparative utilities for detecting and monitoring underground tests must be considered.

10.1.6 Digital Three-Dimensional Modeling

• If digital three-dimensional models of a given test site are to be generated, the stereo data must have significantly better spatial resolutions than that offered by the 10m SPOT system.

- A precise digital three-dimensional perspective view of an identified test should be provided to support analyses of the site, future tasking of collection assets, and decision-maker and analyst viewing.